P O L I T E C N I C O D I M I L A N O

Hydrogen Gas Gap Heat Switches: characterization and life testing

Mauro Prina

XII Ciclo del Dottorato in Energetica

December 1999

POLITECNICO DI MILANO

Hydrogen Gas Gap Heat Switches: characterization and life testing

Mauro Prina

XII Ciclo del Dottorato in Energetica

PH.D Program Director: prof. Gianfranco Angelino

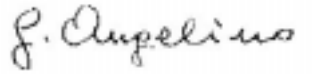

Advisors: prof. Ernesto Pedrocchi

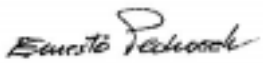

Dr. Robert C. Bowman

December 1999

Acknowledgements

I would like to thank my advisors, Pedrocchi Ernesto and Robert C. Bowman, for all the suggestions, the discrete and constant support that they provided during the time I spent with them. Their attention and loyalty towards what is manifested as an evidence is what I have appreciated the most of them. I am also very thankful to Marco Bersanelli who got me involved in the Planck project. I am proud to contribute to a further development in the understanding of the beginning of the Universe.

With them I would like to thank all the people that have been involved in this adventure, il cavaliere Gianluca Morgante, Pradeep Bhandari, Chris Lindensmith, Toni Loc, Chris Paine, Mike Schmeltzel, Donald Rapp, Larry Wade and all the ones that throughout this years supported me and collaborated on the Planck cooler. I also would like to thank all the proofreaders, Ed and Julie, that reshaped and helped to give a readable aspect to this work.

I am grateful to them and to all my friends that continuously help me in regaining the right perspective each morning making the everyday life an adventure.

Abstract

An 18 K continuous-cycle sorption cryocooler is being developed for the European Space Agency Planck mission, which will be launched into space around 2007 in order to map the anisotropy of the cosmic microwave background. This cooler will produce liquid hydrogen by a closed-cycle Joule-Thomson expansion of gas compressed and circulated using metal hydride sorbent beds in the compressor assembly. The compressor assembly will be located on the spacecraft bus and is attached to radiators for passive cooling to 280 K in order to provide a heat sink for cooling the sorbent beds to their absorption temperature and rejecting the heat of absorption. Each compressor bed will be provided with a gas gap heat switch designed to minimize the overall cryocooler power and to maximize the stability of the cold tip temperature, both of which are strongly affected by the performance of the gas-gap heat switch actuator.

The initial research objective is to define the engineering and operational requirements for the gas gap heat switches to be used in hydride compressor beds of a 20 K Joule-Thomson cryocooler. Furthermore, this project involves the design of hydride gas gap actuators and validation of this design by testing the actuators in a life test. The gas gap heat switches on the Planck sorption cooler alternatively connect and disconnect the compressor units to a heat sink at 280 K. Operational requirements, such as heat conductance and time to switch, have been derived according to the predicted operational behaviors of the sorption cooler and to environmental conditions. The derived requirements have been validated in the laboratory on a prototype compressor unit in terms of pressure vs. gap conductance.

The gas gap heat switch is used to thermally connect or disconnect two objects, by filling the gap between the two surfaces with gas up to a pressure P_{ON} or emptying it down to a pressure P_{OFF}. The primary requirements of the gas used in a gas gap heat switches are a high thermal conductivity and the ability to be stored reversibly by an actuator. The combination of hydrogen and hydrides has selected as a baseline for the switch design. Three different hydride metal systems, Uranium, ZrNi and SAES St 172, were used to build the seven actuators that have been tested.

The initial behavior of the actuators have been determined and their performance degradation due to the switch cycling (up to 13,000 cycles) has been analyzed. The proposed designs have been validated by testing the experimental performances of the

seven switches in terms of pressure swing and power dissipated. The evaluation of those switches has been done considering the cooler requirements that drove their design. The resulting conclusion is that all the switch designs are exceeding the requirements, although they each have advantages and disadvantages which are described in this report. All three the switch designs have been validated, but it is suggested to use ZrNi actuators as the flight unit switches to minimize the risk of components (i.e. heaters) failure.

Contents

1. Introduction and Background

At the end of the XX century it is so common to think that electric current is interruptible that it would seem even strange to pose the question. Nowadays the everyday life of most of the human beings is full of electrical switch applications of every kind. We can generalize the concept of a switch to a device that can allow or prohibit a flux of any kind between two elements. In an imaginary survey, probably a little bit more thinking would be required to answer the question "can you give me an example of a optical switch", and perhaps the camera diaphragm would be the most common example. A completely different treatment has been reserved for the heat switching. It is easy to think of heat insulation, heat transfer optimization, or temperature control; but a clear example of heat switching is difficult to find. Most of the applications requiring alternatively thermal insulation and heat conduction reached a trade off between the two, by optimizing either the thermal insulation or the heating/cooling time constant. For some particular applications, like components used on spacecraft where thermal optimization have major impact on performance and cost, it is valuable to consider designing and building heat switches. This research has its origin in the design and realization of gas gap heat switches for a space flight component, the Planck mission sorption compressor .

A gas gap heat switch is used to connect or disconnect two objects thermally, by filling the gap between the two surfaces with gas up to a pressure P_{ON} or emptying it down to a pressure P_{OFF}. The pressure change in the gap is equivalent to the change in the number of molecules available to transport heat from one surface to the other. At very low pressures the molecules are so few that they will principally strike the walls while at higher pressures they will most likely strike other gas molecules as shown schematically in Figure 1-1. Even though the heat transfer from surface to surface is more efficient at low pressure, there are so few molecules available that the rate of heat transfer is greatly reduced.

Different ranges of the Knudsen number, defined as the ratio of the mean free path of a molecule to a characteristic environmental dimension (for example, the distance between two parallel planes), distinguish two regimes. The *molecular regime* is defined for Knudsen numbers above 1, when the mean free path is longer than the distance between the plates and a molecule has greater probability of striking the surfaces rather than other gas molecules. When the Knudsen number is below 0.01, intermolecular

collision predominates, and the heat transfer is determined by the momentum transfer in the gas: the regime is called *viscous or continuum regime*. Above a certain pressure, depending on the molecular characteristics, the heat conductivity approaches a constant value. The *transition regime* is defined for Knudsen numbers between these two limits. The two orders of magnitude variation in Knudsen number across the transition regime correspond to roughly two orders of magnitude change in the heat conductance. A gas gap heat switch will operate primarily across this regime by appropriately changing the pressure (density) of the gas between two surfaces.

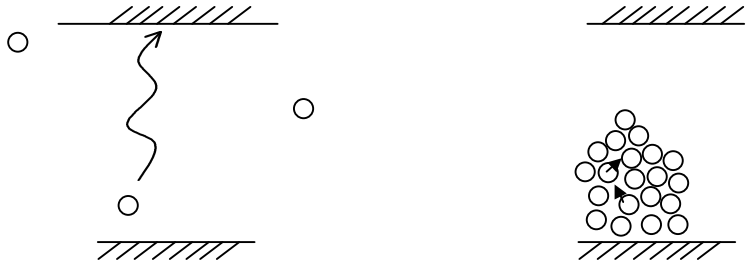

Figure 1-1 Schematic of the heat transfer in molecular and viscous regime.

The design and the development of a gas gap heat switch requires a detailed understanding of the application requirements and of the reversible pump used to evacuate and fill the gap the with gas. In this section a brief description of the PLANCK mission cooling system [section 1.1] and in particular of the sorption cooler will be given [section 1.2] to introduce the application requirements for the gas gap heat switch [section 1.3] that will then be more thoroughly discussed in [section 2]. Since hydrogen has been considered as the conductive gas and hydride as reversible metal pump, a brief theoretical introduction to the hydrogen-metal systems [section 1.4] will then be given followed by the background on the gas gap heat switching technology [section 1.5].

1.1 The PLANCK cooling system

PLANCK [1] is a European space mission whose main objective is to image the temperature anisotropy of the Cosmic Microwave Background (CMB) at high angular resolution. Measurements of the CMB made with the FIRAS instrument on the COBE mission [2] confirmed the hot big bang model. According to this model the Universe was initially hot and dense and has been expanding and adiabatically cooling ever since. When the Universe was ~$3 \cdot 10^5$ years old, its temperature was around 3000 K and protons were able to capture electrons to form neutral hydrogen and helium atoms. Before this

time, the Universe was opaque to radiation and thus the transition at ~3000 K (called recombination), freeing photons for the first time, produced the earliest available image of the Universe. PLANCK will produce high sensitivity maps over 95% of the sky in a wide range of frequencies which have never before been studied at such high resolutions and sensitivities. These maps will have a large number of applications, from cosmological studies (the primary target) to many of the most important subjects and problems of modern astrophysics. The telescope will measure temperature fluctuations in the CMB with a precision of ~ 2 parts per million and an angular resolution ~ 10 arc-min. The analysis of these fluctuations will determine to a precision of few percent the fundamental cosmological parameters (Hubble constant, density of the Universe, cosmological constant etc.), thus answering fundamental questions about our Universe.

Planck will carry two instruments: the High Frequency Instrument (HFI) and the Low Frequency Instrument (LFI). In combination they will observe and image the full sky in nine spectral bands between 30 and 857 GHz. Both the LFI and the HFI instrument sensors need to be cooled to cryogenic temperatures to optimize their signal to noise ratio. The detector cooling system has to minimize the mechanical vibration to reduce the spurious signal generation on the ultra-sensitive detectors.

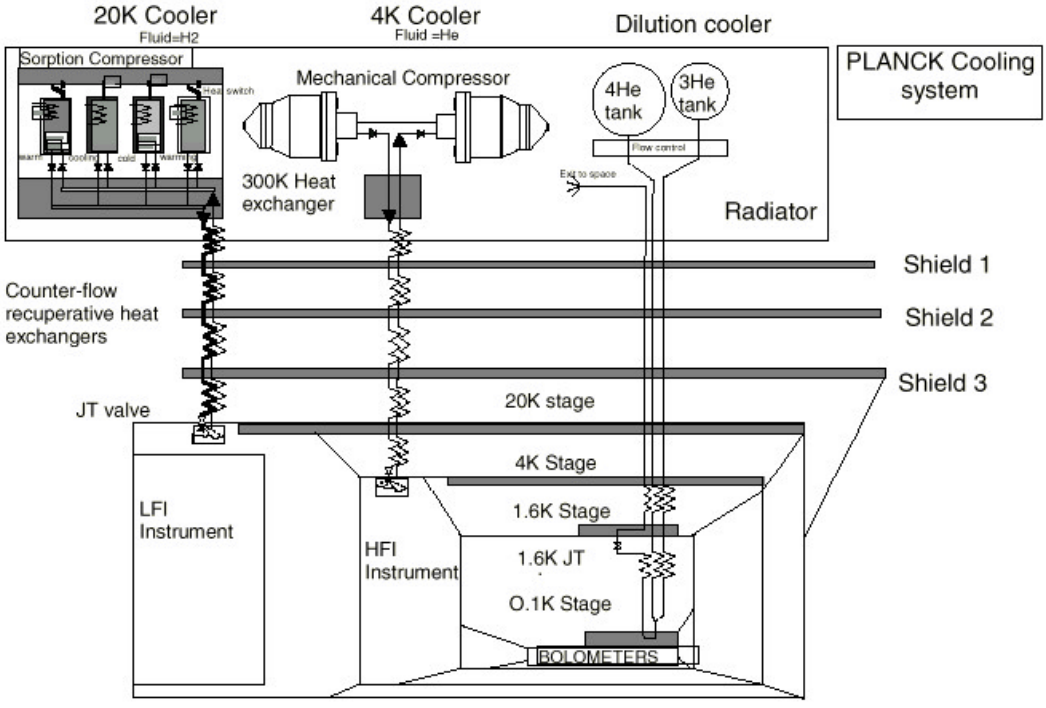

Figure 1-2 PLANCK Cooling Systems [3].

The LFI radiometers need a temperature of 20 K reached through a combination of passive cooling to about 50 K and active cooling using a hydrogen sorption cooler to reach lower temperatures. The HFI uses bolometers cooled to 100 mK through a combination of passive cooling (radiator at 50 K), the 20 K sorption cooler, a 4.5 K Mechanical Joule-Thomson cooler and a Benoit style open cycle dilution cooler (^{3}He-^{4}He). The use of an open cycle dilution cooler will limit the mission life to 1.5 years for the HFI. The thermal environment for the instrument detectors is well described by the schematic in Figure 1-2 and a detailed analysis can be found in [3].

1.2 The 20 K sorption cooler

The sorption cooler performs a simple thermodynamic cycle [4] based on the hydrogen compression up to 6 MPa, the hydrogen gas pre-cooling by the three radiators at 170 K, 100 K and 50 K, the further cooling due to the heat recovery by the cold low pressure gas stream, the expansion through a J-T expansion valve and the evaporation at the cold stage [see Figure 1-2]. The key element of the 20 K sorption cooler is the compressor, an absorption machine that pumps hydrogen by thermally cycling several sorbent compressor units.

The principle of operation of the sorption compressor is based on the properties of a unique sorption material [5, 6] which can absorb large amounts of hydrogen at relatively low pressures and low temperature, and which will desorb to produce high-pressure hydrogen when heated in a limited volume (the properties of a typical hydride sorbent are illustrated schematically in Figure 1-3.). Heating of the sorbent is accomplished with electrical resistance heaters and cooling is achieved by connecting to a radiator. The system is periodically cycled between heating and cooling cycles, producing high-pressure gas intermittently. In order not to lose excessive amounts of heat during the heating cycle, a heat switch is provided to alternately isolate the sorbent bed from the radiator during the heating cycle, and connect it to the radiator thermally during the cooling cycle.

In Figure 1-3, the mass of hydrogen stored in a unit mass of sorbent at equilibrium is plotted on the horizontal axis versus the pressure on the vertical axis. Each curve is an “isotherm” at constant temperature [see section 1.4]. The sorbent in contact with hydrogen gas can exist at equilibrium anywhere on one of the isotherms. If hydrogen is added to or removed from the sorbent at constant temperature, the system will move

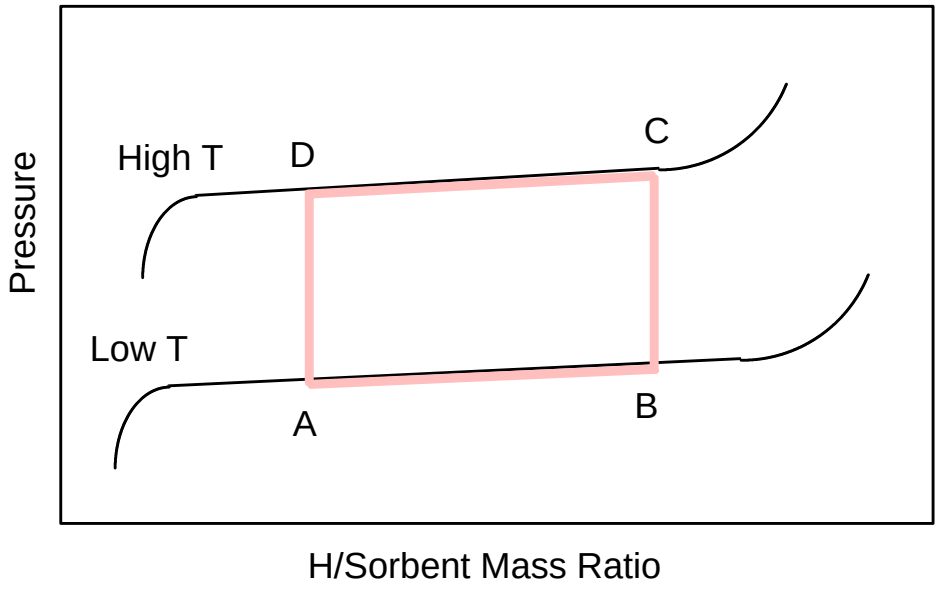

Figure 1-3 Idealized Compression Cycle.

along an isotherm. Absorption of hydrogen at constant low temperature is represented by the line A → B. Heating from low T to high T in a confined space is represented by B → C. Continuously removing hydrogen from the sorbent at constant temperature is represented by C → D. Cooling depleted sorbent from high to low temperature in a confined space is represented by D → A.

As a sorption compressor element (i.e. sorbent bed) is taken through these four steps in a cycle, it will intake low pressure hydrogen and output high-pressure hydrogen on an intermittent basis. If the high-pressure hydrogen is pre-cooled with radiators to below the inversion temperature and then expanded through a Joule-Thomson (J-T) expansion orifice the high-pressure gas will partly liquefy, producing liquid refrigerant at low pressure for sensor systems. Heat from the sensors will evaporate liquid hydrogen, and the low-pressure gaseous hydrogen is recirculated back to the sorbent for compression. This system can be depicted schematically as shown in Figure 1-4. Such a system will periodically produce liquid refrigerant in a cycle involving the four steps shown in Figure 1-3.

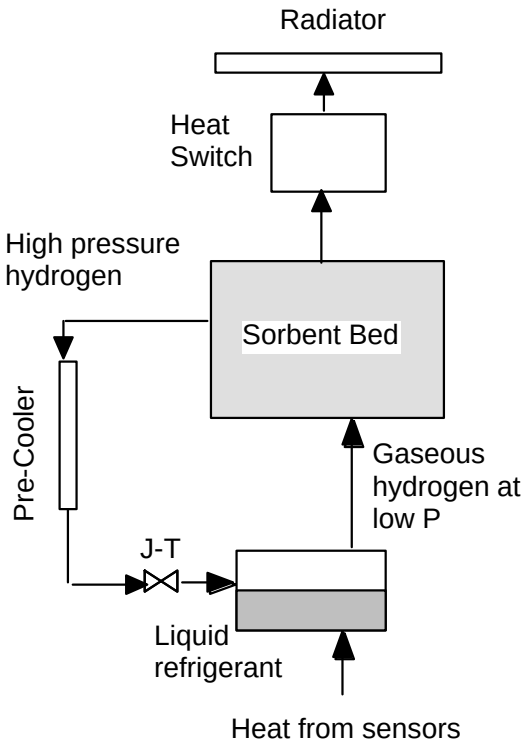

Figure 1-4 Schematic of a single compressor cooler.

In order to produce a continuous stream of liquid refrigerant, we employ several such sorption beds and stagger their phases so that at any given time, one is desorbing while the others are either heating, cooling, or re-absorbing low pressure gas. In such a system, there is a basic clock time period over which each step of the process is conducted. Since the absorption kinetics are relatively slow, the absorption step can be given two or more cycles in order to go to a sufficient state of completeness.

Table 1-1 illustrates such a process for a system of five sorbent beds, as shown in Figure 1-5.

Time Cycle → Sorbent bed↓	1^	2^	3^	4^	5^
1	Heat	Desorb	Cool	Absorb	Absorb
2	Desorb	Cool	Absorb	Absorb	Heat
3	Cool	Absorb	Absorb	Heat	Desorb
4	Absorb	Absorb	Heat	Desorb	Cool
5	Absorb	Heat	Desorb	Cool	Absorb

Table 1-1 Cycles for five sorbent bed system.

In any given clock time cycle, one sorbent bed is desorbing high pressure gas. If it were possible to produce a uniform flow of high pressure gas within a single time cycle, then except for minor discontinuities when switching from compressor to compressor, the production rate of high pressure hydrogen would be constant in time. In actuality, the desorption rate cannot be maintained exactly constant during a single clock time cycle, so a high pressure ballast tank is included in the high pressure manifold to mitigate pressure fluctuations. The flow rate of hydrogen through the J-T orifice is controlled by the size of the orifice and the pressure difference across it.

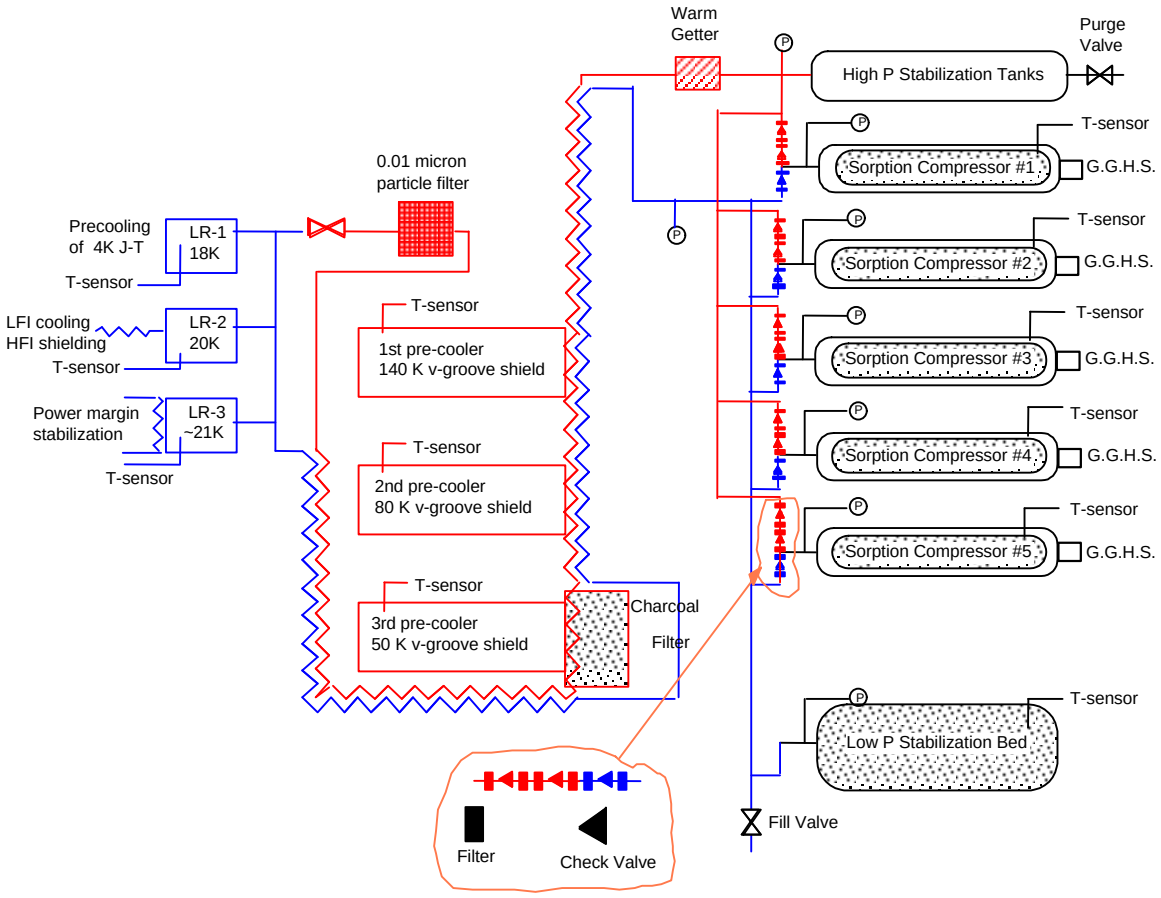

Figure 1-5 Overall Cooler schematic. The high-pressure manifold is shown in red, while the low-pressure manifold is in blue. All of the compressors and the stabilization bed are in good thermal contact with the radiator. A gas gap heat switch (G.G.H.S.) is mounted On each sorption compressor element.

The high pressure ballast tank assures that pressure fluctuations are very small, and therefore flow through the J-T is essentially constant. Similarly, a buffer sorbent bed

(equal to a 200 liter volume) at low temperature is included in the low pressure manifold to minimize low pressure fluctuations. Because of the slope of the A-B line in Figure 1-3, if the pressure in the low pressure manifold drops, this buffer bed will release hydrogen, and if the pressure rises, it will absorb hydrogen.

Figure 1-4 does not show how the gas flows are regulated. Automatic regulation is provided by the use of check valves that are actuated by a small pressure differential. The check valves ensure that when a sorbent bed being cooled reaches a pressure about 7-28 kPa less than that of the low pressure manifold, low pressure gas will flow into the sorbent bed. Similarly, a sorbent bed in the heating mode will drive high pressure gas into the high pressure manifold when its pressure exceeds that of the manifold by ~ 14-54 kPa since two check valves are used in series on the high pressure manifold.

The high-pressure manifold consists of high-pressure lines and stabilization tanks, a getter bed for hydrogen fluid purification and a pressure transducer. A getter, a charcoal filter and a particle filter are located in the high-pressure line to remove contaminants and prevent plugging of the contaminant residual components of the system.

Each single compressor element is comprised of two concentric cylinders closed with end caps as shown in Figure 1-6. The inner of these tubes contains the hydride material (i.e., the sorbent bed) and the outer forms a vacuum jacket around the inner cylinder. This vacuum jacket is used as a gas-gap heat switch by alternately evacuating the jacket region and filling it with gas.

Each compressor sorbent bed is 45 cm long and has an outer diameter of 3.8 cm. The hydrogen gas for the gas-gap heat switch is supplied through a tube protruding from the side of the outer cylinder. A vent tube passes through the center of the hydride material to allow gas to flow out to the compressor inner element [*a* in Figure 1-7]. This vent tube is fabricated from sintered 316 stainless steel, and has a sub-micron porosity,

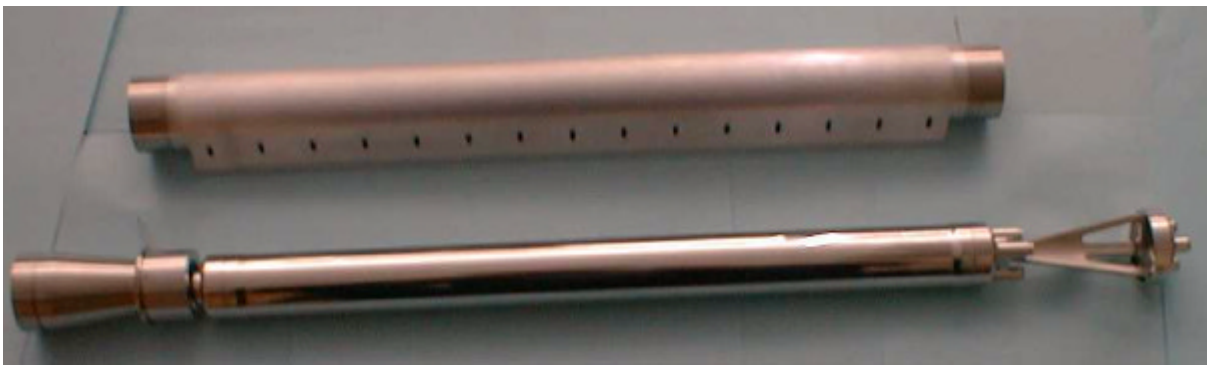

Figure 1-6 Inner and Outer Cylinders.

which prevents the powdered hydride from entering the gas flow lines. A heater tube passes through the hydride material providing a large contact area between the heater and the hydride media, leading to good temperature uniformity [*b* in Figure 1-7].

Additional heat conduction to the hydride is provided by aluminum foam that fills the inner cylinder and makes a tight contact with the heater. The foam is 89% empty, and is cut to allow penetration by the various other components located in the inner cylinder. The heater, sheathed thermocouple, and vent-tube leads run from the end cap of the inner cylinder to that of the outer cylinder [*c* in Figure 1-7]. Each tube has a small bend for stress relief, isolating them from the launch load path. Therefore, the only components that take significant load are those designed to be structural load carrying supports. There are two of these structural end supports; one at either end of the tube assembly. At one end, provision is made for thermal compliance without strain between the inner and outer tubes. The outer tube assembly is fabricated primarily of 6061-T6 aluminum. This is for ease of conduction between the outer tube and the thermal sink to which the outer tube is attached. This outer tube also provides the primary structural attachment point for the single compressor bed. Electrical and plumbing attachments are handled from the three

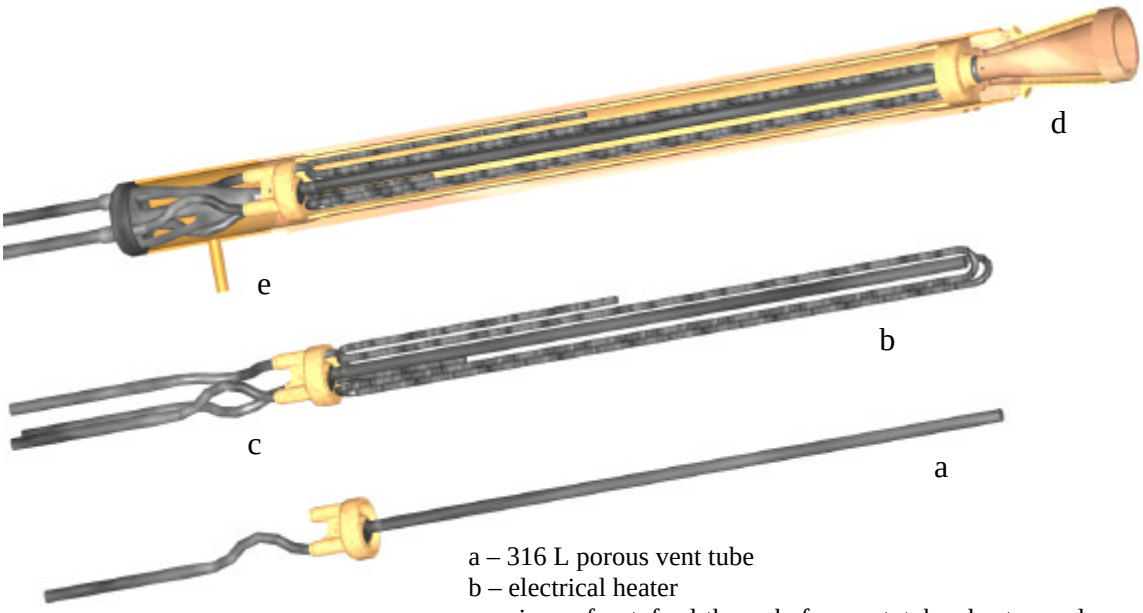

a – 316 L porous vent tube
b – electrical heater
c – inner front feed-through for vent tube, heater and thermocouple
d – section of the compressor unit assembly, with the front and end support coaxially holding the inner element
e – port for the gas gap actuator

Figure 1-7 Compressor unit view of the internal parts of a hydride compressor element

tubes at one end of the device and from the lateral gas gap actuator port [*e* in Figure 1-7]. Nearly all of the parts of the compressors and the gas-handling system which come in contact with hydrogen are made of 316L Vacuum Arc Remelt (VAR) Stainless Steel (SS) which has been electro-polished on the surfaces exposed to hydrogen. The choice of VAR 316 L - SS minimizes the outgassing of surface adsorbed gases, thereby reducing the degradation of the compressor elements hydride by reaction with hydrogen [see section 1.4]. There are two assembly compressor exposed to the hydrogen refrigerant components made of other materials: the aluminum foam, which provides heat conduction to the hydride in the compressor, and the viton seals of the check valves.

A thorough description of current configuration for the Planck 20 K sorption cryocooler is given in Appendix A. This is a preprint of a paper [7] published in the Proceeding of the 1999 Cryogenic Engineering Conference, Advances in Cryogenic Engineering, vol. 45 (in press).

1.3 Role of gas gap heat switch in Planck cooler

The inner and outer cylinders of the compressor are separated by a narrow gap and a means must be provided to alternate between the heating and cooling cycles of the compressor elements over many thousand of cycles. Thermal conduction in the space between two surfaces primarily depends on the gas species and on the gas density, which in turn can be controlled by varying the pressure as illustrated in Figure 1-1. In the heating cycles, heaters imbedded in the compressor elements are turned on. To prevent excessive heat loss and high power requirements, the compressor elements must be thermally isolated during this process by evacuating the gap down to a pressure P_{OFF}. In the cooling cycles the heaters must turn off and the compressor elements must be thermally connected to a radiator by filling the gap with gas up to a pressure P_{ON}. Thus, it is possible to alternately isolate and thermally connect the compressor elements to the radiator during each successive cycle. Objective of this research is to develop and test an initial conceptual design for the gas gap switches to be used in the Planck sorption cooler. The requirements have been developed and seven heat switch actuator have been characterized before a during a long term cycling test (life test).

The inner and outer surface definition and, in general, the overall design of the compressor unit and its environmental conditions drive the heat conductance requirements for the ON and OFF state. A specific ON state requirement [see section 2]

assures that the ON heat conductance in the gap is large enough to be characterized by the viscous regime. The area of the two surfaces, the distance between them and the heat conductivity of the gas separating them thus define the ON heat conductance. The heat conductance must be large enough to remove the heat of absorption in the appropriate cycle time. Hydrogen is the gas with the highest heat conductivity [Table 1-2] and it can be reversibly pumped by hydrides [see section 1.4]. Hence hydrogen and hydrides are a suitable solution for the design and the realization of PLANCK gas gap heat switches.

Gas Species	*Heat Conductivity* W / m K
H_2	$183 \cdot 10^{-3}$
He	$152 \cdot 10^{-3}$
N_2	$26 \cdot 10^{-3}$
CO_2	$16 \cdot 10^{-3}$
CO	$25 \cdot 10^{-3}$
Air	$26 \cdot 10^{-3}$

Table 1-2 Heat conductivity for some gas species at 300 K [8]

A small amount of a low-pressure hydride sorbent is used which can be heated or cooled to increase or decrease the hydrogen pressure in the gap [see Figure 1-8]. This sorbent is so small in quantity that its small heat losses are acceptable; so the actuator is not insulated in the heating mode. The baseline approach for providing gas for the heat switch is a closed-cycle hydrogen/metal-hydride (hydride pumped) sorption pumping system. The hydride-pumped gas-gap uses a small amount of metal hydride, which will not be the same composition as in the compressor bed, to absorb and desorb hydrogen gas

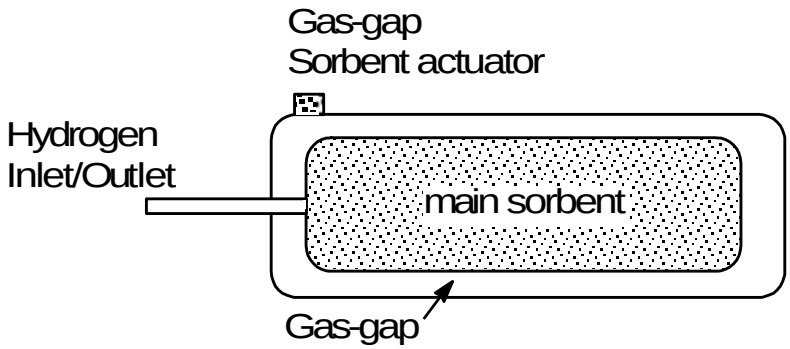

Figure 1-8 Simple Schematic of Compressor with Gas-Gap.

into the gas-gap. The general description of the hydrogen-metal system will be given in [section 1.4] followed by the description of general approach considered in the material candidates selection [section 3].

An alternative system could be a system with a supply of compressed gas to fill the gas-gap when needed, using an active valve with a second active valve used to vent the gas to space to evacuate the gap. The use of valves would results in an increased system mass, due to the need for a compressed gas container, and may increase the risk of losing the use of one or more compressor beds due to the possibility of leaks in the seats of the active valves. The active valve solution was used during the BETSCE experiment which flew on the Space Shuttle STS-77 in 1996 [9, 10].

1.4 Reversible hydrogen storage materials

Since the discovery of the ability of some metals (i.e. palladium) to interact with hydrogen in 1866 by Thomas Graham, many fundamental and practical studies have followed resulting in a vast catalogue of elemental metals, solid solution alloys, amorphous metal alloys and intermetallic compounds that can react with hydrogen in a exothermic reaction. However, it was not until the late 60's that hydrogen storage intermetallic hydrides were systematically studied [11] mainly to identify alloys or compounds suitable for hydrogen fuel storage, chemical heat pumps or hydrogen compressors. Specific metal systems have been used to recover hydrogen and hydrogen isotopes at pressures below 100 Pa [12, 13, 14, 15, 16] or as getter materials [17, 18], which are clean-up reagents for residual gases in vacuum systems[19].

Atomic hydrogen can be chemisorbed onto a metal following the dissociation of hydrogen gas molecules at the surface or by the cathodic dissociation of water molecules at the surface to form chemically adsorbed hydrogen. The adsorbed hydrogen then diffuses through the host material's lattice leaving adsorption sites free for other hydrogen gas molecules to dissociate. Depending on the hydrogen concentration, the temperature and the hydrogen-gas pressure, atomic hydrogen may partially or fully occupy different sets of interstitial sites as schematically represented in Figure 1-9 [20].

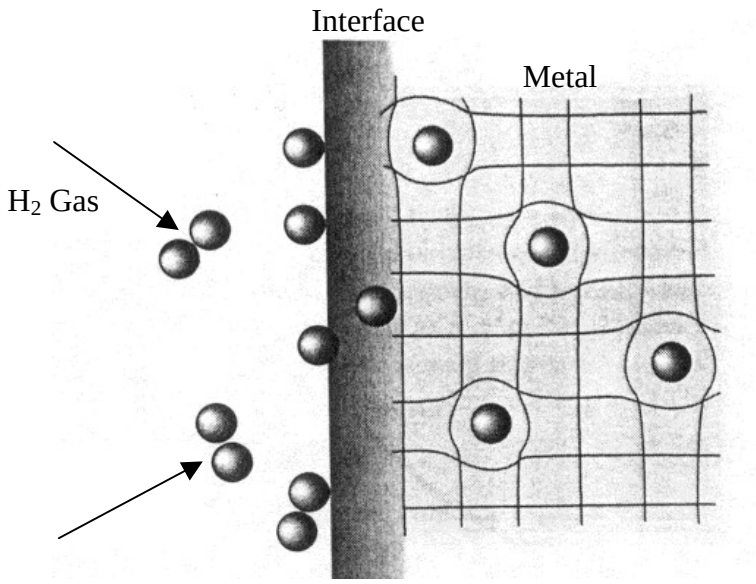

Figure 1-9 Schematic representation of the absorption of hydrogen gas into a metal system

Three physical properties of the interaction between hydrogen and metal systems determine a material's capacity to reversibly store hydrogen: the thermodynamic stability of the hydride, the sorption kinetics and the hydrogen storage capacity of the hydrogen-metal system. The term hydride is used to broadly refer to all the phases of hydrogen-metal system other than interstitial solid solution, which include new crystal structures formed by a change in the original host metal symmetry as well as those unchanged host-metal structures where hydrogen occupy a significant fraction of interstitial sites in either ordered or disordered manner. The absorbed hydrogen capacity is strictly related to the crystal and electronic structures of the metal system and in particular to the distribution and the geometric dimensions of the interstitial sites [21, 22, 23].

The hydrogen-metal system interactions are energetically described by the thermodynamics that is usually derived from the pressure-composition-temperature curves (PCT) as shown in Figure 1-10. Calorimetric investigations have been carried out on Zr [24], Ti [25] and some of their alloys, and the results are consistent with the data derived from the van't Hoff plots.

Following an absorption isotherm shown in Figure 1-10, hydrogen begins to dissolve into the host metal lattice as the pressure of the gaseous phase increases forming a solid solution of hydrogen in the metal (α phase). As interactions among the hydrogen

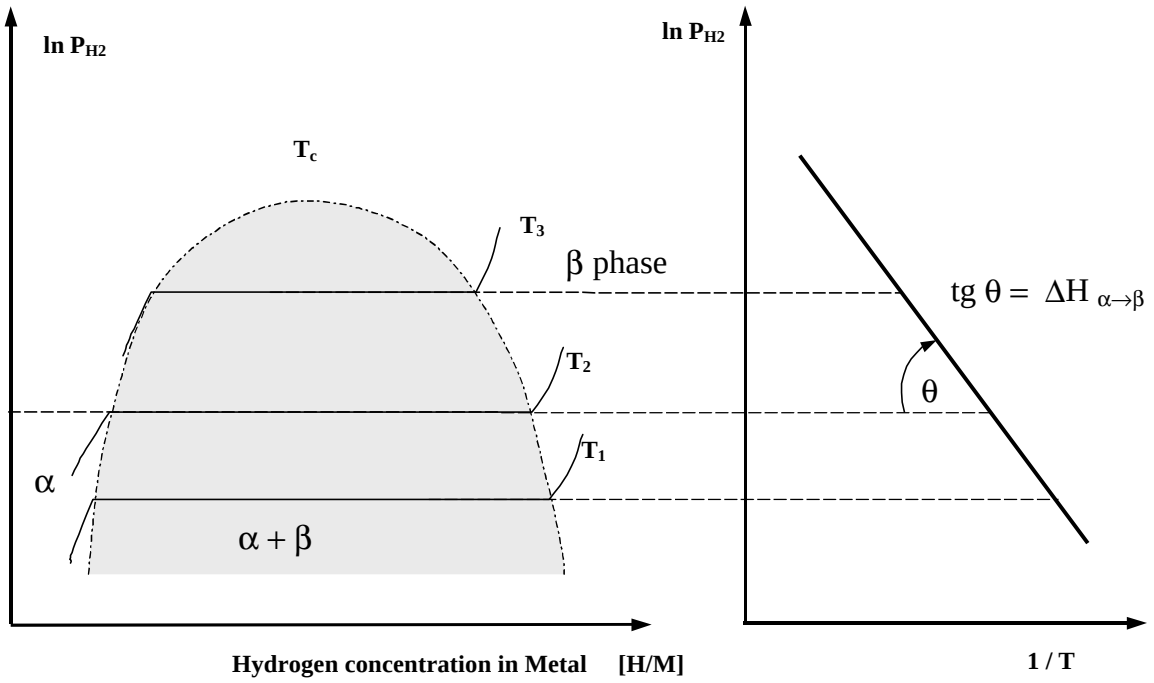

Figure 1-10 Idealized representation of Pressure-Concentration-Temperature (PCT) for solid solution a and hydride phase b. The enthalpy of the hydride formation is the slope of the line in the log(P)-1/T *plot.*

atoms inside the host metal become important, the hydrogen-metal system minimizes the free energy by forming β phase. Hydrogen starts to occupy particular combinations of interstitial sites to nucleate and form the hydride β phase. According to the Gibbs phase rules during the transition, where the two phases co-exist at a fixed temperature, the pressure will remain constant. The density of hydrogen-occupied interstitial sites determines the width of the plateau region between hydride-solid solution phase. When all the solid solution phase has been converted to the hydride phase the pressure increases much more rapidly as more hydrogen is absorbed. This is why the isotherms turn upward at high H/M in Figure 1-10.

Most metals and intermetallic compounds can react with hydrogen to form different hydride phases according to the different occupancies of the host lattice interstitial sites. However some materials form only a solid solution α phase and the β hydride phase – for example uranium and its hydride phase $UH_{3.0}$.

The relationship between equilibrium pressure *P* and Temperature *T* in a plateau region between α-β phase is described by the van't Hoff expression

$$\ln P = -\frac{\Delta H_{a\to b}}{RT} + \frac{\Delta S_{a\to b}}{R} \qquad \textit{Equation 1-1}$$

where *R* is the universal gas constant, $DH_{a\to b}$ and $DS_{a\to b}$ are respectively the enthalpy and the entropy of the β phase hydride formation.

When hydrogen is in solid solution at low concentrations with either the host crystalline metal or the hydride, the pressure *P* versus concentration *x* follows Sievert's law [Equation 1-2].

$$x = \Psi(T)\sqrt{\frac{P}{P_0}} \qquad \textit{Equation 1-2}$$

where Ψ(T) is a coefficient depending on the temperature, the number of interstitial sites in the host lattice, the hydrogen concentration in the phase, etc. A comprehensive description of hydride behavior can be found in [26], which includes thermodynamics and statistical mechanics of the interaction between hydrogen and various metals. Hydrides of amorphous alloys usually behave differently than the crystalline metals or intermetallic compounds. They may absorb substantial quantities of hydrogen but there is no hydride phase transition due to the fact that amorphous alloys do not have a uniform distribution of equivalent interstitial sites.

Two phenomena beyond the ideal behavior shown in Figure 1-10 appear in the behavior of most of the hydrogen metal systems: 1) the sloping plateau and 2) the difference between the hydriding-dehydriding pressure plateaus, referred to as hysteresis. The equilibrium pressure across the plateau region at a certain temperature should be independent of the hydrogen concentration (Gibbs phase rule), or in other words the plateau line of an isotherm should be flat. However many hydrides, if not most of them, have sloping plateaus, although one must be sure that equilibrium pressure is established. Current explanations for sloping plateau involve chemical or structural lattice disorder. The same observation on non-equilibrium measurements can be repeated for the difference in the absorption and desorption pressure-concentration-temperature curves. However, hysteresis has been commonly observed for many hydrogen-metal systems to the extent that the ratio between the adsorption and desorption pressure can be as high as 35, as niobium hydride [27].

Besides the thermodynamic stability of the hydride and the hydrogen storage capacity of the hydrogen-metal system, the sorption kinetic rates for the hydriding and dehydriding reactions often determines whether the metal system is a practical hydrogen pump for the gas gap actuator in an appropriate time cycle. The process rates can be determined by the heat removal/supply during the reaction [28, 29] or by the reaction intrinsic kinetics. It has been observed that temperature plays a central role in the thermodynamics of the hydrogenation reaction and, considering the large heats of formation, the low effective thermal conductivity of metal hydride powders [30, 31, 32], and the restricted flow of hydrogen through the fine hydride powder, kinetic measurements are very difficult and major discrepancies among the experimental results have been observed in the literature [33].

The intrinsic kinetic process for the hydrogenation in the α - β phase transition can be regarded as the combination of the following interacting processes [see Figure 1-11]:

1) hydrogen gas adsorption on the surface
2) hydrogen dissociation on the metal/oxide surface,
3) atomic hydrogen migration through the surface layer
4) atomic hydrogen diffusion into the β phase,
5) nucleation and growth of the hydride phase in the bulk
6) hydride decomposition and diffusion of hydrogen in α phase.

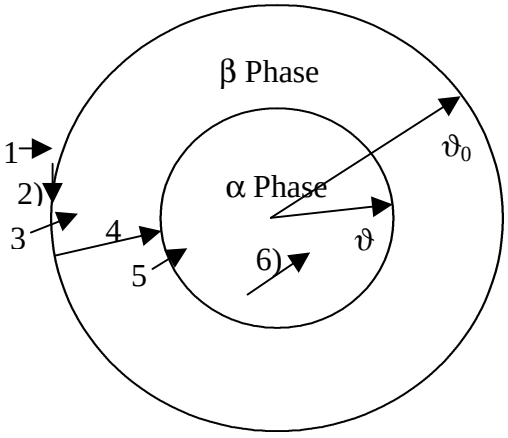

Figure 1-11 Hydrogen absorption kinetic processes [33]

The surface is the solid-gaseous interface through which hydrogen has to travel to reach the bulk in the absorption and desorption processes. The surface crystal structure and its composition are related to the material manufacturing process, its exposure to air (or any other contaminants) during shelf life, and its handling procedures. Usually, all hydrogen metal systems react with oxygen forming a stable oxide layer that, by passivating the surface, impede the dissociation and the hydrogen migration through it [33]. Oxygen is not the only poisoning element for the hydrogen metal system reaction. Carbon monoxide, carbon dioxide, sulfuric acid, water and even nitrogen can inhibit surface active sites by forming stable compounds with a low hydrogen diffusivity thus impeding hydrogen to reach the metal bulk.

For this reason, the first step in a hydrogen-metal system reaction is usually the material activation process, that is a specific sequence of operations to obtain suitable surface conditions for the adsorption/dissociation/migration processes. Normally, it is required to heat up the material under high vacuum to remove the oxygen and other poisoning contaminant concentrations on the surface by either evaporation or diffusion into the bulk lattice. Fromm [33] has proposed that metal oxides are not stable above 800 K and pressure below 10^{-9} bar due to the high bulk diffusion of oxygen and that “the effects of annealing treatments on the kinetics of hydrogen storage materials can be understood as a result of the competition between oxide layer growth and is dissolution in the metal phase”. The surface elements concentration has been studied on some metal hydrogen systems and it has been verified that at high temperatures under vacuum the poisoning elements percentage on the surface decrease [34].

The absorption of hydrogen in the metals causes the host lattice to expand as much as 35% (i.e. uranium hydride), modifying the initial structure, stressing the lattice, and thus often causing a fine powder disintegration of the host metallic bulk. The fine powder cracking enhances the overall kinetic process by offering oxygen (poison)-free surfaces to hydrogen gas, promoting both adsorption and dissociation. This phenomenon was observed during the hydrogenation of the first uranium actuator sample.

Providing that oxygen or other contaminants present in the system do not contaminate the new surfaces of the activated particles, and that the metal system structure is stable, the metal system kinetics shouldn’t vary by cycling after the first hydrogen reaction. Some metal hydride phases are in fact metastable and, depending on the metal atom diffusivity in the structure, more stable structures can precipitate, thus

modifying the initial hydrogen capacity and reaction kinetics. The precipitation of more stable hydrides is called disproportionation [35]. A further discussion of how these studies relate to bakeouts and activation processes in our work is given in section 4.

1.5 Review of past work on gas gap heat switches

Gas gap heat switches can be considered a form of evacuated thermal insulation that can be made conductive by introducing gas in it. Vacuum insulation is a commonly used technology: lamp bulbs and cryogen transportation systems are some of the examples. The technology history of gas gap heat switches dates to early this century when it was originally developed by low temperature experimentalists [36]. Carbon/helium switches are still commonly used on academic research on low temperature physics. Several investigations have been carried out for many sorts of possible applications: (1) dissipating-insulating jackets for high temperature batteries [37], (2) heat retention device for catalytic converters [38, 39], (3) space cryocooler applications [40] and (4) sorption cooler thermal optimization [41]. Most of the studies dealt with the combination of hydrogen and hydride although, for cryogenic applications below 4 K, helium-charcoal switches are commonly used [42].

These investigations have not been followed by comparable product developments. Today the only device commercially available is the INTELLIGETTER by SAES that uses a Zr-V-Fe alloy [St 707] as a sorbent material for hydrogen. This device has been designed to fill a 4.5 l volume to a pressure of 0.8 kPa in the ON state and to reach an ultimate OFF pressure below 10^{-3} Pa. The INTELLIGETTER product specification [43] reports that 25 W are required to turn it ON in 4 minutes and that it takes around 14 minutes to turn it OFF. The limited data are introductory to the challenges that a gas gap heat switch design and development have to face. The switch power, the switching time, the maximum or the minimum heat conductance, the lifetime, or any combination of these quantities can be the governing requirements, depending on the application. For example D. Johnson [40] for his cryogenic space application switch had to minimize the power (300 mW) and to maximize the ON – OFF heat conduction ratio.

It is worth discussing briefly how the previous work dealt with the mentioned parameters:

Heat conductances in the OFF and in the ON state. The heat conductances of the switch are strongly affected by the design of the surfaces exchanging heat and by the gap dimension. Considering the ON state in the viscous regime, the ON conductance is determined by the nature and temperature of the gas and by the geometric dimensions of the switch. The OFF state instead is mostly defined by the conductive and radiative losses between the two surfaces. Various ON-OFF conduction ratios were reached, varying from 55 [38] to 660 [40]. It is interesting to note that with large heat power to conduct in the ON state, as in the catalytic converter application (4 kW) [38], the ON-OFF ratio is lower than in low power application as the space heat switch (8 W) [40].

Switching time. J. Burger [41] is the only investigator who has previously performed an analysis on the required switching time for a sorption cooler. He describes a general process to define the requirements for a sorption cooler gas gap heat switch. He arrives at the conclusion that "with a few more than four sorption cells and a slightly higher input power a sorption compressor can readily be operated without a heat switch at all". However, in his analysis he leaves undefined the question as to whether the sorption cells function by absorption or by adsorption. In fact, he does not impose the requirement that a sorption cell is kept at the absorption temperature during each phase of the sorption process, which is required for the PLANCK cooler [see Table 1-1]. It seems, but it is not explicitly stated, that his calculations are only relevant to an adsorption compressor rather than an absorption one, because the latter continuously desorbs as it is heated and does not need to be held at either high and or low temperature for long times. His conclusions, therefore cannot directly be applied to the PLANCK sorption cooler and consequently to the relative gas gap heat switch. A comprehensive switching time analysis for an absorption compressor unit hasn't yet been done. The switching time requirements are discussed in section 2.3.

Power of the Switch. The power required to run the switch is primarily related to the amount of gas needed to fill the gap, the material used, and the time constant of the switch [40].

Lifetime. Past investigations [38] performed for over hundreds of cycles reported the degradation of the vacuum in the OFF state after few cycles. The performance

degradation was attributed to the jacket assembling procedures resulting in outgassing of the surfaces. In fact, all the gases absorbed on the jacket walls at low pressure and in contact with hydrogen can be desorbed, increasing the gas pressure in the switch OFF state and contaminating the active sites of the sorbent material. The reduction of every contaminant present in the switch is therefore of critical importance, also constituting a major cost driving force for an industrial production of the heat switch. The contamination reduction approach taken in this research effort will be described in section 4.

2. Requirements

The requirements for gas gap thermal switches in sorption cryocoolers are dictated by the operational and environmental conditions of the compressor unit [4]. The radiator temperature, the cycling time, the off and on temperature of the hydride material used in the compressor unit, and other secondary factors such as the pressure drop across the check valves, define the requirements of the gas gap. For example, the fact that the temperature of the cold end of Planck sorption cooler will be 18 K imposes the hydrogen low pressure of 60 kPa. Subsequently, considering the hydride material in the compressor and the pressure drops in the low pressure manifold, a maximum absorption temperature of 290 K is required [4, 44]. Assuming the constant temperature of the radiator is 280 K, the switch must be able to keep the sorbent alloy in the compressor unit below 290 K during the absorption phase.

The critical parameters that determine the viability of the heat switch are:

- "ON" conductance
- "OFF" conductance
- Time lag in rise of "ON" conductance after power switch actuator heater is turned on
- Time lag in decay of "OFF" conductance after heater power is turned off
- Power required in "ON" condition
- Lifetime (number of cycles without significant change in performance)

The objective of the requirement definition process is to estimate the required ranges of these parameters for the gas gap from operational and environmental conditions of the compressor unit in an 18 K sorption cryocooler for the Planck spacecraft.

2.1 ON-OFF Heat Conductances

The gap heat conductances in the OFF and ON states are the main operational switch requirements, since they determine both the power needed to run the cooler and the cold end temperature. The gas gap OFF conductance, G_{OFF}, determines the heat losses

from the inner element to the radiator when the inner element is heated and when heat is applied during the desorption phase, with a maximum ΔT across the gap of 200 K. The maximum allowed conductance in the heating cycle which appropriately limits power requirements for the compressors, is approximately G_{OFF} = ~ 0.03 W/K, depending on the time lags.

The required ON conductance, G_{ON}, is determined by the maximum allowable absorption temperature and the fact that 40 W are generated by hydrogen absorption at the design flow rate. The temperature of the compressor hydride during absorption defines the absorption pressure, which in turn is related to the cold end temperature. G_{ON} during absorption must be > ~ 4 W/K in order to achieve the maximum absorption temperature of 292 K.

The time scales in Figure 2-1 are derived from the nominal cooler sequence [4] for two consecutive 800 second heating steps followed by 3 consecutive 800 second cooling steps, resulting in a 66.6 minute cycle for the heat switch. To simplify the initial analysis, the switching starting time for both the ON-OFF and the OFF-ON operations is phased with the compressor unit operation. The gas gap heat conductance profile for ideal and real switching are reported. An ideal heat switch (continuous line) would require no time to switch states and would immediately reach either the ON or the OFF status. In reality it takes a finite time, defined as $t_{ON \rightarrow OFF}$ and $t_{OFF \rightarrow ON}$, for the gas gap conductance to change between G_{OFF} and G_{ON}, as shown by the real switch line (dotted line). The switching behavior depends on the details of the switch design.

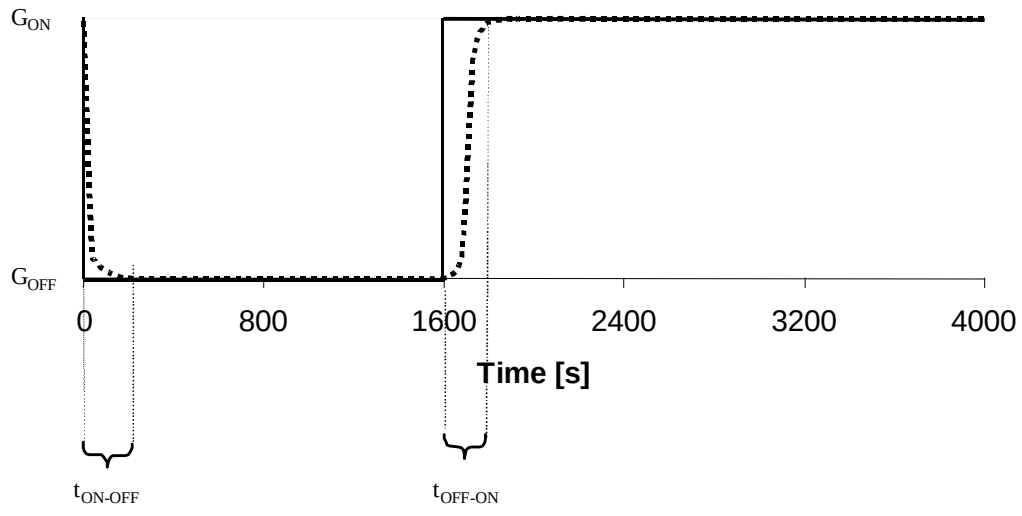

Figure 2-1 Time variation of the gas gap conductance in a compressor allowing for time lags in heating and cooling

The hydrogen pressure in the gap is mainly determined by the gas gap heat conductance. In section 2.2 a theoretical overview of the physical phenomena is given, along with a description on how the compressor unit gas gap conductance was measured.

2.2 Pressure – Gap Heat conductance

The heat transfer in a gas at rest between surfaces at different temperatures has been a subject of interest for scientists since the development of the kinetic theory of gases [45]. The laws governing the basic phenomena in gases were discovered long ago, but it was not until the second part of the last century that Clausius, Maxwell, Boltzmann and others developed an adequate theoretical interpretation. The basic assumptions of the theory are that the gas molecules are negligibly small and that they move freely between relatively rare collisions. The laws of conservative mechanical systems describe the collisions between two molecules that are assumed to behave as small inert elastic bodies. It must be observed that even the description of such a simple phenomenon as the heat transfer between two flat surfaces, actually leads to very complex mathematical expressions. In fact, gas conductivity theory, as well as viscosity theory, was developed as a sequence of approximations that fit the measured behavior of the gases. The kinetic theory was initially developed for a gas at rest in equilibrium. Boltzmann derived the velocity distribution $f(\mathbf{v})$ for a gas in that condition. Subsequently the Boltzmann's theory was used to explain many other phenomena.

The kinetic theory approach has its major limitations in the definition of the boundary conditions. The need for knowledge of the velocity distribution on the surfaces $f_0(\mathbf{v})$ and $f_L(\mathbf{v})$ implies a detailed description of the gas molecules-surface interaction [46, 47]. It can be observed that the unsatisfactory description of the low-pressure gas heat conductivity at the beginning of this century led some scientists towards the development of the surface science. The pressure boundary condition is also unclear. The definition of pressure acting across a surface as "the net rate at which momentum normal to it is being transmitted across it per unit area" implies that pressure is a tensor under general conditions and can be considered a scalar under specific conditions, as a gas at rest. If the two plate temperatures are not very different, the hypothesis of an average temperature and the ideal gas law can be used to determine the pressure. When one of the two hypotheses does not hold true, the pressure boundary condition is very difficult to

quantify. It also is important to note that pressure cannot always be measured in the gap. However measuring pressure outside the gap adds another variable to the system.

These two difficulties have directed scientists to look for some semi-empirical solutions. Most of the work was done at the end of last century and at the beginning of the XX century. Von Smoluchowsky, Knudsen and Langmuir developed three semi-empirical models; the first one deals with the transition between the molecular and viscous regimes, the second one only with the molecular regime; and the last one with conduction and convection in a low pressure gas. The Von Smoluchowsky and Knudsen models are briefly described in the next paragraphs. Since the early studies, no major improvements have been made.

Further development of the topic followed when the quantum mechanics was introduced, especially in the definition of the scattering of gas molecules by a solid wall. In [48] Loeb stated “It is thus seen that in the study of specular reflection the latter must be regarded as a problem of reflection and diffraction of matter waves from surfaces rather than from the particulate point of view” as it was demonstrated by some experiments by Knauer and Stern and by Estermann and Stern. A quantum mechanical description of the phenomenon will not be given here considering the difficulties involved, as well as the fact that the heat transfer characterization here is not intended as a comprehensive study of general gas solid interactions, but rather as a definition of the requirements for the gas gap actuator. Instead, a description of the experimental measurement of the gas gap heat transfer for the sorption compressor element will be given and the results will be presented.

2.2.1 Temperature Discontinuity (Von Smoluchowsky)

After the early development of gas kinetic theory, Poisson suggested that, in analogy with the viscous slip, there might be a temperature discontinuity in an unequally heated gas in the vicinity of a boundary wall. Von Smoluchowski performed some experiments and he found what Poisson had expected; he noted that the jump distance g is inversely proportional to the pressure and therefore is directly proportional to the mean free path. In developing the theory, he introduced a constant to define the energy interaction during the collision between a gas molecule and the wall. The expression for the heat transfer rate per unit area is

$$H = \frac{l_m}{d + g}\left(T_{hot} - T_{cold}\right)$$ *Equation 2-1*

where l_m is the average thermal conductivity in the gas between T_{hot} and T_{cold} in the plateau region at high pressure, d is the distance between the two plates and g is the layer thickness where the temperature discontinuity occurs. g can be expressed as

$$g = \frac{2 \quad f}{f} \cdot \frac{9g \quad 5}{2\left(\quad +1\right)} L$$ *Equation 2-2*

where γ is ratio of specific heat at constant pressure to that at a constant volume, L is the mean free path and f is a parameter representing the fraction of the "molecules 'absorbed' and re-emitted" by the surface with a temperature characteristic of the surface. It should be noted that it is not clear which temperature should be used in the calculation of the mean free path when there is a significant difference in the two surface temperatures. The experimental fit of the expression proposed is acceptable, but Von Smoluchowsky admitted that the Knudsen model has a "more satisfactory general point for very low pressures than his own"[45].

We can examine the behavior of Equation 2-1 and Equation 2-2 over a wide range of pressure. At very high pressure, the mean free path L becomes small, and therefore g becomes small. In this region

$$H \approx \frac{l_m}{d}\left(T_{hot} - T_{cold}\right)$$ *Equation 2-3*

and the heat transfer rate is inversely proportional to d. At low pressures, the mean free path is large and $2g >> d$. In this molecular region,

$$H \approx \frac{l_m}{2g}\left(T_{hot} - T_{cold}\right)$$ *Equation 2-4*

and since g is inversely proportional to pressure, H is small and directly proportional to pressure.

2.2.2 Knudsen theory

Knudsen addressed the problem of heat conductivity in the molecular regime for Knudsen numbers greater than 1. The Knudsen number can be defined as the ratio of the mean free path of a molecule to the critical dimension, i.e. the difference of the two concentric cylinder radii. He considered the heat transfer between plates as determined by

two Maxwellian streams leaving the surfaces at different temperatures. In order to determine stream wall temperature he introduced the accommodation coefficient α. The accommodation coefficient can be defined "as standing for the fractional extent to which those molecules that fall on the surface are reflected or re-emitted from it, have their mean energy adjusted or 'accommodated' toward what it would be if the returning molecules were issuing as a stream out of a mass of gas at the temperature of the wall". [45].

The expression for the free molecular heat transfer rate per unit area, *H*, that Knudsen derived is

$$H = \frac{a_1 a_2}{a_1 + a_2 - a_1 a_2} \cdot \frac{(g+1)c_v}{\sqrt{2pRT_{cold}}} P_{gas}\left(T_{hot} - T_{cold}\right) \qquad \textit{Equation 2-5}$$

where P_{gas} is the pressure of the surrounding gas, c_v is the specific heat at constant volume, R is the universal gas constant, and a_1 and a_2 are the accommodation coefficients. It is interesting to note that the heat transfer rate is not a function of the distance between the two surfaces, as is the case in von Smoluchowsky's expression at low pressure.

Dushman [49] reported that the von Smoluchowsky and Knudsen expressions are equivalent in the molecular regime assuming a particular expression for the viscosity of the gas (used in the determination of the mean free path) and if we assume that

$$a_{tot} = \frac{a_1 a_2}{a_1 + a_2 - a_1 a_2} = \frac{f}{2 - f} \qquad \textit{Equation 2-6}$$

In the simplification that led Knudsen to the definition of his model, i.e. to consider two Maxwellian streams defining a temperature of the gas in the gap, was based on the critique that he received from Langmuir. After the development of the thin film theory of heat conduction Langmuir [50] stated, "The definition of the accommodation coefficient is open to the objection that the concept of a temperature of the molecules leaving the surface has no clearly defined meaning unless the molecules leave the surface with a Maxwellian distribution of velocities. If thermal equilibrium is not reached, it is almost certain that the distribution is not Maxwellian."

The accommodation coefficient depends upon the specific gas-surface combination, in particular whether the wall surface is clean or covered with other gases adsorbed films [50] and whether the surface is mechanically smooth or rough. Several

investigations were performed to determine accommodation coefficients with both methods (temperature discontinuity and Knudsen) with a poor agreement between the two methods [51] and often even within each method. The measurement disagreement can often be related to the difficulty in reproducing equivalent experimental conditions to the gas-surface interactions. However some investigators [52] did not consider the Knudsen accommodation coefficient a equivalent to the one obtained with the substitution proposed by Dushman on the temperature discontinuity measurement.

Table 2-1 reports some accommodation coefficient measurements for hydrogen gas with a description of the solid surface.

Acc. Coef.	*Surface*	*Ref.*
0.35	Polished Platinum	[49]
0.712	Platinum coated with black	[49]
0.2	Tungsten	[49]
0.2	Tungsten	[50]
0.3	Tungsten	[53]
0.1	Tungsten clean	[54]
0.2	Tungsten with oxygen adsorbed	[54]
0.64	Tungsten with nitrogen adsorbed	[54]

Table 2-1 Accommodation coefficient measurements for hydrogen gas at » 300 K

Some attempts [55] to predict the accommodation coefficient by the molecular size of the gas and of the surface species did not generate clear experimental validation.

2.2.3 Test apparatus and test procedures

The experimental determination of the heat transfer in hydrogen at low pressure was done on a compressor element with an inner element that was designed to enhance gas gap conductivity measurements. The stainless steel inner vessel did not contain aluminum foam and hydride powder, but instead, a solid piece of copper was inserted to enhance the temperature uniformity throughout the entire inner element. The temperature uniformity for the Planck sorption compressor unit filled with the relatively low conductance aluminum foam, hydride and hydrogen gas reaches 12 K during normal desorption phase. The gas gap heat transfer is determined, as described in 2.2.1 and 2.2.2, by the gas in the gap and by the two surfaces. The inner element and the outer shell of the

compressor element used to determine the gap heat transfer were electro-polished and then gold-plated to assure the same surface conditions as a regular compressor element.

The temperature of the copper element, the temperature of the water-cooled outer shell and the power supplied to the heater were used to define the heat transfer between the inner element and the outer shell. An ammeter and a voltmeter on the heater element monitored the power supplied to the inner element. After assembling the test element, a PRT - platinum resistance thermometer - was attached to the outer shell and the element was bolted to a water-cooled aluminum plate. The cooling system was operated at fixed temperature. During the test a substantial temperature difference was observed between the water temperature and the outer shell temperature due to the cooling loop performance.

The inner element was initially equipped with 6 PRTs (4 wires resistance measurement method) mounted on the inner copper element equally partitioning its length. To extend outside the inner element, the copper lead wires had to go through a small diameter support tube imposing a very thin (0.1 mm) wire diameter. Before the thermal characterization of the gap, reported in Table 2-2 and Table 2-3, all of the PRTs were lost due to wire breakage. The test assembly could not be rebuilt and a different temperature sensing system had to be implemented. It was decided to introduce a thermocouple in one of the tube supports, as shown on Figure 2-2, and to verify by an X-ray analysis where the thermocouple was located. It was found that the thermocouple was inserted in a gap between the heater coil and the copper inner element and that the inner bed was parallel but not concentric to the outer shell.

When the inner element was equipped with PRTs it was filled with 1 atm of hydrogen gas to reduce to contact resistance between the element components (copper element, heaters and vessel). Hydrogen gas was initially used as filling media after the thermocouple was inserted and the set of measurements reported in Table 2-2 was obtained.

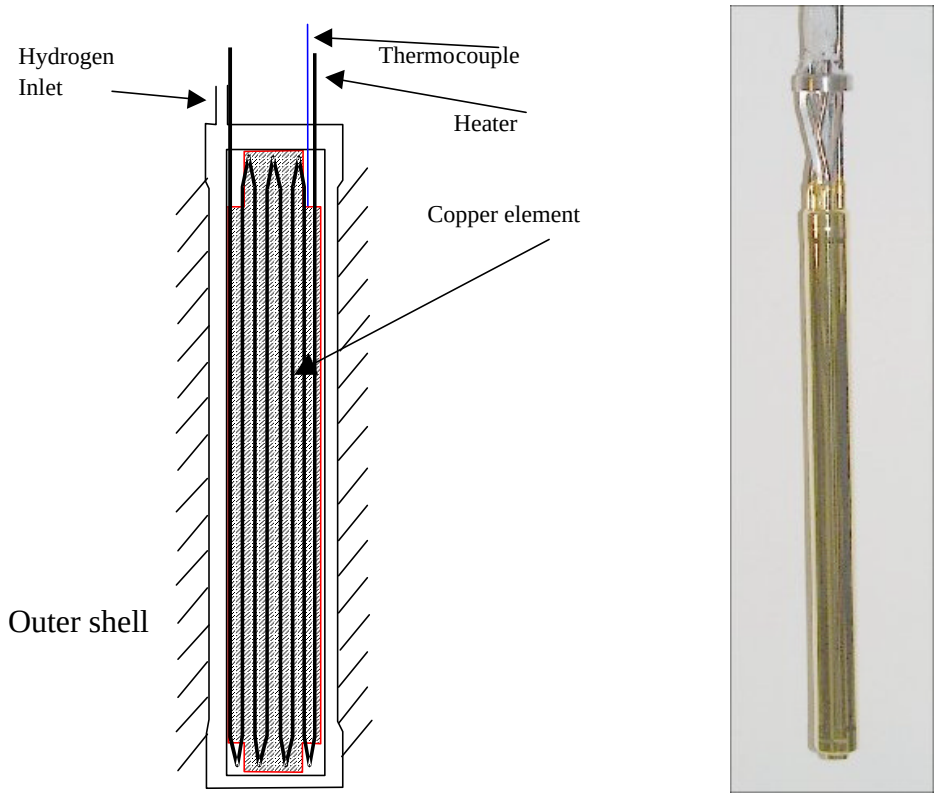

Figure 2-2 Heat transfer test element schematic and the inner element used in the heat transfer measurements.

It was observed that when the gap was flooded with hydrogen it was not possible to obtain the viscous heat transfer measurement; we obtained twice the expected temperature difference between the inner element and the outer shell . The thermocouple was reading a temperature higher than the inner element surface temperature due to substantial thermal gradients inside the element. To reduce the temperature gradient inside the inner element, it was filled with distilled water. Water was selected to allow natural convection inside the vessel; the copper element was in fact gun-drilled and the compressor element was mounted vertically [see copper element drawing in Appendix B]. The specified uncertainty in the heat transfer mechanism inside the element sets the confidence level in the accommodation coefficient measurements. Some gap conductance data obtained with hydrogen as filling media in the inner element are reported in Table 2-3.

The hydrogen was introduced into the gap by the gas gap hydrogen inlet. The inlet was connected to a 2 liter volume to stabilize the pressure in the gas gap, to three

MKS Baratron 622 capacitance manometers (with different dynamic range: 0.13 Pa – 266.6 Pa, 6.66 – 13 kPa and 660 Pa – 13 MPa) and to an hydrogen pumping and filling station, as shown in Figure 4-4.

The turbo-molecular pump of the filling station was used to evacuate the gas gap volume while the inner element was heated at 200 C for two days to let the inner element surface out-gas. The pressure reached in the system after the initial bake out was below 10^{-6} Pa.

2.2.4 Data analysis and pressure requirements

The test apparatus was designed to measure the gas gap heat conductance at various pressures. In order to eliminate the parasitic heat losses in the measurement of the gas gap heat conductance, the vacuum conduction and radiation losses were measured while pumping continuously on the gas gap volume. The pressure in the gap during these measurements was always below $1*10^{-5}$ Pa. The test results are reported in Table 2-2.

T_{Bed} [K]	T_{out} [K]	Power [W]	GAP CONDUCTANCE [W/K]
334.4	288.80	0.98	0.0215
360.3	288.90	1.60	0.0224
396.0	288.83	2.64	0.0246
419.1	288.88	3.30	0.0253
441.4	288.90	4.20	0.0275
474.2	289.00	5.75	0.0310

Table 2-2 Heat losses from the inner element to the outer in vacuum

A curve fit of the losses using a statistical model with two parameters as expressed in Equation 2-7 was performed.

$$Power = G \cdot (T_{Bed} - T_{Out}) + Radiative\_component \cdot (T_{Bed}^4 - T_{Out}^4) \qquad \textit{Equation 2-7}$$

where G is the conductive heat loss component, *Radiative_component* is the radiative heat loss component and T_{Bed} is the temperature of the inner element surface. T_{Bed} was calculated assuming the inner copper element was uniformly heated at the temperature

read by the thermocouple and considering a 346 W/K heat conductance in the stainless steel vessel. The maximum temperature correction was 0.7 C.

The curve fitting leads to the definition of a conductive heat loss component *G* of $9.2 \cdot 10^{-3}$ W/K with a standard deviation σ of $1.4 \cdot 10^{-3}$ W/K and a radiative component of $91 \cdot 10^{-12}$ W/K^4 with a standard deviation σ of $7 \cdot 10^{-12}$ W/K^4. The χ^2 of the curve fitting is 0.0176. The conductive parasitic component is due to the front and to the back stainless steel supports that coaxially hold the inner element and the outer shell.

After the measurements of the parasitic heat losses, the gap was filled up to a set pressure and the power needed to keep the inner element at a temperature T_{bed} was measured. The outer shell temperature was monitored and recorded during the entire test. The experimental results are reported in Table 2-3 where the net power is calculated by subtracting from the measured power the heat losses previously measured in vacuum [see Table 2-2]. To determine the mean free path the hydrogen temperature was assumed to be the average between T_{hot} and T_{cold} and by using the expression for viscosity proposed by Dushman [see section 2.2.2]. To calculate the Knudsen number, the gap distance was taken to be 0.762 mm.

Pressure	T_{bed}	T_{out}	Knudsen number	Net Power	Gap conductance
[Pa]	[C]	[C]		[W]	[W/K]
3.06	173.9	16.52	6.43	13.15	0.08
8.26	170.2	17.61	2.27	39.09	0.26
24.66	166.7	20.47	0.7960	96.10	0.66
27.99	83.8	23.31	0.624	44.28	0.73
71.31	166.9	26.12	0.277	218.99	1.56
77.31	78.6	24.63	0.229	87.43	1.62
154.63	80.1	25.60	0.113	143.29	2.63
283.9	76.8	26.65	0.0613	184.72	3.68
575.9	73.4	28.55	0.0301	222.02	4.95
1,120	66.6	29.32	0.0153	222.37	5.96
2,111	62.6	29.46	0.0081	222.46	6.71
3,668	60.8	29.47	0.0046	222.85	7.11
10,400	59.1	29.37	0.0016	222.88	7.50
30,526	58.5	29.41	0.0005	222.90	7.66
75,181	57.9	29.33	0.0002	222.91	7.80

Table 2-3 Heat losses from the inner element to the outer shell for different hydrogen pressures

It can be observed that the first measurements at low pressure were done with the inner element substantially hotter than in the later measurements. In the beginning, hydrogen gas was used as a filling media in the inner vessel and there was no concern about the inner pressure of the vessel during the tests. When the inner element was filled with water, the inner pressure became a safety concern and it was decided not to exceed the atmospheric water boiling temperature. It is interesting to note that at low pressure there is not much difference between measurements obtained with hydrogen and water as the inner element filler. In fact, the heat conductance at 24.66 Pa (with hydrogen in inner element) and 27.99 Pa (with water in inner element) are very similar.

The accommodation coefficient α was inferred from low pressure measurements using the Knudsen method assuming identical accommodation coefficients for the two gold plated surfaces with $\alpha_1 = \alpha_2 = \alpha$. Considering only the measurements at Knudsen number above 0.5 and using Equation 2-5, an accommodation coefficient α of 0.30 was estimated with a standard deviation of 0.01.

The net power was fitted with Equation 2-8 to infer the value of the f using the weighted least square minimization method.

$$Net\ Power = \left[\frac{l_m Area_{0.762}}{0.762 + 2g} + \frac{l_m Area_{1.524}}{1.524 + 2g} \right] \left(T_{hot} - T_{cold} \right) \qquad \textit{Equation 2-8}$$

Account was taken of the fact that different sections of the inner cylinder had different radii, and therefore different gas-gap distances. In the determination of f the measurements at “low” pressures are more important then the ones at “high” pressure as described in section 2.2.1. In fact, when the pressure is adequate to establish the viscous regime the heat transfer is pressure independent. Different ranges of the Knudsen number distinguish the molecular and viscous regimes. Knudsen numbers above 1 indicates the molecular regime in the gap; as it decreases the viscous regime develops. For Knudsen numbers below 0.01, the viscous regime is fully established. In carrying out the curve fit, points at low pressure were weighted more heavily to make best fit at lower pressures where α is more sensitive to the curve shape. The weights for the data fitting were determined by normalizing the series of Knudsen number reported in Table 2-3.

To determine the heat conductivity l_m the temperature in the gas was considered the average between T_{hot} and T_{cold}. Since the hydrogen viscosity expression proposed by Dushman was used in the calculation of the mean free path, the two parameters α and f

should be identical [see Equation 2-6 with $\alpha_1 = \alpha_2$]. A *f* of 0.30 was estimated with a curve fitting χ^2 of 4.5 10^{-5}.

In Figure 2-3 the heat conductance in the gap is reported against the hydrogen pressure with the curve fitting done with Equation 2-8 and the estimated accommodation coefficient α=0.303.

It has to be noted that the experimental measurement of the heat transfer in the viscous regime suffered an average - 5.4 % error (- 0.44 W/K). It is most probable that the thermocouple, even with water as conductive media in the inner element, was still sensing a higher temperature than the outer shell surface temperature due to the proximity of the heater.

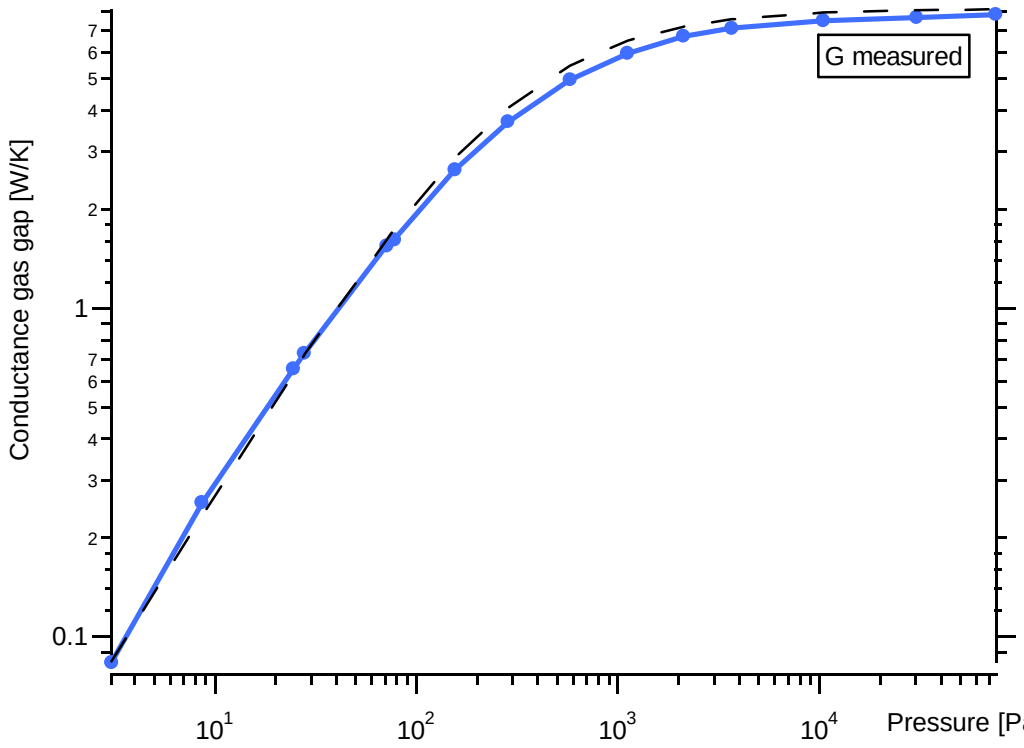

Figure 2-3 Curve-fitting on heat transfer experimental data (line with markers). The dotted line is the curve fitting assuming a f of 0.302.

2.3 Timing and dynamics

The amount of time allowable to reach temperature in switching from "ON" to "OFF" and vice-versa is not immediately evident (see Figure 2-1). Obviously, we desire these times to be as short as possible, with step functions being the ideal, but since the overall cycle time for the heat switch is 66.6 minutes, a few minutes of lag might not be a major problem. In general, it is important that the time lag when the switch is opened for the heating cycle be as short as possible to reduce heat losses to the radiator. A short time lag in the cooling cycle appears to be less important provided that the cooling cycle allows the compressor element to cool down fully over its cycle time of 33.3 minutes. However it is required that the compressor cool down time to 290 K in 800 seconds.

To reduce the thermal load into the radiator, the time required for the transition from G_{ON} to G_{OFF} should be minimized. The time to switch to a high conductance state (which is not necessarily the highest conductance obtainable) must be short enough to allow the compressor unit to cool to the absorption temperature in the time required by the operational cycle of the system.

For both of the switching operations, the process to verify the attainment of the compressor unit requirements will be described without giving any specific time requirement. For any given curves of conductance vs. time, the ultimate test is to use these curves to assess their performance.

2.3.1 Switching OFF→ON

The switching OFF→ON must be fast enough that the compressor unit will reach a temperature of 290 K in 800*s* after the compressor unit power is turned off. The heat balance of the compressor unit at any given time can be written as

$$Power-(mc_p)_{Comp.unit}\frac{dT_{Comp.unit}}{dt}-(G_{Gap}+G_{parasitic})(T_{Comp.unit}-T_R)=0 \qquad \textit{Equation 2-9}$$

where $G_{Parasitic}$ indicates the heat losses through the metal supports and the radiation losses expressed in Equation 2-7, mc_p is the thermal mass of the compressor unit, $T_{comp.unit}$ is the temperature of the compressor unit and T_R is the temperature of the radiator. During the cool down of the compressor unit no heater power (*Power*) is supplied.

Three simplifying assumptions were made to formulate the requirement criteria: (1) a constant compressor unit thermal mass of $(mc_p)_{Comp.\ Unit}$ = 826 J/K (the maximum value in the considered temperature range), (2) a constant temperature of the radiator T_R of 280 K, and (3) to neglect the $G_{parasitic}$. Equation 2-9 can be simplified for as

$$-826\frac{\partial T_{Comp.unit}}{\partial t} = G_{Gap}\cdot\left(T_{Comp.unit} - T_R\right) \qquad \textit{Equation 2-10}$$

where G_{Gap} is derived from Equation 2-8. Equation 2-10 cannot be solved explicitly in $T_{comp.unit}$ because G_{Gap} is a function of pressure (function of time) and of $T_{comp.unit}$, used in the determination of the hydrogen thermal conductivity l_m. A gas gap thermal switch, validates the OFF→ON requirement when, by substituting its OFF→ON transition pressure in Equation 2-8 and then G_{Gap} in Equation 2-10, the solution $T_{comp.unit}$ of the latter equation verifies that $T_{comp.unit}$(800s) ≤ 290 K.

2.3.2 Switching ON→OFF

The gas gap heat switch begins to switch from ON to OFF at the completion of the absorption phase, in preparation for the heating of the compressor unit which initiates the desorption phase. If the switching operation is slow, a substantial amount of heat will be conducted directly to the radiator, increasing the energy needed to heat the compressor unit up to 450 K in 800s. The power needed to heat the compressor unit, derived from Equation 2-9, can be expressed as

$$Power = \frac{1}{1600}\left[\int_{290}^{470} MC_p\partial T + \int_{0}^{1600} G_{parasitic}(T - T_R)dt + \int_{0}^{1600} G_{Gap}(T - T_R)dt\right] \qquad \textit{Equation 2-11}$$

In the cooler modeling and design it was assumed that the second term in Equation 2-11, namely the heat conduction through the mechanical supports and the radiative loss, would account for 10 W (split between 5W conductive and 5 W radiative) considering a linear increase of the compressor unit temperature and a fixed radiator temperature of 280 K. By using Equation 2-7 it has been verified that the second term accounts for 3.8 W if one assumes a linear temperature increase.

The last term of Equation 2-11 is the power increase *DPower* due to the slow gas gap actuator switching behavior. A specific requirement will not be given in term of switching ON-OFF but *DPower* will be use to evaluate the gas gap actuator as a figure of merit.

Considering a linear compressor unit temperature increase, the expression for the increase in power required due to the residual gas OFF state conductance is:

$$\Delta Power = \frac{1}{1600}\int_0^{1600} G_{Gap}(t)T_{Comp\ .unit}\,dt$$

$$T_{Comp\ .unit} = \begin{cases} \frac{160}{800}t + 10 & 0 < t < 800 \\ \frac{30}{800}(t - 800) + 170 & 800 < t < 1600 \end{cases}$$

Equation 2-12

in which the temperature of the compressor unit varies from 10 C to 170 over the first 800 s, and from 170 C to 200 C over the next 800 s. The increase in power required to heat the compressor unit has three parameters: the time required to switch $t_{ON\rightarrow OFF}$, the G_{OFF} conductance, and the switch behavior during the transition. The G_{OFF} heat conductance is the most important parameter in the computation of *DPower* increase. After the ON→OFF transition period (of 200-300 s) there will be a large temperature gradient across the gap and small changes in the heat conductance will drive large *DPower* increase. For example an ideal abrupt switch going immediately to 0.03 W/K OFF state conductance would result in a 4.35 *DPower* increase.

2.4 Power of the "ON" State

The power required by the heat switch is very small compared to the power required for the compressors (typically about 1%) and therefore the power required for the heat switch is not a critical factor in heat switch design. In the initial cooler design a 8 W upper limit was established.

2.5 Lifetime

The heat switches for the compressor assembly of PLANCK sorption cryocooler will undergo roughly 12,000 cycles during 1.5 years of operation while in space. Since about six months of operation will be required in ground testing, the total number of cycles will be roughly over 16,000 cycles. The heat switch for each hydride compressor element component should be designed to operate reliably with minimal changes in the ON and OFF conductances as well as switching time constant for this lifetime.

3. General Approach

The operational principle of the gas gap heat switch and the critical requirements imposed on it have been described in the previous sections. In this section a general approach to the switch design will be discussed with a particular focus on the sorbent materials selection and the actuator test design. The sorbent material screening was dictated by the requirements previously expressed and led to the selection of three metal systems: Uranium, ZrNi and St 172 SAES getter alloy. The actuator test unit design required an initial numerical modeling of the system to optimize some of the parameters, such as the dimension of sorbent material containment unit, the operational temperatures, the hydrogen used in the initial filling etc. Numerical modeling was performed by predicting the actuator performance against the previously measured gap heat conductance.

3.1 Schematic design

The position of the heat switch on a typical metal hydride compressor element is shown in Figure 1-8. The gas gap actuator is a simple device. It includes the active material, a filter to prevent particulate matter from moving into the gas gap, an external heater to heat the material, and a connecting tube to connect the device to the outer wall of a compressor element. Since the outer wall of the compressor element is in contact with the radiator, it tends to remain near the radiator temperature. The design has the natural form shown in Figure 3-1.

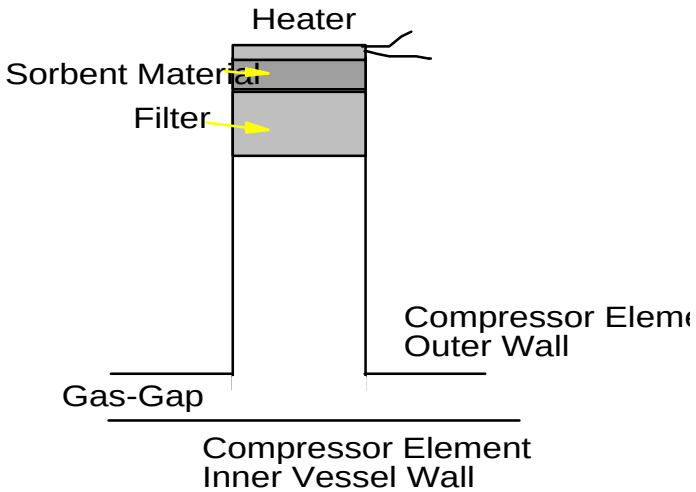

Figure 3-1 Schematic actuator design

The parameters that can be chosen to optimize the design include:

- the type and the amount of sorbent material,
- the total amount of hydrogen to use in the hydrogen-sorbent system,
- the type of filter,
- the type and power of the heater,
- the dimensions (diameter length and wall-thickness) of the connecting tube.

The type of sorbent material is of critical importance in determining what values of P_{ON} and P_{OFF} can be achieved over any given temperature range. Sorbents that require high temperatures to achieve adequate ON pressures may limit the life of heaters. Sorbents need to establish the OFF pressure at radiator temperatures (~ 280K). The amount of hydrogen must be properly metered to assure that the sorbent material is at the right place in its isotherms when in the ON and OFF positions. Each different sorbent material has different kinetic behavior and will absorb and desorb at different rates, which in turn will affect the heating and cooling time lags. In addition, the type and amount of sorbent are the principal factors in establishing the thermal mass of the tip.

The filter acts as a flow barrier and delays the transport of hydrogen to and from the sorbent. To improve the gas flow through the filter it is desirable to have pores as large as is allowable while still preventing transport of particulate matter from the sorbent to the gas gap region.

The heater must be properly chosen to endure the large number of on/off cycles. It must be attachable to the outside of the tip and make good thermal contact without greatly increasing the thermal mass of the tip and thus extending the thermal lags in switching operations.

The dimensions of the connecting tube (length, diameter, wall-thickness) are important parameters which particularly control the heat flow from the sorbent tip area to the compressor outer shell bolted to the radiator. In the compressor unit cooling phase when the heat switch is ON, the heat conductance from the heat switch tip to the compressor wall should be as small as possible to keep the switch sorbent hot. Conversely in the compressor unit heating phase with the heat switch OFF, it is desirable to have a large conductance to reduce the tip temperature as fast as possible and therefore

the hydrogen equilibrium pressure in the gap. Thus, a compromise must be reached between these two opposing needs to optimize the switch overall performance.

3.2 Material candidates

The material requirements are derived from the gas gap switch specifications and by the fact that the minimal temperature that the switch actuator could achieve is the radiator temperature [see Figure 3-1]. The materials that can be used as hydrogen reversible pump have to allow a pressure ratio of around 500 and a reasonable temperature range in order to obtain the pressure switching. As a general specification the absorption pressure should be lower than 1 Pa based on the 0.03 W/K requirement and the experimental data on the gas gap heat transfer [Equation 2-8] and the desorption pressure should be in the 500-1000 Pa range. A coarse screening of materials based on the above criteria for appropriate equilibrium pressures was performed [56, 57] upon known metal systems resulting in the list of materials and their behavior reported in Figure 3-2.

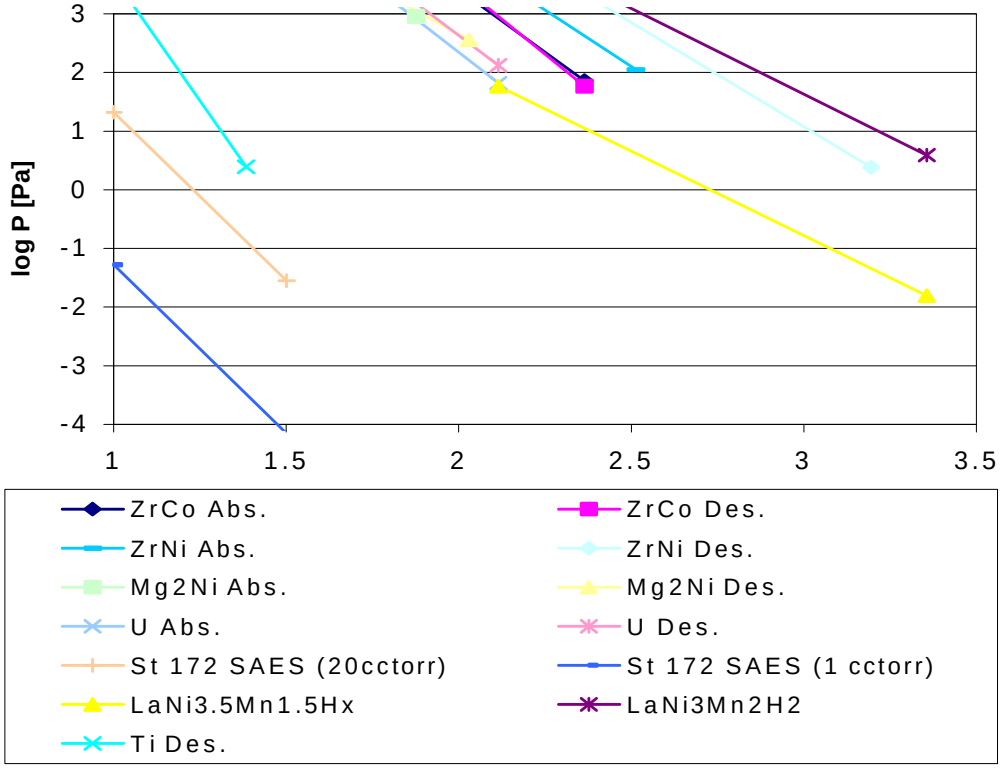

Figure 3-2 Van't Hoff plots for the first screened materials. The data are reported in Table 3-1.

Hydride	*Absorption*			*Desorption*			*H/M*	*Ref.*
	Range [K]	A	B	Range [K]	A	B		
$ZrCoH_x$	423-573	4261	11.93	423-573	4764	13.03	0.8-2	[56]
UH_x	473-700	4570	11.48	473-700	4450	11.53	≈ 3	[56]
TiH_x				723-1023	8424	14.16	1-1.5	[56]
$LaNi_3Mn_2H_2$	298-573	2923	10.40				0.5-3.8	[56]
$ZrNiH_x$	398-673	3853	11.52	313-723	3552	11.74		[57]
Mg_2NiH_x	533-593	3306	9.16	493-593	3245	9.14		[57]
$LaNi_{3.5}Mn_{1.5}H_x$	298-473	2874	7.84	423-523	D28.6	58.1		[57]

Table 3-1 First material selection based on the equilibrium pressure requirement. A and B are referred to a van't Hoff equation logP=-A/T+B *assuming pressure in Pa and the temperature in Kelvin. The van't Hoff data have been selected between as an average between the many measurements of thermodynamic hydride properties. For ZrNi, ZrCo and U thermodynamic properties survey see [64]*

The St172 SAES is a mixture of zirconium and the pseudo-binary intermetallic compound Zr-V-Fe. For hydrogen concentration in the material below 2.5 mgH_2/g its behavior can be expressed by

$$\log P[Pa] = 4.705 + 2\log(concentration[mgH_2 / g]) - \frac{5730}{T[K]} \qquad \textit{Equation 3-1}$$

$LaNi_3Mn_2H_2$ and $LaNi_{3.5}Mn_{1.5}H_x$ are intermetallic compounds derived from $LaNi_5$ with substitution of Ni atoms by manganese to reduce the plateau pressures of the original alloy [58]. The same idea has been used to design the alloy used in the compressor unit [5]. The major concern in selecting these materials is the fact that the OFF pressure is reached for temperatures very close to minimum temperature. Consequently the small margin on the switch OFF state increases the risk of substantial heat losses from the compressor unit to the radiator despite the ease with which the ON state can be reached with a switch temperature [~400 K] to desorb in the required pressure range. In addition, initial thermodynamic and degradation studies were performed on these alloys [59] showing a performance degradation of the alloy. Conversely TiH_x, is a stable elemental hydride and high temperatures are required to desorb hydrogen in the selected pressure range arguing against its use as gas gap sorbent material. The same observations can be repeated for Zr $H_{2.0}$ hydride.

The hydrogen capacity and the thermodynamics of Mg_2NiH_x are very promising and its kinetics for hydriding/dehydriding reactions are reasonably rapid above 470 K but there are substantial discrepancies between reported parameters in the kinetics at low

temperatures [57]. Also, Mg_2NiH_x is a semiconductor insulator [60] and thus its thermal conductivity and hydrogen diffusion coefficient are much lower than in most metallic hydrides, which degenerates the overall reaction kinetics. The metal system characteristics suggest that Mg_2NiH_x is not a suitable gas gap sorbent material.

ZrCo has been evaluated by several groups as a uranium replacement in tritium handling storage [56, 61, 62]. Its van't Hoff curve is located between ZrNi and Uranium and it appears as a suitable gas gap sorbent material; the ON pressure can be reached at around 500 K and an equilibrium pressure below 0.13 Pa can be reached at 330 K. Irvine and Harris [63] showed that although in the PCT diagram only one plateau region can be identified, there are actually two hydride phases, β_0 and β_1 distinguished by the crystal structure. They also verified that their results are dependent on the thermal history of the samples by observing the plateau region width reduction and shifting after thermal cycling at 623 K. In addition to the disproportionation of the starting intermetallic compound, it has been observed that the hydride behavior is also strongly and negatively affected by nitrogen, oxygen and methane exposure to the metal [64, 65]. The reported data on contamination sensitivity and disproportionation were not encouraging to the selection of ZrCo as gas gap sorbent material and it was decided to keep it as a backup option to candidates Uranium, ZrNi and the SAES St172, whose characteristics will be briefly discussed in the following sections.

3.2.1 UH_x

Uranium reacts readily with hydrogen to form the stable ternary hydride UH_3 in a high exothermic reaction. As previously mentioned, the hydrogen-uranium system has only one hydride phase [see Figure 3-3] and it is characterized by broad and flat plateaus. Consequently, it can be considered as favorable hydrogen reversible storage over a wide temperature range. The uranium hydride history, as well as the pure metal application history, is very much related to the fission nuclear studies and energy conversion. The earliest investigations on the solubility of hydrogen in the bulk metal were done during the Manhattan Project (a comprehensive description of the hydrogen-uranium system can be found in [66]). Since that time, its major hydride application has been the recovery of tritium in the fission and fusion reactors.

The hydride crystal structure has been identified [66] as a cubic structure with eight uranium atoms per unit cell with twelve hydrogen atoms surrounding each uranium

atom. The hydride structure is thermodynamically very stable. Its heat of formation, 63.8 KJ/gH, is much larger then most of the ternary intermetallic compounds hydrides such as ZrNi, Mg_2Ni, ZrV_2. Even though the hydrogen-uranium system has been widely characterized by many groups over a wide range of temperatures and pressures, some differences were observed in the thermodynamic data [67]. The thermal history along with the surface contamination and the particle size play an important role in the system thermodynamics. The heat of formation of 63.8 KJ/mol-H and a 90.6 J/Kmol-H entropy that were measured by Wicke and Otto [68] have been used for the mathematical modeling of the gas gap actuator.

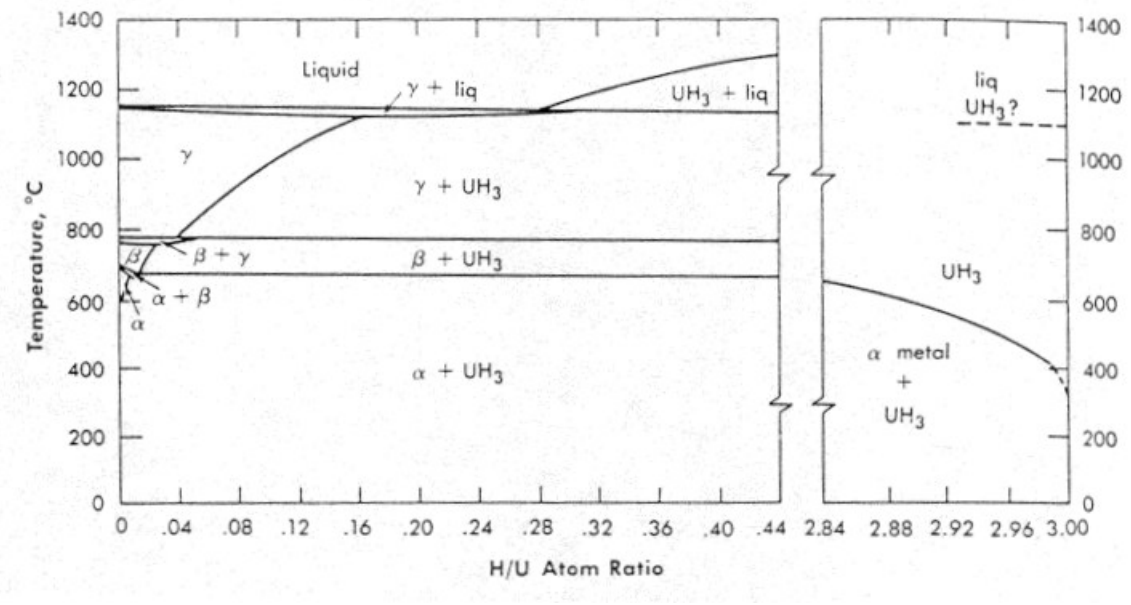

Figure 3-3 Hydrogen uranium phase diagram [66]

During the initial hydrogen reaction the metal is disintegrated into fine powder by the large expansion of the hydride phase into the metal structure. The large discrepancy between the metal (19 g/cm^3) and the hydride (10.95 g/cm^3) density causes the rupture of the solid structure exposing clean metal surface to hydrogen thus increasing substantially the reaction kinetics. Many investigators [33, 69, 70, 71] have extensively studied the kinetics of the hydrogen-uranium reaction and substantial differences are reported in their experimental measurements of the rate of absorption. Lindner [67] suggested that the rate of the dehydriding reaction has a logarithmic dependence on the ratio P_0/P where P_0 is the corresponding PCT plateau pressure, while Condon and Powell have suggested a first

order and a ½ order rate of the reaction depending on the pressure and temperature range. As previously expressed, measurements on kinetic rate are very difficult, especially with such a high heat of formation, but the studies performed by Powell [72] indicated that the reaction kinetics can be slow and strongly affected by contaminants.

3.2.2 $ZrNiH_x$

ZrNi has already been tested and used as a gas gap switch hydride by J.Wu [40] at JPL and as low pressure absorber for a closed cycle 10 K sorption cooler [9, 10]. Like uranium, it has also been used for hydrogen isotopes recovery [74]. The stoichiometric 1:1 alloy is one of the nine intermetallic compounds of the ZrNi system and among them it has the highest hydrogen storage capacity [75] forming two hydrides phases as shown in Figure 3-4. A ZrNi-H system phase diagram has been presented by Kronski and Schober [76] but it hasn't been completely accepted. Although ZrNi-H system was the first intermetallic compound hydride characterized and many investigators have studied its properties, there remain some experimental questions still unsolved.

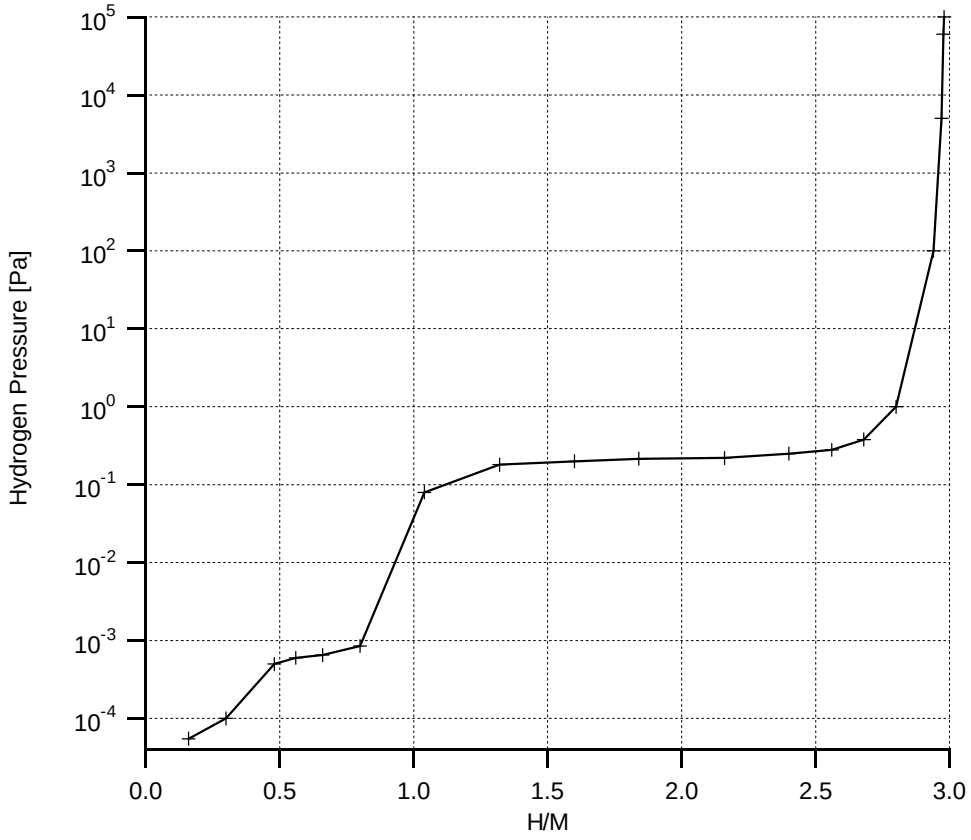

Figure 3-4 The 293 K absorption isotherm for ZrNi [73].

The first plateau region, between the solid solution α and the β phase is located around the 0.2 hydrogen /metal ratio [H/M]. The enthalpy $\Delta H_{\alpha\rightarrow\beta}$ of the β phase hydride formation is 47.5 kJ/mol-H while the $\Delta S_{\alpha\rightarrow\beta}$ is 59 J/Kmol-H. Above 0.6 H/M concentration only β phase is present up to a 1.0 H/M, where another plateau region indicates the β to γ phase change. The second plateau region indicates the second phase transformation, for a H/M ratio between 1 and 2 H/M. The enthalpy $\Delta H_{\beta\rightarrow\gamma}$ of the γ phase hydride formation was found [77] to vary substantially depending on the material thermal history as well as the annealing procedure. As shown in Figure 3-5, there is hysteresis between the absorption and desorption plateau in the β- γ phase transition. For the absorption of an annealed alloy a $\Delta H_{\beta\rightarrow\gamma}$ of 34.1 kJ/mol-H and a $\Delta S_{\beta\rightarrow\gamma}$ of 62.7 J/Kmol-H were measured. For the desorption of the same system different enthalpy and entropy values were derived ($\Delta H_{\gamma\rightarrow\beta}$= 36.8 kJ/mol-H and $\Delta S_{\beta\rightarrow\gamma}$=63.8 J/Kmol-H). As in the case of uranium, in the hydrogenation reaction produces a 14 % volume expansion cracking the initial solid pellets into fine powder [56].

Recently it has been observed [35, 78] that degradation of the $ZrNiH_x$ system occurs at elevated temperatures (675-700 K) jeopardizing its use for applications requiring simultaneous large hydrogen concentration and high temperature. The degradation product were more stable binary hydride compounds (i.e. zirconium hydride)

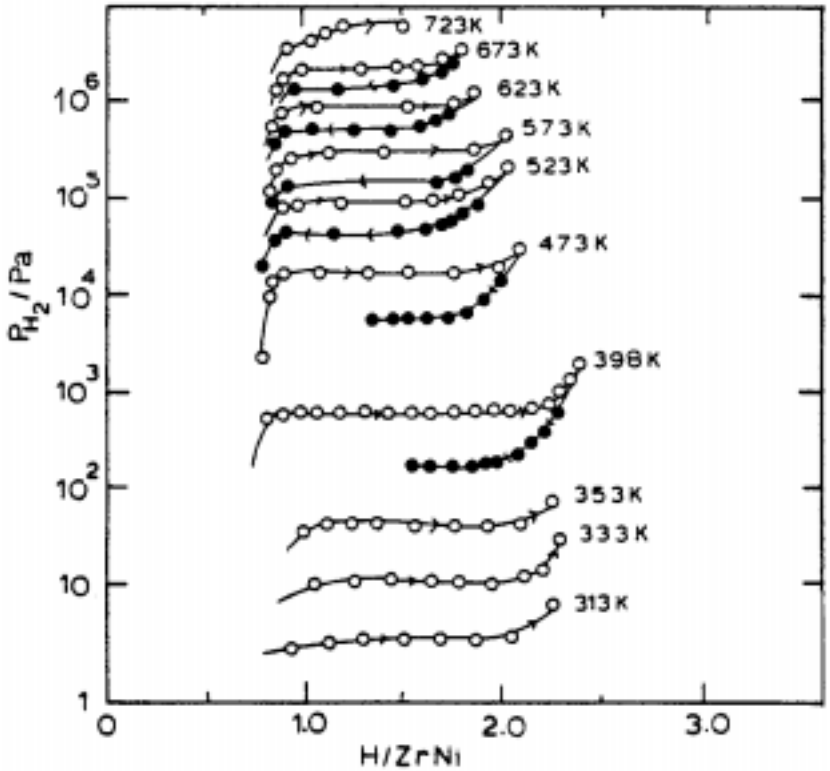

Figure 3-5 Isotherms for the (β +γ) plateau for ZrNi-H system [77]

degradation product were more stable binary hydride compounds (i.e. zirconium hydride) [35, 77]. The nickel was instead separated over time either as a pure nickel phase [34] or as $ZrNi_3$ [77]. The precipitation process decreased the reversible hydrogen capacity and it shifted the isotherms towards higher pressures. Consequently, the metal system was not able to re-absorb the initial stored hydrogen quantity. Some investigators [35] observed also traces of zirconium oxide in the analysis of the cycled material that have contributed to the hydrogen capacity deterioration. A well-defined explanation of the degradation phenomenon has not been described. In addition, all the experimental data were obtained at high temperatures (T > 650 K), where the disproportionation phenomenon is supposed to be faster. ZrNi has been considered as gas gap sorbent material for its fast kinetics and because the temperature required for the ON state (450 K) is substantially lower than the degradation tested temperatures. The stability over a long term cycling of the vacuum reached in each cycle is likely to be the key factor in the selection of ZrNi as the gas gap sorbent material due to the contamination effects.

3.2.3 St 172 SAES Getter Alloy

The St 172 is a sintered porous alloy composed of a mixture of a Zr-V-Fe (St 707) alloy and zirconium in about the same proportions. The alloy is sintered in a high vacuum, high temperature furnace to obtain a solid pellet. Little information can be found beyond the SAES product brochures about St 172; while St 707 has been widely characterized by many investigators. As in the case of most of the hydrogen storage materials reviewed in this work, St 707 had been previously studied as tritium storage media [79, 80, 81, 82]. St 707 is a ternary alloy whose nominal composition is 70% Zirconium, 24.6% Vanadium and 5.4% Iron in weight with nominal atomic composition is $Zr_{57}V_{36}Fe_7$. A previous investigation by C. Boffito et al. [83] characterized the St 707 by X-ray analysis using Cu Kα radiation as a pseudo-binary intermetallic compound $Zr(V_{0.83}Fe_{0.17})_2$ and Zirconium α phase. In the same paper, the maximum hydrogen capacity for the St 707 was found to be 16.24 mgH_2/g of alloy. The investigators noticed that the alloy did not show “any appreciable tendency to form fine powder”, but in the product technical information it is suggested to not exceed the embrittlement limit over which the integrity of the solid pellet is not guaranteed. In fact, the St 172 was developed as a low temperature activation getter for specific applications where only low temperature (i.e. < 400 C) could be tolerated and no particles are generated. The presence of the Zr-V-Fe powder is found to give the porous alloy material a high mechanical

adherence due to some bonding formed with other components at the sintering conditions. The porosity, combined with the high diffusivity of the sorbed species of the Zr-V-Fe, make available to the gases a high surface gettering area. The accessibility to the gas to be sorbed is also proven by a BET surface area measurement to be 10 m^2/g with Krypton as a test gas.

Based on the St 172 composition and the St 707 hydrogen capacity it is possible to infer a 19 mg_H/g of alloy hydrogen capacity for the St 172. The Zr hydride, a major constituent of the St 172 alloy, is thermodynamically very stable and therefore it requires high temperature to release the absorbed hydrogen.

The available data on the PCT diagram are limited by the embrittlement limit (around 2.5 mgH_2/g [84]) and are not very favorable for the gas gap application [see Figure 3-6]. At least 700 C would be required to desorb hydrogen at 30-50 Pa with a concentration below that limit. Considering the rapid kinetics reported by most of the investigators, it was decided to verify the St 172 hydrogen capacity above the embrittlement limit and to contain it in a closed container as show in Figure 3-1, as used for uranium and ZrNi. The material properties for elevated concentration have been measured by a volumetric Sievert apparatus [see description in Appendix C].

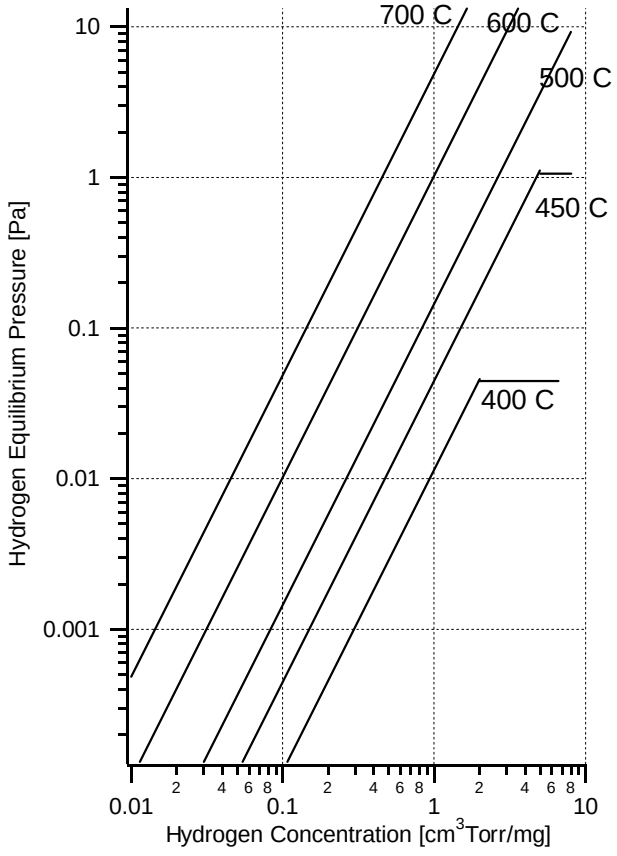

Figure 3-6 The PCT curves for SAES St 172, derived from manufacturer product literature

3.3 Gas Gap Actuators modeling and design

Numerical modeling of all gas-gap actuator components has been used to perform a parametric study of the selected baseline sorbent materials. The objective of the actuator modeling is to evaluate performance levels by predicting the gap heat conductance as a function of all the parameters listed in section 3.1. The evaluation of alternatives is accomplished by attributing to each switch configuration two figures of merit: the *Total power* and the *cooling-time Margin*.

It has been described in section 2 that the power required to run the switch is directly related to the switch cooling time and subsequently to the ON-OFF switching operation. The *Total Power* has been introduced to combine the two effects. It has been defined as the sum of the constant power to run the switch in the ON state plus the increased *DPower* due to the residual gas OFF state conductance [see Equation 2-12].

The *cooling-time Margin* is a figure of merit to appraise the capacity of the switch to cool the compressor unit in the appropriate cycle time (800 s). Considering the *cooling time* as the time needed to cool the compressor unit from 480 K to 290 K [see Equation 2-10] the *Margin* can be defined as:

$$Margin = \frac{800 - Cooling\ \ time}{800}$$

Equation 3-2

The modeled actuator performance, in combination with the measured heat transfer equations (Equation 2-8), are used to evaluate the proposed design against the switch requirements by returning the two defined figures of merit. The modeling for the two switching operations can be summarized as in Figure 3-7.

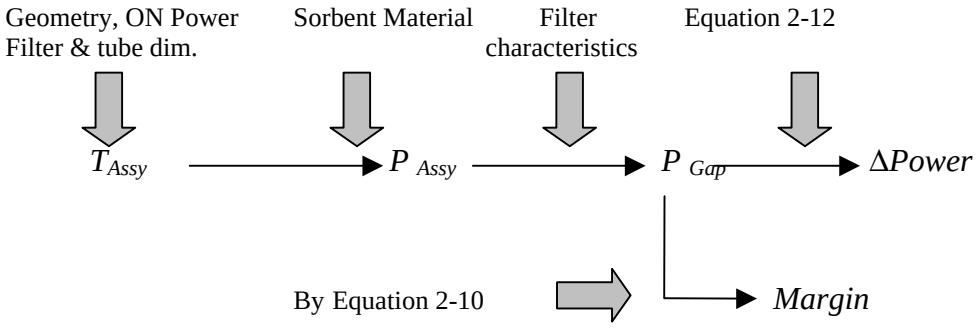

Figure 3-7 Diagram of the actuator modeling

Several hypotheses were introduced to simplify the actuator thermal modeling:

- Constant power is supplied to the heater during the switch ON state.
- The actuator switching operations are time-phased with the compressor unit [see Figure 2-1].
- The heater thermal mass is estimated to be equivalent to the actuator assembly thermal mass. This hypothesis has been introduced as an initial estimate because the heater configuration has been determined after the switch design.
- The switch assembly (sorbent containment, sorbent and filter) is considered isothermal. A detailed analysis of the thermal gradients in the switch assembly depends in fact on the heater configuration [section 4.5].
- The heat of absorption is neglected. This hypothesis allows the separation of the thermal behavior modeling of the switch from the gap conductance calculation.
- The kinetics of the H_2 absorption desorption reaction is assumed to be fast enough. The hydrogenation reaction is usually very fast and, as previously mentioned, there is not a general agreement on the sorption kinetics theory.
- In the expansion into the volume and compression into the sorbent material hydrogen has been considered as an ideal gas (which valid as $P_{ON} < 10$ kPa).

For the thermal modeling of the switch actuator as shown in Figure 3-1 the lumped capacitance method has been used, with a node for the switch assembly and few nodes for the supporting tube. Only conduction and radiation have been considered, due to the fact that the switch will work in space and that it has been tested in a vacuum chamber. The geometry, the heaters, the supplied power, the sorbent material and the materials used in the sorbent containment determine the temperature of the switch assembly $T_{ASSY}(t)$ as a function of time. The power to keep the actuator assembly (filter, sorbent material and sorbent containment) at T_{ON}, temperature of the ON state, is the power to run the switch.

The relationship between temperature and the equilibrium pressure of the material $P_{Assembly}$ has been discussed in section 1.4 [the van't Hoff equation, Equation 1-1]. The

two constants, $DH_{a\to b}$ and $DS_{a\to b}$, are respectively the enthalpy and the entropy of β phase specific hydride formation.

The presence of a porous filter affects the switching operation by introducing a flow resistance between the gap volume and the H_2 storage material. In fact, the hydrogen flow conductance to the sorbent material is primarily determined by the pressure difference across the filter and the effects of the restricted flow conductances in the gap and in the T-tube [Figure 1-7] can be neglected. The pressure difference-flow relationship used in filter modeling has been derived by experimental measurements on a similar filter at the Jet Propulsion Laboratory and agreed with the manufacturer specifications [85]. The expressions used are

$$\dot{n} = \frac{V_{Volume}}{RT_{Volume}}\left(\frac{dP_{Volume}}{dt}\right) \qquad \textit{Equation 3-3}$$

And

$$\left(P_{Volume} - P_{Assembly}\right) = \frac{4\dot{n}M_{H_2}RT_{Assembly}}{pD^2\sqrt{\frac{T_{Assembly}}{294}}C_T\frac{L_{Filter}}{L_T}} \qquad \textit{Equation 3-4}$$

Where D is the diameter of the porous filter (the same of the tube), L_T is the thickness of the filter tested at 294 K giving the flow conductance C_T, L_{Filter} is the thickness of the filter modeled and V_{Volume} is the volume between the inner and the outer element in the compressor unit [see Figure 1-7] (163 cm^3).

The heat conductance can be than inferred using Equation 2-8, derived by the experimental measurement of the heat conductance [see section 2.2.4].

In order to clarify the effect of each single parameter on the switch actuator in the ZrNi actuator modeling section [section 3.3.1] the effect of every single parameter has been considered keeping constant all the others. For each a hydrogen storage material different configurations have been analyzed and as reported in the next sections.

3.3.1 ZrNi actuator design

The ZrNi actuator was designed based on a operating region of the hydrogen-hydride system in the β to γ phase transition. Considering the full reversible hydrogen

capacity of the β - γ plateau 40 mg of ZrNi would be needed. However, attempting to evolve all the reversibly stored hydrogen during the ON-OFF cycle would not leave any margin to potential contamination or hydride system disproportionation. To mitigate those potential risks it was decided to use a much higher quantity of ZrNi (0.25 - 0.3 g) and to cycle the hydrogen-metal system in the mid-plateau region (around 1.5 H/M [see Figure 3-5]). The hydrogen concentration would not vary much when 500-1000 Pa of hydrogen are desorbed in the gas gap volume during the ON state period.

In the determination of the optimum filter pore size an accurate hydride grain size distribution should be known. Watanabe [86] reported the ZrNi size distribution after the alloy had been reacted with deuterium for 85 cycles. He found that more than 50 % of the material still had a grain size higher than 50 μm. However, our ZrNi actuators have to be cycled for much longer than this, and his results cannot be used as an appropriate estimate of the end-of-life grain size distribution. In addition, many other experimental conditions heavily affect the extent of pulverization of the alloy and consequently an a-priori estimate of the distribution can only be approximate. Nevertheless the filter pore size has to be designed. Considering that the flow conductances of both 5μm and 0.5 μm pore size filters are more than adequate in the gas gap actuator mass flow range, it was decided to use a 316 L – SS sintered filter (0.5 μm) manufactured by Mott Corp.

The ZrNi hydride is contained in a cylindrical volume above the filter with a diameter equivalent to the inner diameter of the connecting tube. The same wall thickness has been utilized for the containing unit and the connecting tube. The height of the cylindrical containment has been derived considering a 35 % packing density of the hydride in the sorbent containment.

Considering a particular actuator design, the sensitivity on the components physical dimensions and properties has been evaluated in terms of total power and margin. The pivotal design that was then used to design the ZrNi actuators can be summarized as:

- Temperature ON state = 444 K
- Diameter connecting tube = 12.7 mm (½ inch)

- Length of the connecting tube = 4 mm
- Wall thickness of the connecting tube = 0.150 mm
- Hydride mass = 0.28 g.
- Power in the ON state = 3.82 W.

The effects of the connecting tube dimension, the temperature of the ON state, the thermal mass of the switch assembly, and the temperature of the switch radiator are shown in Figure 3-8.

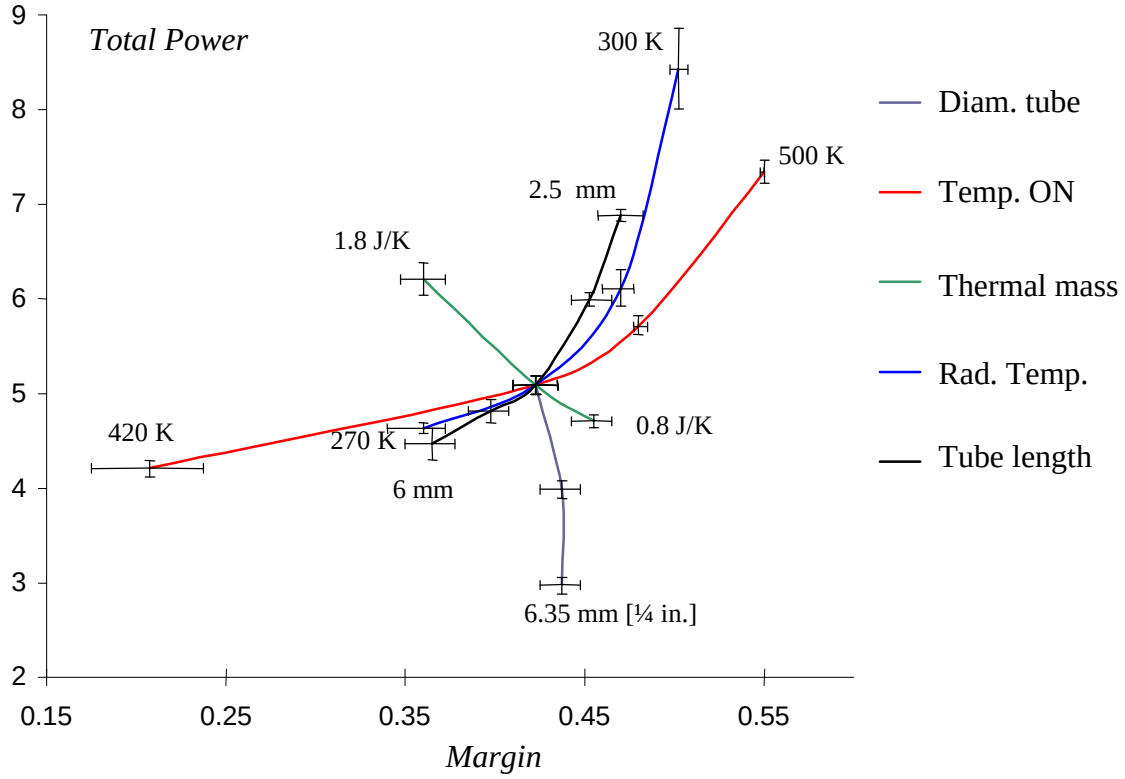

Figure 3-8 Evaluation of different ZrNi actuator designs in terms of Total Power and Margin. The error bars have been determined considering a 2s interval in the accommodation coefficient as estimated in section 2.2.4. The ranges of the variables are: (1) 6.35 mm [¼ in.] – 9.35 mm [½ in.] for the diameter of the tube, (2) 500 K – 420 K for the ON state temperature (3) 1.8 J/K – 0.8 J/K for the thermal mass, (4) 270 K – 300 K for the temperature of the radiator (Rad. Temp.) and (5) 2.5 mm to 6 mm for the connecting tube length.

3.3.1.1 Tube design

The connecting tube design determines the major heat conductance of the switch assembly to the radiator. The tube design is therefore the principal factor in the ON state power requirement.

In Figure 3-8 are reported two variations of the pivotal tube diameter, 9.535 mm ($^3/_8$ inch) and 6.35 mm (¼ inch). Decreasing the diameter reduces the total power. However, the hydride layer thickness in the sorbent containment increases and, considering the poor thermal conductivity of the hydride powder, the assumption of an isothermal switch can no longer be justified.

The effects of the diameter and tube length in terms of total power and margin are almost orthogonal. A longer tube reduces the power to run the switch in the ON state but it delays the switch assembly cool down, increasing the *DPower* due to the residual gas OFF state conductance. Considering the concerns on the alloy performance degradation, especially of the OFF state, it was decided to design a fast actuator and to not emphasize minimizing the total power.

The radiative heat exchange has been considered assuming that the actuator is enclosed in a black body at the radiator temperature and the emissivities were assumed to be 0.3 for the stainless steel tube and of 0.5 for the heater.

3.3.1.2 Temperature of the ON state

The temperature of the ON state primarily determines the margin of the switch. In Figure 3-8 a 420 – 500 K range variation is reported. It should be noted that the ZrNi switch is very controllable: increasing the power to run the switch (that is increasing the equilibrium temperature of the ON state) increases the margin.

3.3.1.3 Temperature of the radiator

The ZrNi switch is very sensitive to the radiator temperature. A higher OFF state temperature would immediately increase the OFF state pressure of the switch and consequently the *DPower* [Equation 2-12].

3.3.1.4 Thermal mass

The thermal mass of the switch assembly (filter, cap and sorbent material) decreases the switching speed of the actuator, thus degrading its performance. Therefore

it has to be minimized by reducing the sorbent containment wall thickness, the filter's thickness and the thermal mass of the heaters. The thermal mass of the pivotal design point is 1.18 J/K.

3.3.2 Uranium actuator design

The uranium actuator was designed based on a operating region of the hydrogen-hydride system in the α to β phase transition [see Figure 3-3]. The hydride containment, in terms of tube diameter and wall thickness, filter porosity and thickness, has not been redesigned but it has been assumed equivalent to the ZrNi actuator's containment. The hydride quantity that can be contained in this volume is in the 0.4- 0.5 g range depending on the hydride packing density. The uranium amount exceeds the minimal quantity required to reversibly evolve hydrogen in the gap at the ON pressure providing a margin for a possible degradation. The hydrogen concentration in the metal system is not a critical parameter due to the fact that the plateaus are fairly flat. The hydrogen concentration would practically not vary during desorption when the switch is ON.

The uranium design parameters are:

- Diameter	12.7 mm
- Wall Thickness	152 μm
- Power of the ON state	3.1 W
- Operating temperature (ON state)	558 K
- Filter thickness	1.00 mm
- Tube length	9.0 mm

Considering the actuator design, the sensitivity on the length of the connecting tube, the T_{ON}, and of an additional thermal mass has been evaluated in terms of *Total Power* and cooling time *Margin*, as shown in Figure 3-9.

The connecting tube design determines the major heat conductance of the switch assembly to the radiator. The radiative heat exchange has been considered assuming that the actuator is enclosed in a black environment at the radiator temperature and the emissivities were assumed to be 0.3 for the stainless steel tube and of 0.8 for the heater. A parametric study on the emissivity has not been done considering the strong dependence

on the heater configuration. In section 4.5.2 the description on a finite element analysis on the specific uranium actuator is reported.

In Figure 3-9 are shown the effects of the connecting tube length, the temperature of the ON state, and the thermal mass of the switch assembly. The temperature of the ON state play an important role in determining the cooling time margin of the actuator as happened for the ZrNi actuator. In Figure 3-9 the equilibrium temperature of the ON state vary between 520 and 575 K

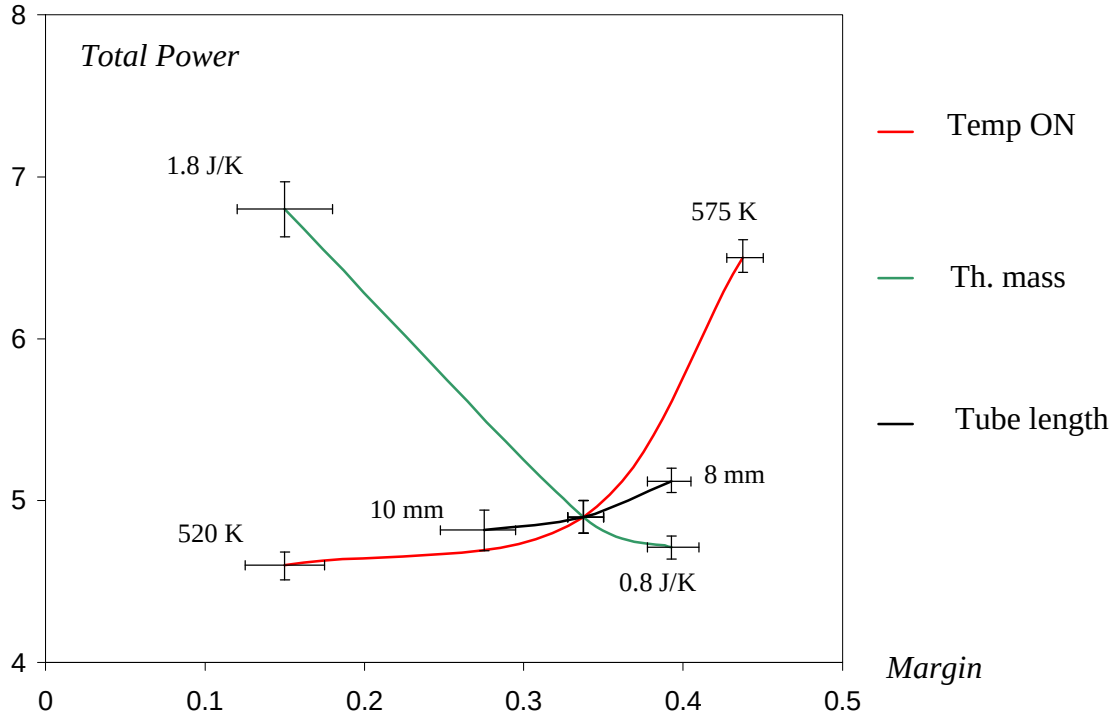

Figure 3-9 Evaluation of different uranium actuator design in terms of Total Power and Margin. The error bars have been determined considering a 2s interval in the accommodation coefficient as estimated in section 2.2.4. The ranges of the variables are: (1) 520 K – 575 K for the ON state temperature (2) 1.8 J/K – 0.8 J/K for the thermal mass, and (3) 8 mm to 10 mm for the connecting tube length.

The estimated thermal mass of the actuator is 1.15 J/K. It is interesting to observe how an increase in the thermal mass degrades the overall actuator performance by increasing the total power and diminishing the cooling time margin.

3.3.3 St 172 actuator design

The St172 actuator was designed before measuring the hydride isotherms at high hydrogen concentrations. In fact, at that time the Sievert's apparatus was not available at

JPL. As an initial estimate, it was supposed to operate the material at high temperature (around 350 C) and therefore to use a long connecting tube to minimize the ON state power. A 15 mm tube was considered with an actuator assembly, in terms of porous filter and hydride containment, equivalent to the uranium and ZrNi ones.

4. Actuator Test Assembly

4.1 Hydride container design

The general configuration of a gas gap heat switch actuator is reported in Figure 3-1. The volume containing the hydride is a cylinder with a radius 12.395 mm and a 1 mm height, as shown schematically in Figure 4-1.

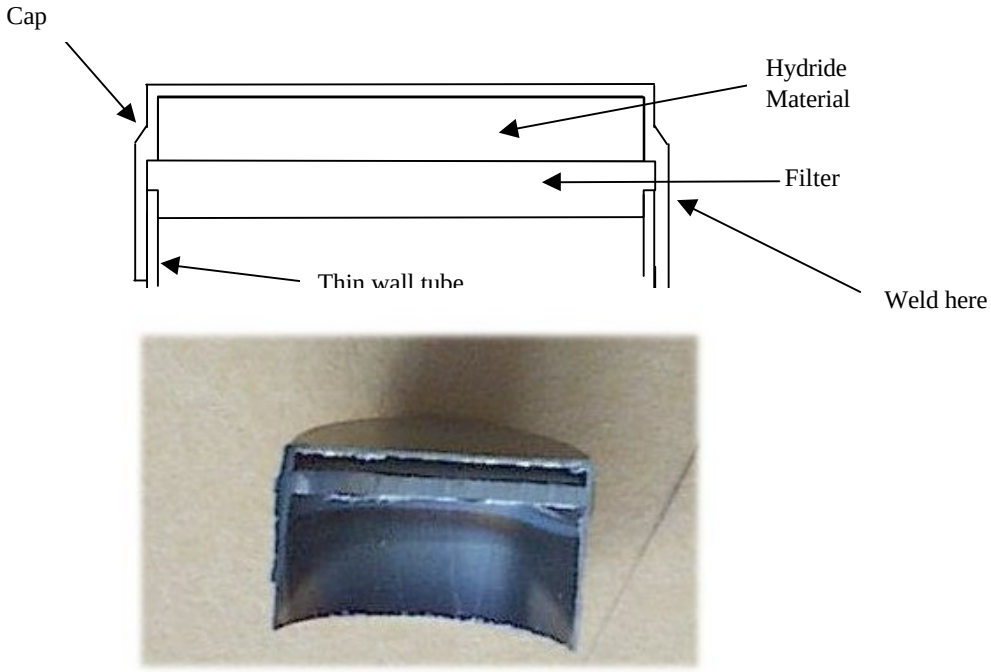

Figure 4-1 Gas Gap Actuator Assembly schematic and a section of a weld test

The cap and the thin wall tube have a wall thickness of 150 μm. The filter has a thickness of 0.78 mm and a porosity of 0.5 μm, in order to contain the material after it is transformed into fine powder by the reaction with hydrogen. The porosity of the filter was selected based on the known granular distribution of the three hydrides.

The filter was mounted on the top of the tube with a tight fit. The cup was filled with the specified amount of material and then the tube, with the filter mounted on top, was slid into it and held in place by a tight press fit. The actuator assembly was then ready to be welded.

4.2 Test plans

The actuator tests were intended to characterize the initial performance of the three different actuators and to verify the changes in behavior with time by cycling ON-OFF the actuators. Three uranium actuators (U-1, U-2, U-3), three ZrNi (ZrNi-1, ZrNi-2, ZrNi-3) and one St 172 (St 172-1) were tested. The initial performance parameters of the actuators are intended to be the relationships between power, temperature and pressure and the behavior changes are changes of those relationships with time due to the thermal cycling. An electrical heater supplies the heater power for the actuator and a cool temperature sink is obtained by thermally connecting the actuator to a cooled plate with a copper clamp.

The pressure, the temperature of the hydride encapsulation and the supplied heater power to the switch will be recorded. The actuator test unit is shown in Figure 4-2. The control volume simulates the net volume for the PLANCK sorption compressor element.

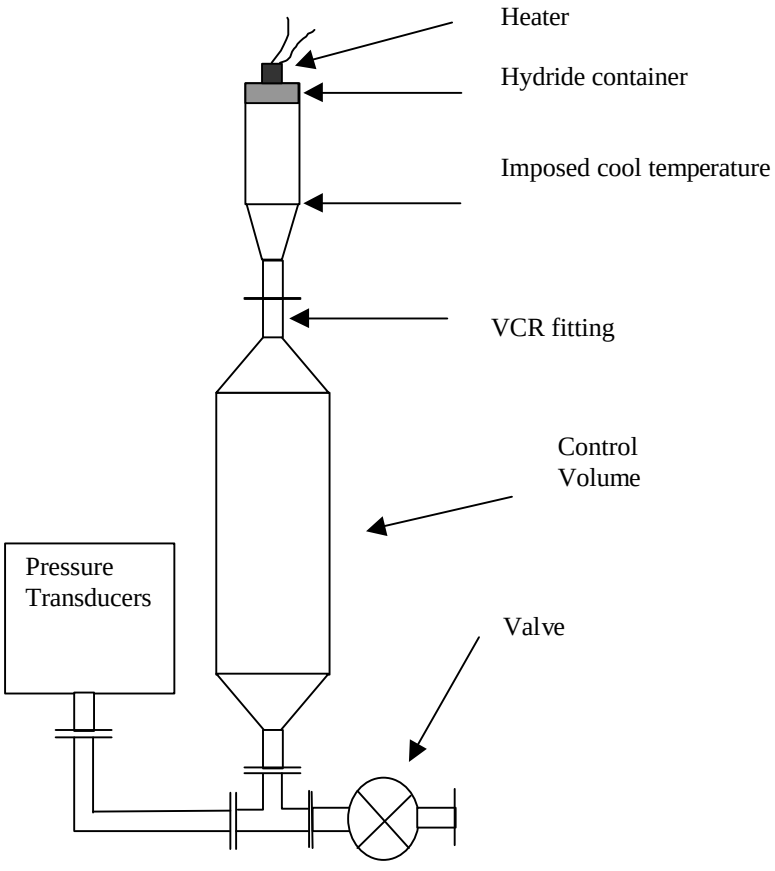

Figure 4-2 Actuator Test Assembly schematic

4.3 Actuator Unit Assembly procedure

The assembly procedure of the gas gap actuator test can be summarized as follows:

1. The thin wall tube was e-beam welded onto a thicker wall concentric reducer [12.7mm (½") to 6.35 mm (¼")]. The thicker wall tube is used in order to have mechanical strength to permit a good thermal connection to the cold reference for testing. The thin wall tube was then trimmed to the appropriate length and a VCR fitting was attached to the ¼" end. As reported in the previous section, the length for the three different material are

- Uranium 9 mm
- Zirconium – Nickel 4 mm
- SAES 172 15 mm

2. The control volume was built and all the VCR fittings were attached on the tubing components. Every component was leak-tested before assembly. An initial measure of the control volume was made by pouring isopropyl alcohol in the volume and measuring the amount poured. The volume of the entire test assembly was later calibrated against a secondary reference volume. All the parts used in the test assembly and in contact with hydrogen gas are made of stainless steel 316L and Inconel (only the sensor part of the capacitance manometer). The inner surfaces of the tubing parts, the VCR connectors and a valve, were electro-polished.

3. All the parts were cleaned to minimize contamination of the hydride material. (The contact of hydrogen gas with an adsorbed monolayer of non-inert gases may activate some chemical reactions. The products of those reactions may either react with the hydride or constitute a constant residual gas in the gas gap.)

   The Electro-polished parts were initially rinsed in isopropyl alcohol and then cleaned in an ultrasonic cleaner for ½ hour. The parts were then dried with dry nitrogen.

   The caps were rinsed and cleaned with a degreaser, water and isopropyl alcohol in the ultrasonic cleaner. They were then inserted in a previously

cleaned volume and baked out under vacuum for a few hours at 300 C. The volume was then sealed under vacuum and moved into an argon controlled atmosphere where it was opened. The caps were then ready to be assembled.

The filters were rinsed and cleaned successively with a degreaser, water and isopropyl alcohol in the ultrasonic cleaner. They were dried in the passing box of the argon atmosphere chamber and then introduced into the argon controlled atmosphere. They were inserted in a previously cleaned volume that was then sealed using a valve, removed from the inert atmosphere and connected to a pumping station. The volume was filled with hot hydrogen at 1 atm and then it was baked out under vacuum at a temperature of 300 C overnight. The residual gas in the volume was then analyzed showing traces of argon, hydrogen, water, methane, ethyl alcohol, carbon monoxide and propene. No clear explanation was found for the presence of propene. The most likely hypothesis is that it was a by-product of the filter manufacturing and cleaning process but the manufacturer [Mott Metallurgical Corp.] wouldn't validate it in order to keep the process confidential. The volume was then sealed under vacuum and re-inserted into the inert atmosphere where it was open to remove the filters.

The pressure transducers were rinsed with isopropyl alcohol and dried with dry nitrogen.

4. The volume, the valve and the pressure transducer were assembled as shown in Figure 4-2.

5. The hydride materials were prepared and cleaned with a different procedure before being inserted into the cap as shown on.

   The uranium discs, as received, had a black layer of uranium oxide on the surface and were introduced in the inert atmosphere chamber in order to reduce the oxide formation. To remove the oxide, the discs were cleaned in nitric acid 8 N solution, rinsed in water, rinsed in high purity ethyl alcohol and dried in the passing chamber of the inert atmosphere glove box by pulling vacuum on them. The discs were then inserted into the inert atmosphere. The result of the cleaning operation was a smooth metallic surface. It was noticed

that once they were cleaned, a paler layer reformed on the discs. This second layer was more difficult to remove than the first one.

The zirconium nickel [ZrNi] material was cut into thin slices (thickness 330 μm) out of a solid piece by wire Electro-Discharge-Machining at JPL. The material initially had a shiny metallic surface but the machining operation left the slices covered with a black layer, suggesting that some carbonates or oxide were formed on the re-cast layer. The surface black layer was tentatively removed by scratching on the surface with fine sandpaper in the inert atmosphere chamber. However it was not possible to remove completely the black surface layer and to obtain a very smooth clean metallic surface.

The SAES 172 alloy was received from the manufacturer in solid pellets mounted on a Inconel rod [St 172/HCS/7-6/150C]. It was not cleaned with any particular method but only grounded in the glove-box to obtain small size grain that could fit into the volume.

6. The three test materials were inserted in the cylindrical volume. The operation was done in an inert atmosphere chamber [shown in Figure 4-3].

Figure 4-3 Argon controlled atmosphere glove box.. The water and oxygen level was continuously monitored and kept below few parts per million by an active getter bed through which the argon was flowed.

7. The caps were welded on the thin wall tube and on the filter in order to attach the three parts together, as shown in Figure 4-1. Initially the welds on the thin wall tube, the cap and the filter was done using a WeldLogic orbital tube welder. It was chosen to try a “in-house” welding solution to reduce the contamination of the hydride material by doing the weld in the inert atmosphere. Out of the ten actuators built (4 with Uranium, 4 with ZrNi and 2 with the SAES 172) only two were built in this way, one with uranium [U-1] and one with ZrNi [ZrNi-1]. It was very difficult to reproduce the weld with the same welding schedule. In fact, the orbital arc welder requires a fine tuning of many parameters (the material of the weld parts, the gap between the tungsten and the elements, the welding gas, currents and timing, etc). The tolerances (especially the tight fits), given the dimension of the parts, played an important role. A small region where the parts were not in perfect contact would cause an overheating of the cap and consequently a hole. It was then decided to e-beam weld the parts. The actuators were assembled inside the argon inert atmosphere chamber and then bagged. The bags were open for the e-beam welding. Immediately after the e-beam weld the actuators were mounted on a valve and helium leak tested. After the leak test the actuators were left under vacuum by closing the valve. On the uranium and on the SAES 172 actuators the heater support and the heaters were then welded on the top of the cap before reintroducing them into the argon atmosphere. The ZrNi actuators were instead re-inserted immediately into the argon atmosphere chamber. The heater and the temperature sensing on the cap will be described in 4.5.

8. The actuator test unit was assembled inside the inert atmosphere chamber. It was then removed and connected to a pumping station, leak tested and baked out under vacuum at 250 C overnight to reduce the gases adsorbed on the internal surfaces of the test actuator assembly. The test actuator unit was then ready to be filled with hydrogen and to be tested.

4.4 Hydrogen reaction and filling procedure

The hydrogen quantity absorbed by the metal system is an important parameter in the definition of switching operation. The system shown in Figure 4-4 was used to fill the actuator test sorbent material to its proper concentration.

The II (secondary) reference volume (218.75 cc) and the line volumes were initially calibrated against two primary reference volumes of 294.35 cc and 534.19 cc using research grade argon. Argon was then evacuated and the pressure transducers of the

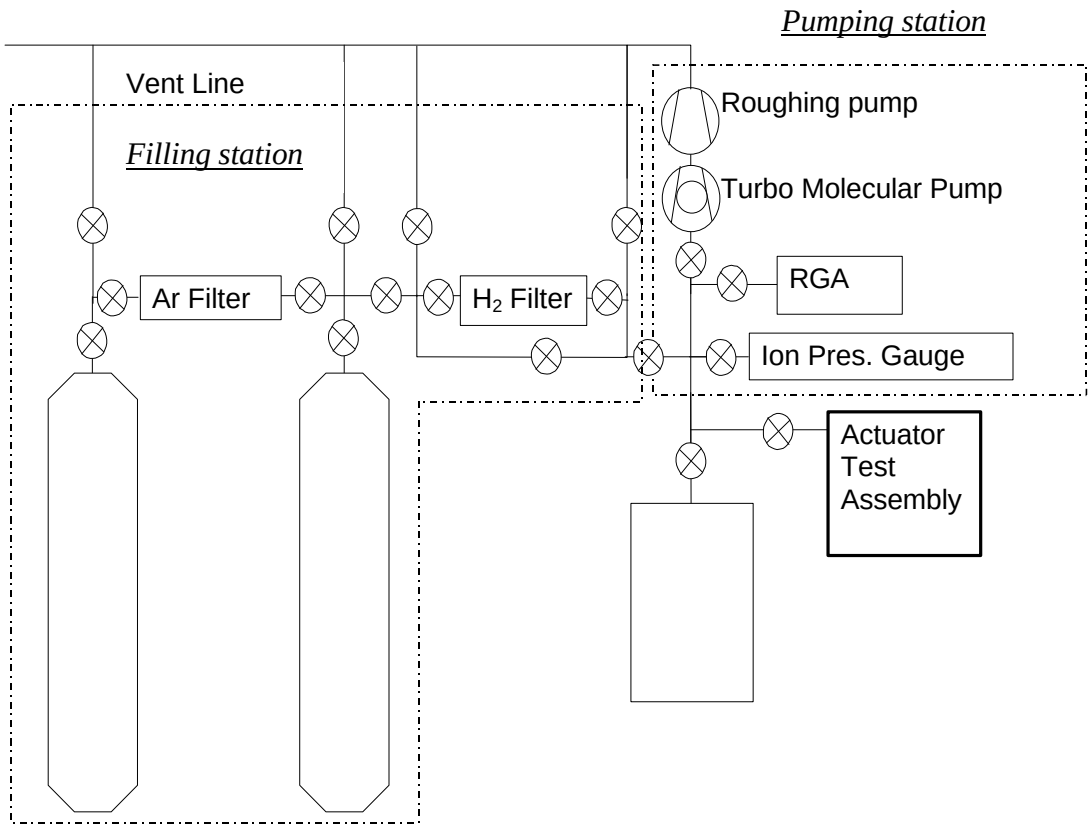

Figure 4-4 Hydrogen filling-pumping station

II reference volume and of test actuator assembly were zeroed against the Bayard - Alpert ionization pressure gauge mounted on the pumping station. Hydrogen was then flowed through its proper filter and purification apparatus to the II reference volume and its accessing valve was closed. The known amount of hydrogen was then expanded to the actuator test assembly and absorbed by the metal system.

The hydrogen reaction operation was usually repeated twice on each actuator for two reasons: 1) to remove some impurities that could have formed during the hydride formation, especially for ZrNi, and 2) to expose to hydrogen clean metal by cracking the initial metal pellet. [see section 1.4]. After the first reaction the material was heated up to a temperature above 300 C actively while pumping on it for 1 hour. Table 4-1 the hydrogen quantity absorbed by each actuator test are reported.

Test Actuator	Sorbent Quantity	Assembly Volume	H_2 Absorbed	[H/M]	H_2 left for cycling	[H/M]
	[g]	[cc]	[mg_H]		[mg_H]	
ZrNi-1	0.280	189.05	4.94	2.6		
			4.82	2.6	2.55	1.4
ZrNi-2	0.275	195.61	5.20	2.8		
			4.88	2.7	2.97	1.6
ZrNi-3	0.280	200.19	5.18	2.8		
			4.99	2.7	2.75	1.5
U-1	0.50	184.40	6.25	3.0	6.25	3.0
U-2	0.401	194.15	5.00	3.0		
			4.32	2.6	4.86	2.9
					3.68*	2.2*
U-3	0.411	186.75	4.85	2.8		
			4.82	2.8	3.32	1.9
St172-1	0.28	195.96	5.19	18.5 mg/g	2.84	10.14 mg/g

Table 4-1 Hydrogen quantities absorbed by the actuator tests. The [H/M] ratio has not been calculated for the St172 because it is a multi-phase metal system. The H_2 amount left in the test assembly has been calculated by subtracting the removed H_2 from the first absorption hydrogen amount

[The quantity in U-2 has been reduced during the actuator life testing].*

After the material had reacted for the second time some hydrogen was removed in order to fill the actuator with the proper amount of hydrogen. The actuator was then ready to be instrumented and tested. The temperature sensor was mounted on the top of the cap after the filling operations.

It is interesting to note that hydrogen quantity absorbed by the St172-1 at room temperature is very similar to the estimate made on the manufacturer's data composition.

4.5 Actuator Instrumentation

There are three major requirements for the temperature sensor and the heaters: (1) a small thermal mass, (2) the ability to sustain the ON state temperature and (3) a good reliability. Based on these requirements, platinum resistance thermometers (PRT) were selected for both the temperature sensors and for the heaters. The heaters had to satisfy the additional requirement of a high flat surface-to-volume ratio for heat transfer optimization.

	Configuration [dim. in mm]	**Temp. Range**	**Mass** [g]	**Area** [mm^2]
F3101	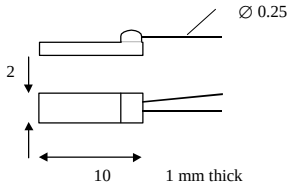	-50 to 600 C	0.09	20
F3102	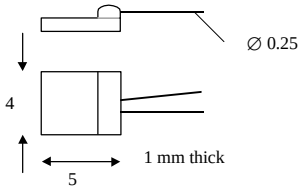	50 to 600 C	0.09	20
F3105	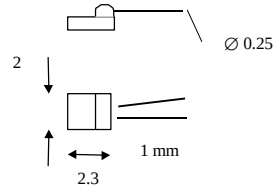	50 to 600 C	0.05	4.6
WS81	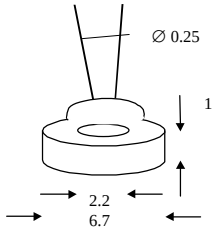	50 to 850 C	0.31	31

Table 4-2 PRT characteristics and dimensions.

For this reason F3101, F3102 and WS81 OMEGA (characteristics are reported in Table 4-2) were considered and initially tested to verify the maximum power that they could supply. The PRTs were attached to a large aluminum bar (5.48 cm diameter, 35 cm length). By measuring the power and the resistance of the heater, the Power vs. ΔT curve

was determined as summarized in Figure 4-5. The ΔT is defined as the difference between the PRT temperature derived from its resistance and the temperature of the aluminum bar. Thermal grease (AREMCO 640 Heat away) was inserted between the heaters and the aluminum bar to increase the heat transfer rate between the PRT surface and the aluminum bar.

F3101 and F3102 have the same surface area (20 mm^2) but there is almost a factor of two difference between the two heat conductances. The heat transfer not only depends on the surface area but also on the layout of the resistance embedded in a ceramic body. The temperature gradients between the heater and the cap are considerable and will affect the PRT attaching technique and the selection of media used to attach them. The PRT selected as the heater, the attaching technique and the powering circuit to it will determine the electrical power dissipation of the element and the heat carried to the hydride container.

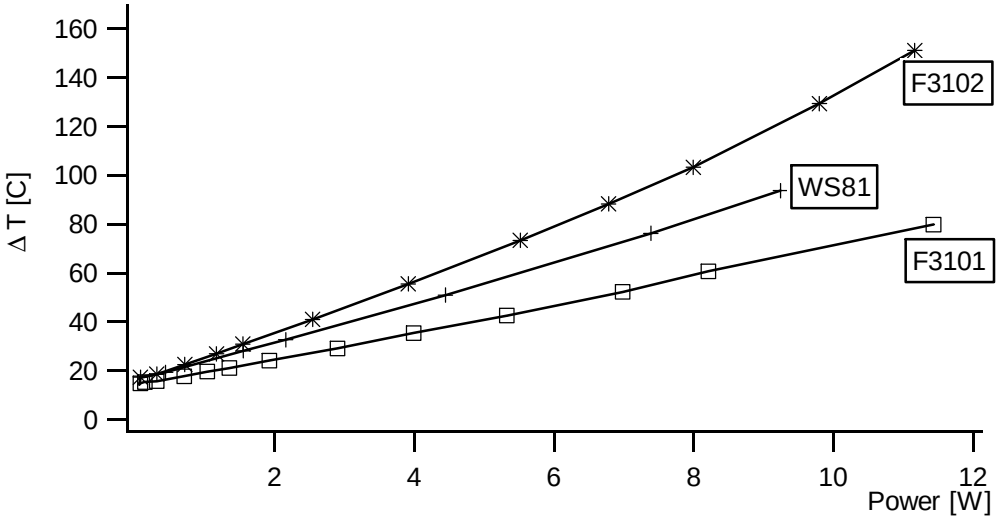

Figure 4-5 DT across the three heaters as a function of power transferred.

The powering circuit was designed to simulate, with a simple circuit, a constant power supply [see Figure 4-6]. It was decided not to use a power supply for each actuator in order to reduce costs. A variable resistor was used for the fine-tuning on the supplied power. The power supplied to each actuator is determined by measuring the Power Supply voltage and V_{R2} and by the values of the variable resistor, R_1 and R_2.

The power supplied to the heater depends on three parameters: the power-supply voltage, the variable resistor and the temperature of the heater itself. The temperature of the heater determines its resistance and consequently the power dissipated by it.

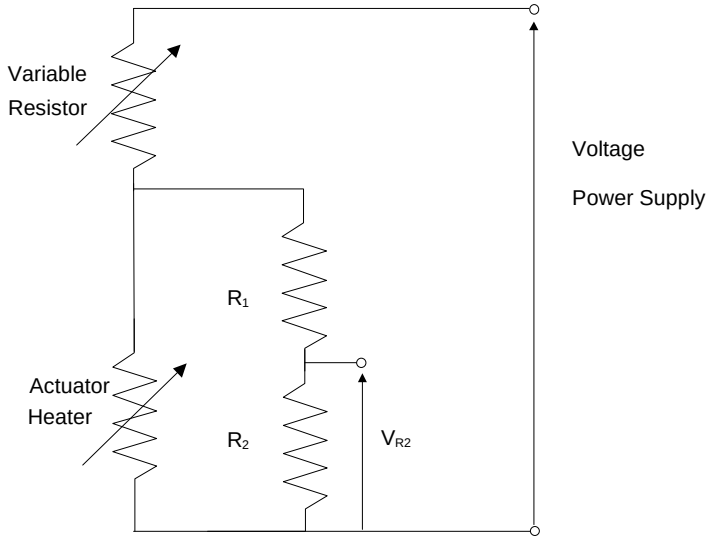

Figure 4-6 Power heater circuit. The power on the Actuator Heater is determined by measuring V_{R2} and the voltage Power supply and by initial measure of the variable resistor and of R_1 and R_2

According to the two substantially different heater configurations, two independent power supplies were used: (1) a Kepco 125-60 M for all the ZrNi actuators and Uranium 1 and (2) a Lambda LH 128 AFM for St-172 and Uranium 2 and 3. The stability of the two power supplies has been verified by conducting tests for one month giving a ±0.05 % variation around the setting voltage for the Kepco kept at 22.05 V and a ±0.8 % variation for the Lambda kept at 36.5 V.

The heater temperature is related to the entire actuator thermal distribution summarized in Figure 4-7. The actuator assembly, the temperature sensor, the heater and the environment are connected by thermal heat conductances that define the heat transfer between the elements.

- The heat conductance from the heater to the cap, $G_{H\text{-}Cap}$, is related to the heater attaching media and on how the operation was performed. The $G_{H\text{-}Cap}$ is a very important parameter, as a poor heat transfer will require a higher temperature of the heater PRT, thereby increasing the possibility of exceeding the PRT maximum

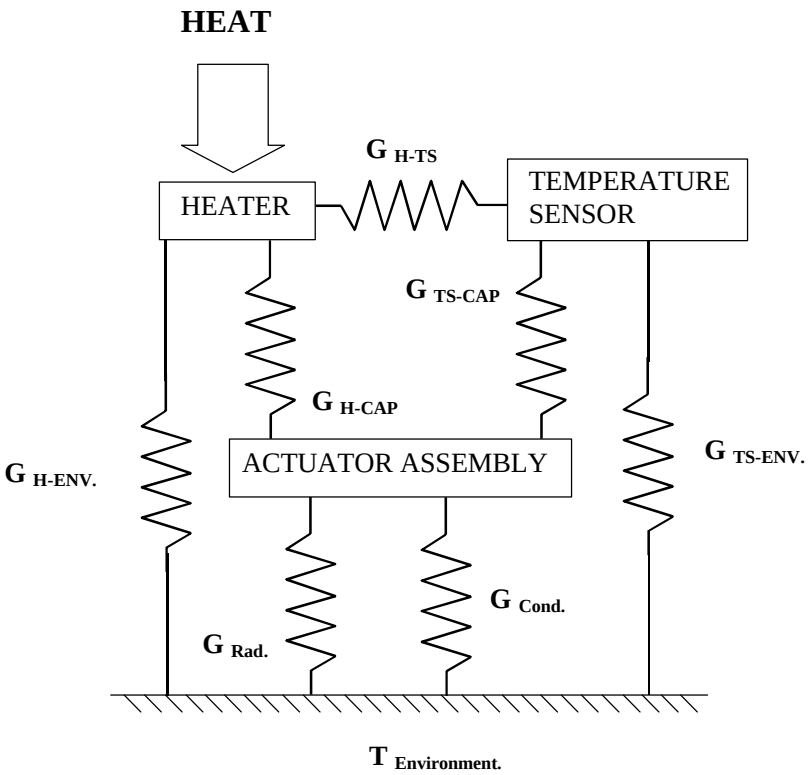

Figure 4-7 Heat conductance schematic

temperature. Depending on the actuator operation temperature different techniques were used.

- The heat conductance from the heater to the environment, $G_{H\text{-}Env.}$, depends on the surface of the heater element and the wiring to the power supply.
- The conductance between the temperature sensor and the heater, $G_{H\text{-}TS}$, depends mainly on their position on the cap and the media that connects them.
- The heat conductance between the temperature sensor and the environment, $G_{TS\text{-}Env}$, depends on the electrical wiring and on the surface of the temperature sensor element.
- The heat conductance $G_{TS\text{-}Cap}$ between the actuator assembly and the temperature sensor depends on the attaching media.
- The heat conductance from the actuator assembly to the environment was modeled in section 3.3 for each different material and can be split into the thin wall tube conductance G_{Cond} and the radiation coupling G_{Rad}.

The most important variable in the switch performance characterization is the temperature of the hydride material. Along with the hydrogen concentration it determines the equilibrium pressure of the hydrogen-metal system. In all the characterization and life data tests reported in the next chapter, the temperature of the hydride is assumed to be equal to the sensed temperature (i.e., it is assumed that the heat conductance $G_{TS\text{-}Cap}$ is very large).

It is interesting to see the effects of the of G_{Cond}, G_{Rad}, $G_{H\text{-}Cap}$ and $G_{H\text{-}Env}$ heat conductance variations on the power supplied to the actuators. As a general case, Figure 4-8 presents two curves, the heat supplied by the powering circuit, and the heat dissipated

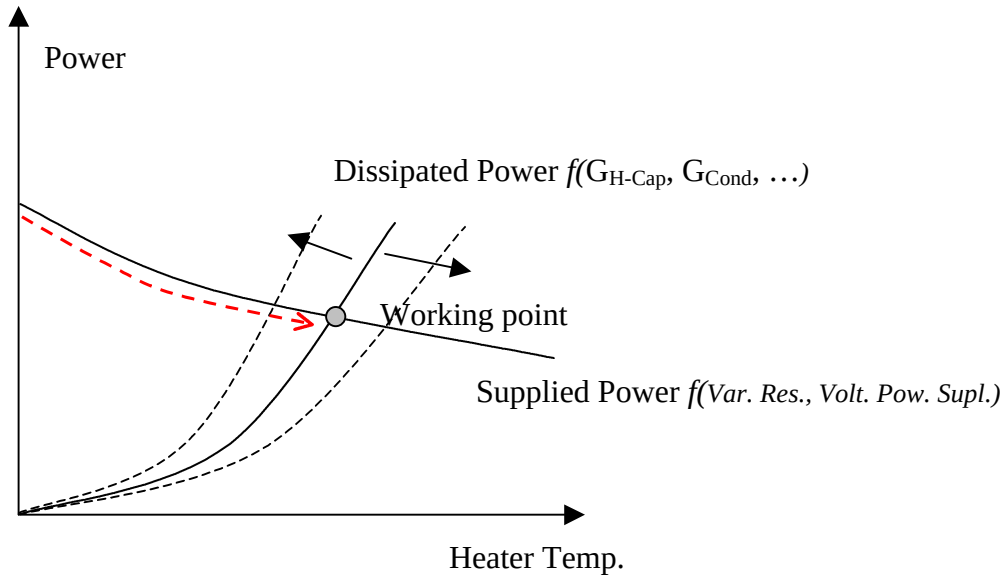

Figure 4-8 Heat supplied to the switch as a function of temperature. Effects of the heater attachment conductance and of the environment heat losses of the heater. The Power dissipated *is the heat dissipated by the heat switch [*Heat *in Figure 4-7]. When the heater is turned ON the power supplied to the actuator follows the dashed arrow, as a function of the heater temperature.*

by the actuator, as a function of the heater temperature. Their intersection determines both the power dissipated and the temperature of the heater/(s). Ideally, once the system is designed and set to work, the two curves should not move and their intersection should be fixed. However the heat conductances and the supplied power can change in time causing the working point to move. Many reasons could induce those variations, such as degrading of the heater attachment to the cap due to the thermal cycling, deterioration of the heater surface increasing the emissivity, etc.

An increase in the heat conductance from the switch assembly to the environment, either radiative or conductive, would cause the working point to move left, increasing the power dissipated and decreasing the heater temperature. The opposite effect would derive instead from an increase of the heat conductance from the heater to the environment. The effect of the variation of the heater attachment to the cap would, instead, move the working point to the right, increasing the heater temperature and decreasing the power dissipated. Working point variations can be caused also by changes in the supplied power curve deriving from resistance changes and power supply voltage fluctuations.

When the heater is turned ON, its temperature is equal to the radiator temperature. The initial power supplied to the heater is the intercept on the y axis of the supplied power. As soon as the heater gets hotter, the power decreases asymptotically reaching the working point shown in Figure 4-8.

4.5.1 ZrNi heater configuration

The ZrNi actuator heaters and temperature sensors were located on the cap of the actuator assembly as shown in Figure 4-9. They were attached with a high temperature epoxy, AREMCO 805 to the cap and cured according to the manufacturer indications. The epoxy used is aluminum filled and according to the manufacturer, can stand 300 C. It has a thermal conductivity of 21.6 W/mK defining a heat conductance in the glue line (0.02 –0.12mm) of 21.6-3.6 W/K . Considering the power supplied to the switch there will be a ΔT of less than 1 C between the surface of heaters and the cap.

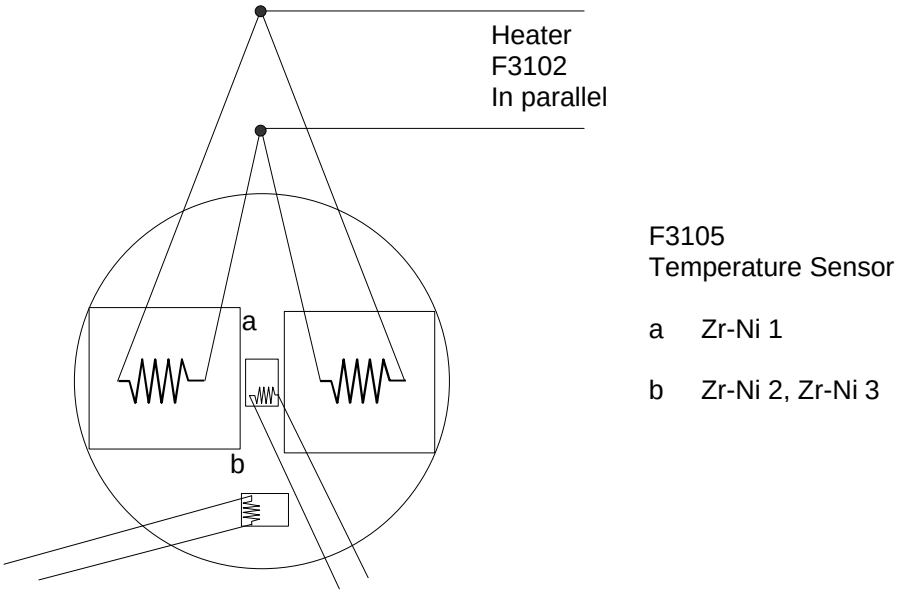

Figure 4-9 Heater and temperature configuration for the ZrNi actuators

The two F3102 heaters leads were crimped together using a small iron cylindrical tube (2 mm external diameter, 0.1 g) and two Nichrome V Pyre-MLH-MIL coated wires (0.25 mm diam. and 20 Ω/m.) were used to connect the heaters to the power supply connector. Nichrome V was chosen to minimize the heat losses in the wires. Each F3105 temperature sensor lead was crimped to two copper wires (0.1 mm diam.) for a 4 wire resistance measure. Considering an alumina specific heat of 1.1 J/gK, the thermal mass of the heater and of the temperature sensor is 0.25 J/K and the estimated thermal mass of the switch assembly of 0.85 J/K, below the estimated value during the switch modeling and design (1.1 J/K). As a result, according to the modeling diagram [Figure 3-8], the three ZrNi actuators are expected to have a lower *Total Power* (4.7 W) and a higher *Margin* (0.46) than the predicted values in section 3.3.1.

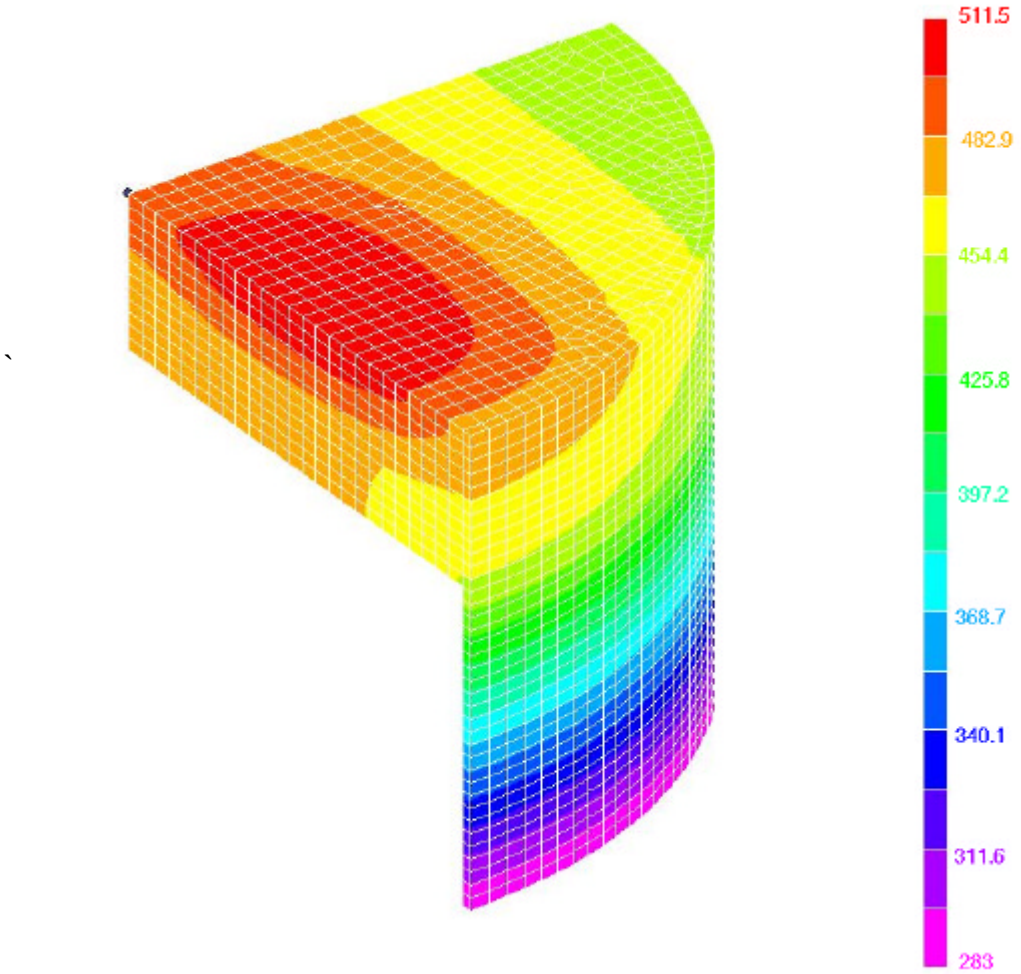

Figure 4-10 Finite element method analysis of the temperature distribution [K] in the ZrNi actuator. Considering the symmetries only a quarter section of the switch assembly has been analyzed. The heater has been modeled as a uniform heat flux generator (3.2 W on the 2x20 mm^2 heaters area). A constant 1.6 W/mK hydride thermal conductivity has been assumed [31]

ZrNi-1 has been the first ZrNi test assembly to be built with three heaters F3102 mounted on the cap with the temperature sensor in the center. During the wiring one of the heater wire broke and the defective heater was removed. A finite element model was used to predict the thermal gradients in the ON state. A JPL staff member, Anthony Loc, performed the analysis using ANY-NASTRAN (finite element solver) and FEMAP (pre and postprocessor). The modeled temperature distribution is reported in Figure 4-10. According to the finite element analysis, the temperature sensed on ZrNi-1 (position "a") is expected to be closer to the heater temperature than to average material temperature (better sensed by the thermometer in position "b", as on ZrNi-2 and ZrNi-3). The temperature sensor in the "a" position shown in Figure 4-10 is located in the center of the actuator assembly which is the hottest spot on the part of the cap not covered by the heaters. Consequently, it can be indicative of the stability in time of the heat conductance between the heater and the cap, $G_{H\text{-}Cap}$, and the heat conductance between the heater and the environment, $G_{H\text{-}Env}$.

4.5.2 Uranium and St 172 heater configurations

The high temperature required for the uranium and St 172 ON states was difficult for the heater attachment to withstand and there were many failed attempts before settling on the final technique. Initially the AREMCO 805 epoxy was used but it could stand only few cycles before detaching from the cap due to the high ON state temperature. Several cements (AREMCO CERAMABOND 503 and 571, OMEGA OMEGABOND 400) and

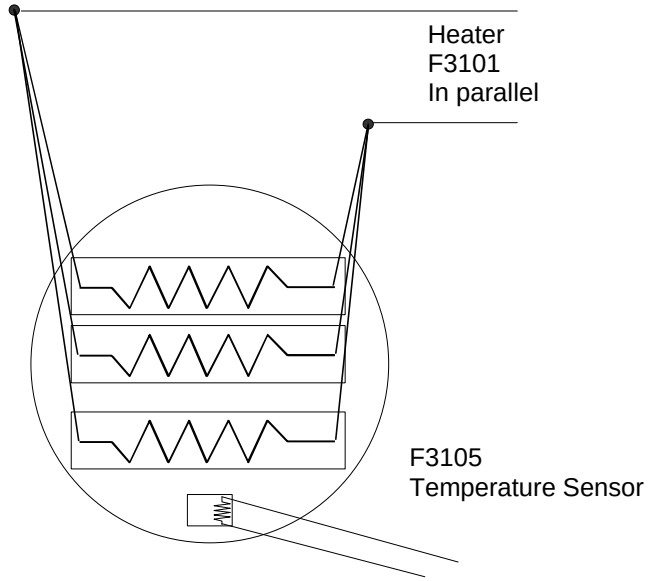

Figure 4-11 Heater and temperature configuration for Uranium test sample (U-1)

their combination were tested, but the difference in C.T.E. (coefficient of thermal expansion) between stainless steel and the PRT's alumina body caused the attachment to degrade after a few cycles. The difference in temperature shrinkage between stainless steel and alumina was particularly evident during the ON-OFF switching operation. The metal cap, coupled to the cold sink by the thin wall tube, was cooling faster than the alumina thereby amplifying the thermal expansion difference. Only unit U-1 survived more than few hundred cycles with the heater configuration reported in Figure 4-11, where the F3101 PRTs were embedded in the cement. In this configuration the heat transfer from the heater to the cap is very efficient; the heaters cover 50% of the cap area. Therefore there should not be large thermal gradients in the switch assembly and the temperature sensed should be very close to the hydride temperature.

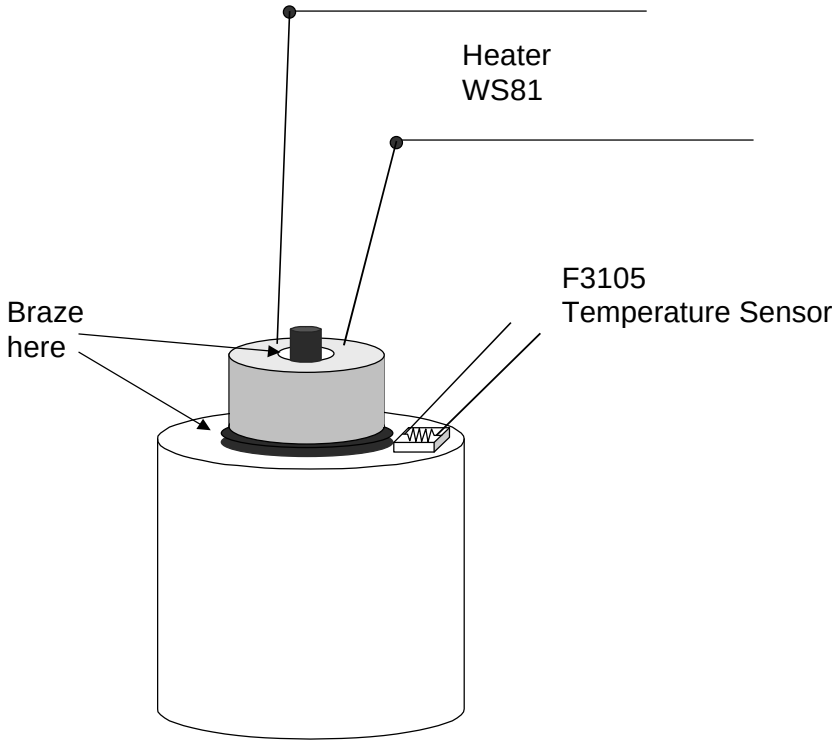

Figure 4-12 Uranium and St 172 heater and temperature sensor attachment.

The data on U-1 presented in section 5.2 are the only those obtained using the final PRT attachment technique. The previous data (around 300 cycles) have not been reported because they are strongly affected by the quick heater attachment degradation.

In addition, the heater's configuration difference did not allow a confident comparison of the initial data with the ones obtained by the final technique.

The other actuators for uranium and St172 were heated using WS81 OMEGA mounted on a copper post [see Figure 4-12]. The copper post was brazed on the cap using a high temperature brazing material (600 C liquidus temperature). The WS81 heating solution, compared to the ZrNi configuration, substantially increased the thermal mass of the hydride containment structure (1.2 J/K) considering that the heater has a mass of 0.31 g and the copper post an average mass of 0.22 g. The heater brazing attachment is however more robust than the epoxy or cement configuration and it can be considered as the first step towards the development of a heater configuration sufficiently robust for space flight. The WS81 holding structure imposed mechanical stresses on the ring-shaped PRT that could eventually break its internal resistance.

The WS81 heating configuration has also been modeled by finite elements method to estimate the thermal gradients in the actuator assembly. The modeling, as for the ZrNi heater configuration, was performed using NASTRAN. Considering the axial symmetry of the assembly only a sector as been modeled and the results are reported in Figure 4-13. A more uniform temperature distribution can be observed in the hydride compared to the ZrNi distribution.

The robustness of the WS81 heater configuration was tested on an empty actuator, lately referred as heater-test, instrumented with a temperature sensor and with a WS81 in positioned as in the St-172 and U-2, 3 heater configuration [Figure 4-12].

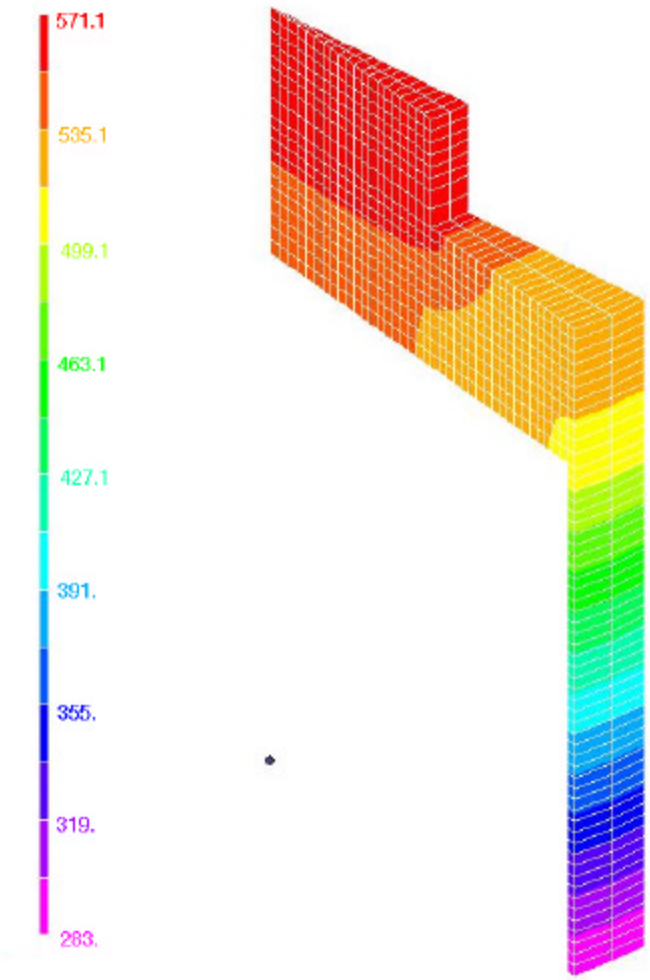

Figure 4-13 Finite element method analysis of the temperature distribution [K] in the WS81 heater configuration. Considering the axial symmetry only a sector of the switch assembly has been analyzed. The heater has been modeled as a uniform heat generator (3.6 W). A constant 1.6 W/mK hydride thermal conductivity has been assumed [31]

The heater-test was thermally cycled ON-OFF for more than 5,400 cycles before the heater failed. The test provided informative results concerning the heating supply degradation. The highest temperature achieved decreased cycle by cycle. At the beginning of the life test the heater-test maximum ON temperature was set to 350 C and the temperature gradually decreased to 246 C, as shown in Figure 4-14.

The decrease in ON state temperature can be related to the degradation of the thermal contact between the heater and the cap, $G_{H\text{-}Cap}$, and to the increase in the heat losses to the environment. In fact, it was noted that the surface of the WS81 became

gradually darker and darker, probably due to the residual of the acid flux used during the brazing operation. A darker surface promote an increase in the $G_{H\text{-}Env}$, that decreases the power going to the actuator assembly and consequently lowering its temperature.

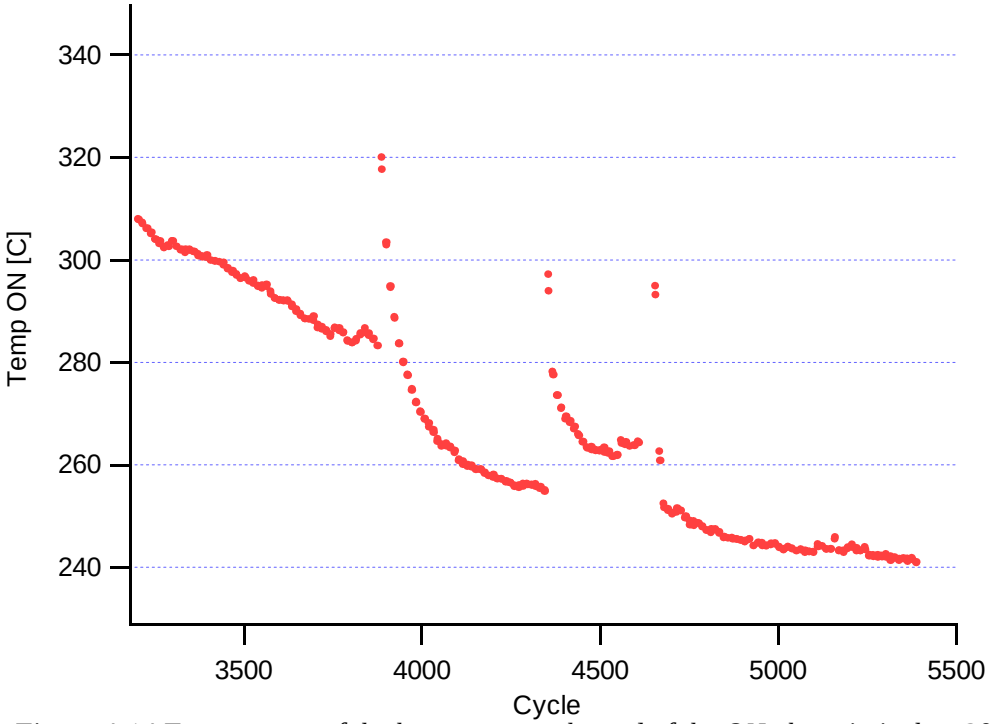

Figure 4-14 Temperature of the heater-test at the end of the ON phase in its last 2000 cycles.

It is also interesting to observe the spikes in the maximum temperature Figure 4-14. They correspond to the first cycles run after the vacuum chamber was exposed to air. It is proposed that the water vapor adsorbed on the contact surface between the heater and the cap would improve the heat transfer between the two. Each time the heater would get hot some vapor would be released by the surface and pumped out by the system used to keep vacuum in the chamber. The same phenomenon was observed on the actuator tests [as also reported in section 5].

After the heater failure, the heater was removed and its surface was examined on a microscope to verify if mechanical fractures could have determined the rupture of the resistance inside the alumina body but no evidence of mechanical fractures were found

OMEGA F3105 PRT's were used as temperature sensors and they were cemented using AREMCO CERAMABOND 571.

4.6 Test layout and data acquisition

The actuator test assemblies were mounted on a copper support inside a vacuum chamber. The copper support was used to establish a thermal sink acting as the radiator reported in the Figure 4-2. An external temperature controlled water cooler kept the copper plate at a temperature of 10 C. Figure 4-15 shows the copper support slots for the switch actuators and several of them connected.

During the initial characterization of the actuator, information were recorded when the operator verified that steady state conditions were reached for each set of measurements: temperature, power and pressure. The life test, which in November 1999 is still going on, was instead unattended and was set up to save *x* cycles of data every *y* cycles (*x* and *y* were set by the operator, normally 2 cycles every 10 cycles). The data acquisition system was used to constantly monitor the actuator temperature, the voltage on the heater, and the pressure. Almost all the actuator test assemblies were equipped with two pressure transducers to monitor precisely the ON and the OFF pressure; a 266 Pa [2 Torr] and a 13.3 kPa [100 Torr] range MKS Baratron capacitance manometers.

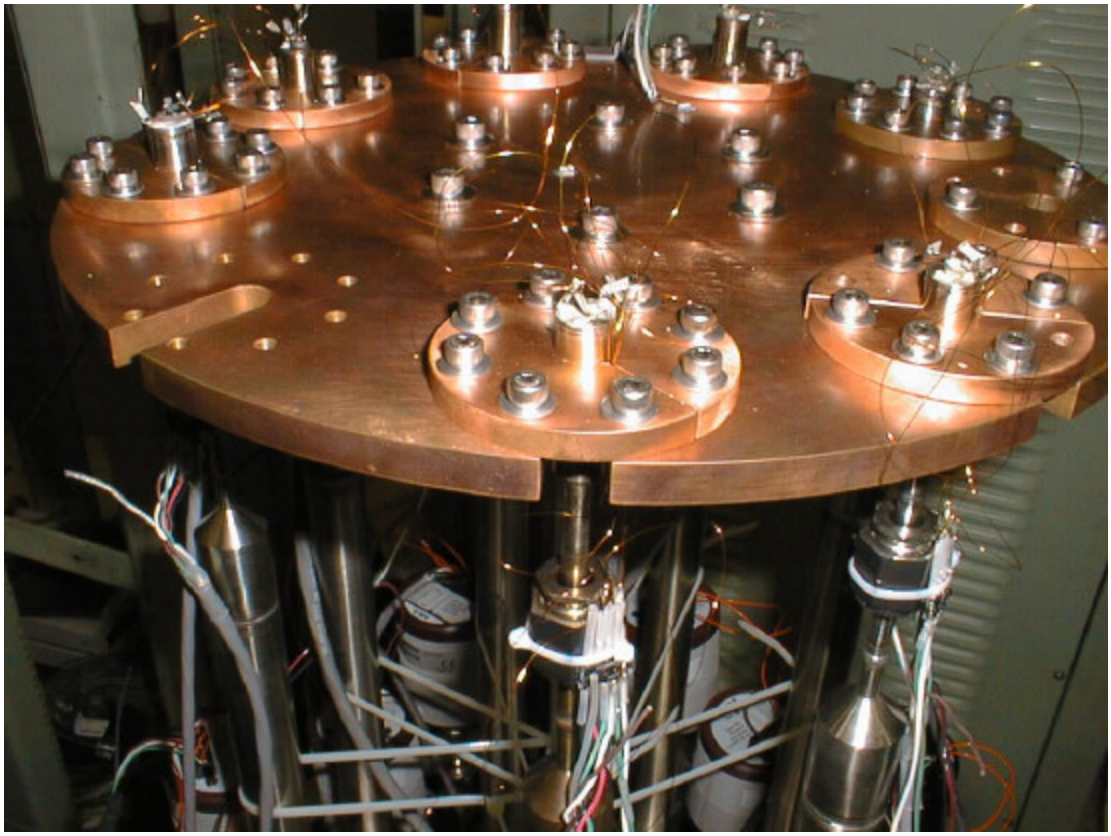

Figure 4-15 Actuator test assemblies in the vacuum chamber.

U-1 was equipped with only the 13.3 kPa pressure gauge and ZrNi-3 was equipped with a 13.3 kPa and a 1.33 kPa for specific laboratory circumstances. It was decided not to upgrade ZrNi-3 and Uranium 1 once they were in testing. To be upgraded the actuator test assemblies would need to be disassembled inside the argon controlled atmosphere to avoid contamination of the hydrides. Moreover a successive reactivation of the hydride material would be needed erasing the previous hydride history.

5. Experimental Results

The test assemblies have been initially characterized by measuring the pressure-temperature-power relationship to verify the hydride behavior and to produce reference points for the life-test data analysis. The characterization data were also compared to the literature van't Hoff absorption and desorption data. If the hydride were isothermal and its temperature were coincident with the temperature sensor measurement, the characterization data should coincide the desorption van't Hoff line. However no precise agreement is expected. In fact, it has been observed in the previous section that there are thermal gradients in the hydride material and that the temperature sensor is not closely monitoring the average hydride temperature.

After the initial characterization the test actuators were cycled for several months with few interruptions. However, each time a new assembly was built and was ready to be cycled, the vacuum chamber had to be opened. The life testing was therefore stopped for usually one to two days. The vacuum chamber was then closed again and the test cycles were restarted. A summary of the life cycling for each selected sorbent material data is reported and discussed in the following sections. Objective of the life testing was to verified the performance variation in time in the actuators. The summary of the life testing results consist of the analysis of the steady states reached at the end of cycle phases (both ON and OFF) in terms of pressure, temperature and power and a comparison of specific cycles to verify dynamic behavior changes. The test ON-OFF phase times were tuned separately for each actuator test according to its own kinetics. We try to minimize the ON-OFF cycle times to accelerate the life cycling tests (i.e. increase the total number of cycles).

The evaluation of the actuator has been performed to summarize all the cycle data. The same criteria used in the alternative evaluation has been adopted to verify how the actuators performed with respect to their initial estimates and how they changed their behavior over time. For each cycle, the *Total Power* and the cooling time *Margin* have been calculated. Considering that the test cycles were shorter than the sorption cooler cycles, it has been assumed that the heat conductance reached at the end of the test cycle was the equilibrium heat conductance.

5.1 ZrNi test results

5.1.1 Initial Characterization data

For the three ZrNi actuator test units, pressure vs. temperature curves are shown in Figure 5-1. The data points are well fitted by a line, but they do not closely resemble the literature data reported [77]. ZrNi-2 and ZrNi-3 curves are located between the absorption and desorption curves reported by Luo et al. [77]. Furthermore, their slopes are very similar to the Luo derived data for absorption. ZrNi-1 curve is instead located below the data of Luo et al. At the same measured temperature the equilibrium pressure is lower. It is interesting to note that at low temperatures the ZrNi-1 curve is located between the two literature data representative curves. It is believed that the characterization data discrepancy can be attributed to the different locations of the temperature sensors on the top of the switch assembly. It has been observed (as shown in Figure 4-10) that there is a temperature difference between the two temperature sensor

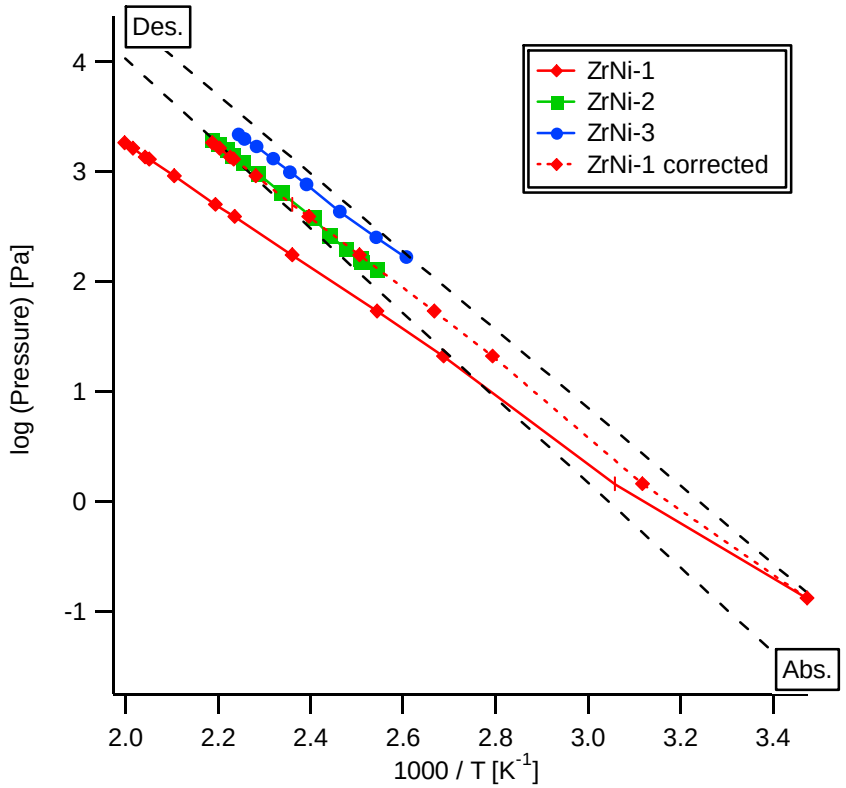

Figure 5-1 ZrNi characterization data: van't Hoff plot. The black dotted lines are the Luo's [77] absorption and desorption data. The red dotted line is ZrNi-1 with the temperature correction

locations of about 40 K at the same input power of 3.2 W. By proportionally scaling the temperature difference between the two sensor's location on the power supplied to the ZrNi-1 actuator, it is possible to correct the ZrNi-1 temperature, using expression Equation 5-1.

$$T_{Corr} = T_{Measured} - \frac{40}{3.2} Power \qquad \textit{Equation 5-1}$$

where $T_{Corr.}$ is the corrected temperature, $T_{Measured}$ is the ZrNi-1 temperature measurement and *Power* is the heater power supplied to the actuator. In Figure 5-1 it is shown that, when the initial ZrNi-1 characterization pressure is plotted as a function of the corrected temperature the new line lies on top of the ZrNi-2 line.

According to the present actuator characterization data, by interpolating the characterization data lines (with the least square minimum method) and extending the interpolated lines at low pressures it is possible to estimate the temperature required to reach 1 Pa [7.5 mTorr], the OFF pressure requirement. The required temperature is 317 K for both ZrNi-1 and ZrNi-2 (1000/T=3.15 K^{-1}), and 302 K for ZrNi-3 (1000/T=3.31 K^{-1}). The fact that the required temperature to reach 1 Pa is identical for ZrNi-1 and ZrNi-2 confirms that the difference in the characterization line between the two is determined by the temperature difference on the cap. It is suggested that the small temperature difference (about 5%) between ZrNi-3 [1.5 H/M] and ZrNi-2 [1.6 H/M] are caused by small differences in the temperature sensor positioning.

5.1.2 Life data analysis

The three ZrNi actuators have been cycling for several months and they will continue cycling up to 25,000 cycles, if possible. The summary of the data that has been presented is referred to the ON and OFF steady state analysis and to the actuator kinetic comparison.

5.1.2.1 ON state

The three ZrNi actuators performance showed a maximum pressure decreasing with continuous cycling, decreasing almost 40 % in pressure. The performance degradation has been found not to be primarily caused by changes in the hydrogenation behavior of the sorbent alloy, but rather to the decrease in the maximum temperature of the ON state.

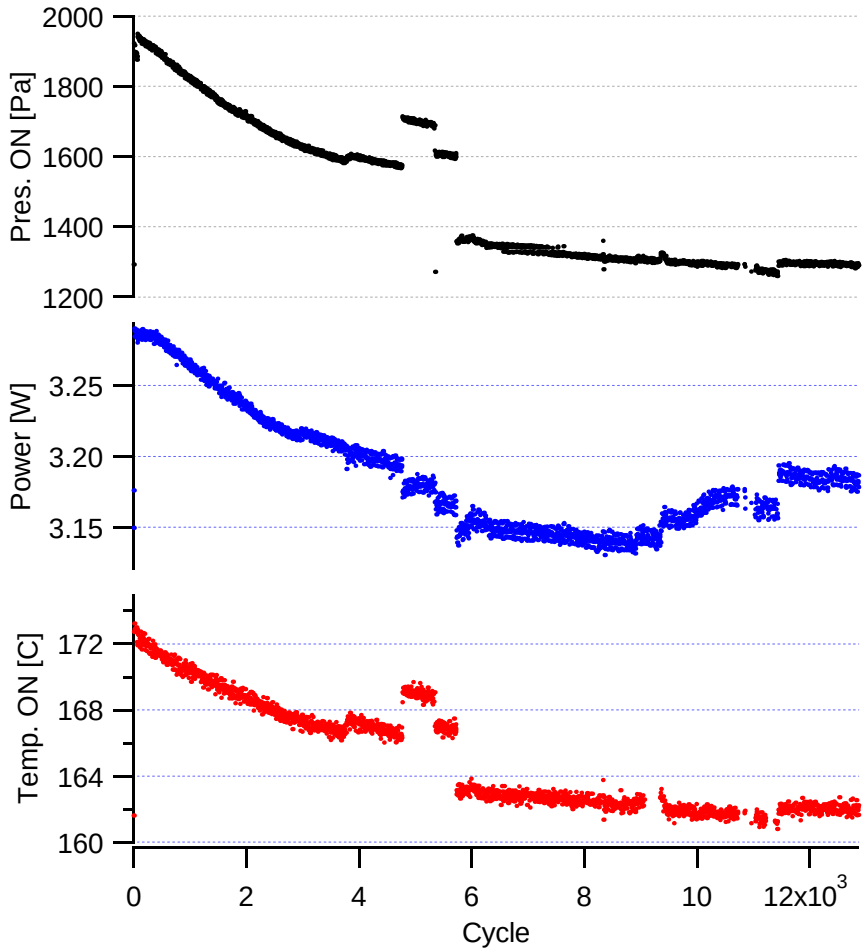

Figure 5-2 Pressure, Power and Temperature at the end of the ON phase for the ZrNi-3 actuator.

Figure 5-2 shows the how the pressure decreased in 12,000 cycles for unit ZrNi-3. The two major discontinuities correspond to repositioning of the switch assembly in the test chamber. In fact, ZrNi-3 was removed twice during life testing: once to verify and recalibrate its pressure transducers and once to analyze the residual gas of the OFF state [see section 5.1.2.2]. The copper clamps holding the switch assembly to the copper chilled plate were not welded to the actuators [see Figure 4-15]. The heat transfer from the sorbent containment to the chilled plate, is therefore affected by the thermal contact between the copper clamp and the connecting tube. The same contact between the two parts couldn't be reproduced each time the test assembly was placed in its proper location, causing the discontinuity in the switch behavior.

It is also interesting to note in Figure 5-2 how very small changes in the power supplied to the heater, (i.e., or in the order of less than 3 %) generate a significant

pressure change. A small temperature decrease, derived from the reduced supplied power, induce a large variation in pressure as expected since log(Pressure)$\propto T^{-1}$ (T is the absolute temperature).

The role of the ON-state temperature variation in the ON pressure is made more clear by plotting pressure and temperature ON state data in a van't Hoff diagram, as Figure 5-1. In Figure 5-3, the temperature and the pressure at the end of the ON state are reported with the previously determined ZrNi-3 characterization line. The narrow axis ranges can mislead the close proximity of the set of points and the characterization line (presented in the expanded view). But the major evidence for the pressure dependence on

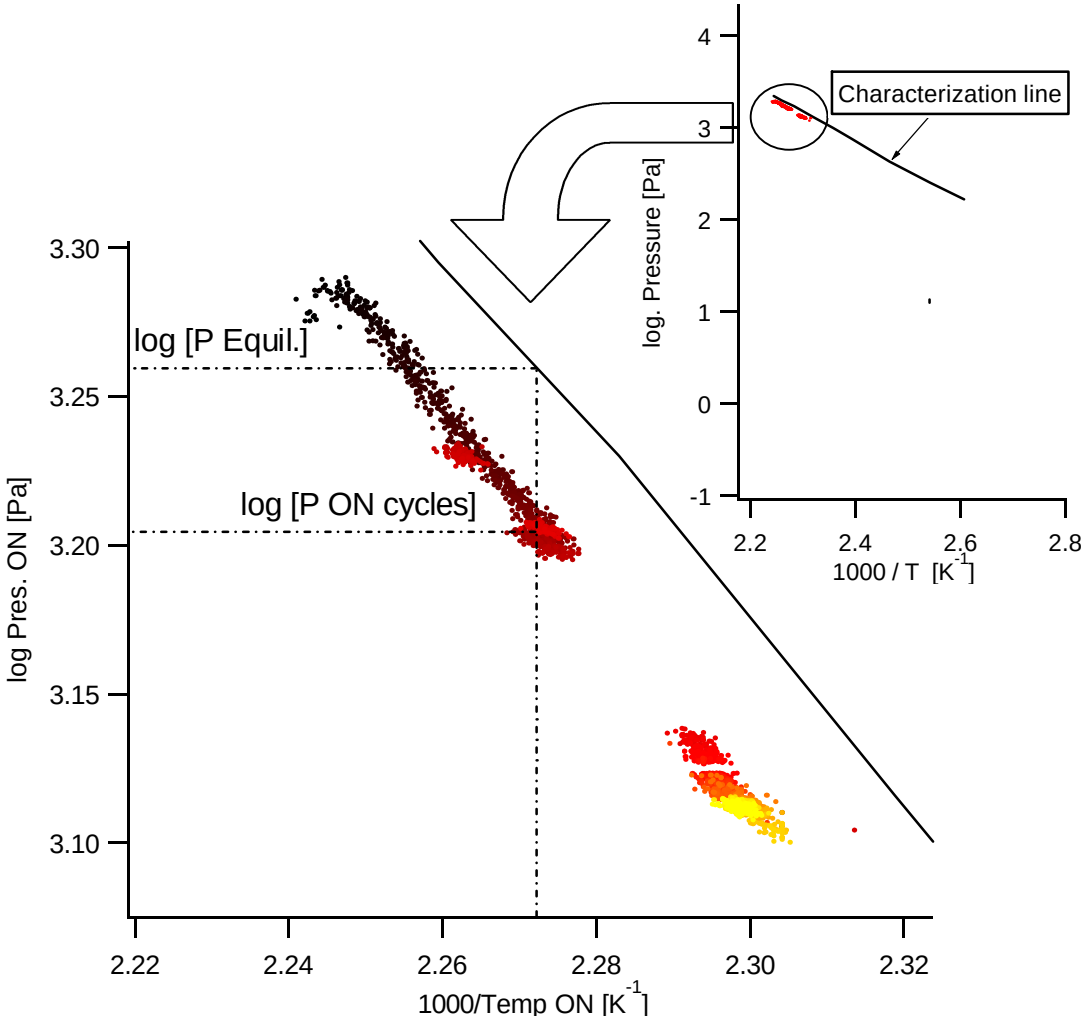

Figure 5-3 Pressure at the end of the ON phase versus 1000/T for the ZrNi-3 actuator. The red color intensity increases as a linear function of the cycle number.

temperature is the strong similarity of the slopes. In fact, the actuator ON state points are parallel aligned to the characterization line. Furthermore it should be noted that at any temperature corresponding to the ON pressure, the pressure for the actuator is always below the initial characterization line, indicating that equilibrium pressure is never reached at the end of the ON phase of each cycle.

The monitored voltage variations of the power supply have not been considered as the source of the power decay because they [see section 4.5] were symmetrical around the set value 22.05 V and therefore would have generated symmetrical oscillation in the power dissipated [see Figure 4-8]. Assuming that the temperature sensor is working properly, it is believed that the decreasing in power and temperature is caused by the deterioration of the heater attachment to the cap due to the thermal cycling [the reliability of the temperature readout is derived by observing the operational stability of the sensor during the whole life test].

It has been observed in section 4.5 that when a lower power is supplied to the switch assembly the heater temperature increases [see Figure 4-8]. The temperature of the heater at the end of the ON state can be determined by the ON state power measurement. Considering the powering circuit presented in Figure 4-6, with a variable resistor value of 5 Ω, the two resistance R1 and R2. of 10 kΩ, the supplied power to ZrNi-3 is presented in Figure 5-4.

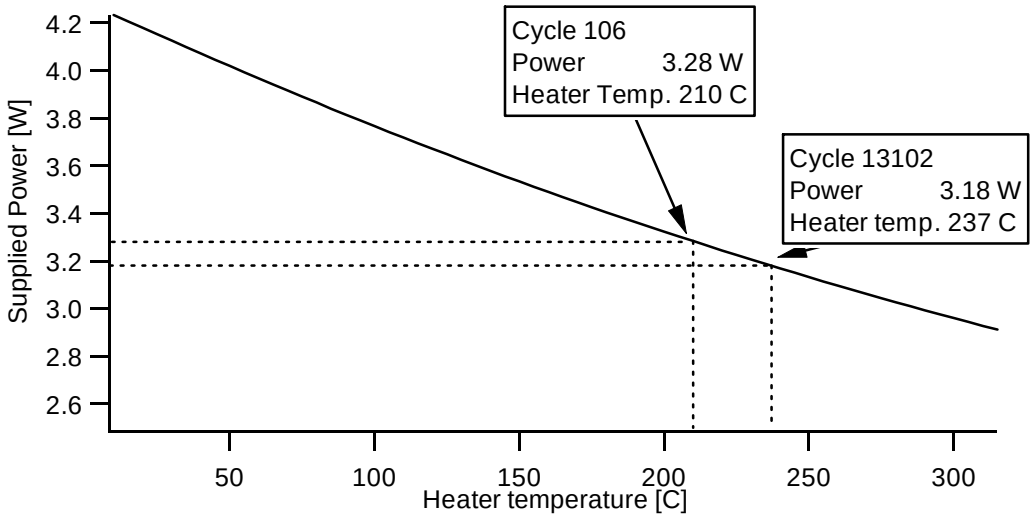

Figure 5-4 Power supplied to the ZrNi-3 actuator as a function of the heater temperature. The heater temperature for cycle 106 and 13102 are determined intercepting the supplied power curve at the ON state power of the two cycles.

The heater temperature increase could be caused by a degradation of either the heat conductance between the heater and the cap or the heat conductance between the cap and the environment. The temperature of the heater prompts one to estimate an upper limit of the heat losses from the cap to the environment at 10 C by radiation (assuming an emissivity of 1) and by conduction through the Nichrome wires (2 wires 0.25 mm diameter and 10 cm long) in 0.1 W at 210 C and 0.14 W at 237 C. The heat losses limit can be used to determine the $G_{H\text{-}ENV}$ ranges in the two cycles, respectively 0-0.0005 W/K for cycle 106 and 0-0.0006 for cycle 13102. The heat conductance ranges calculated by solving the conduction electrical analysis are presented in Figure 5-5.

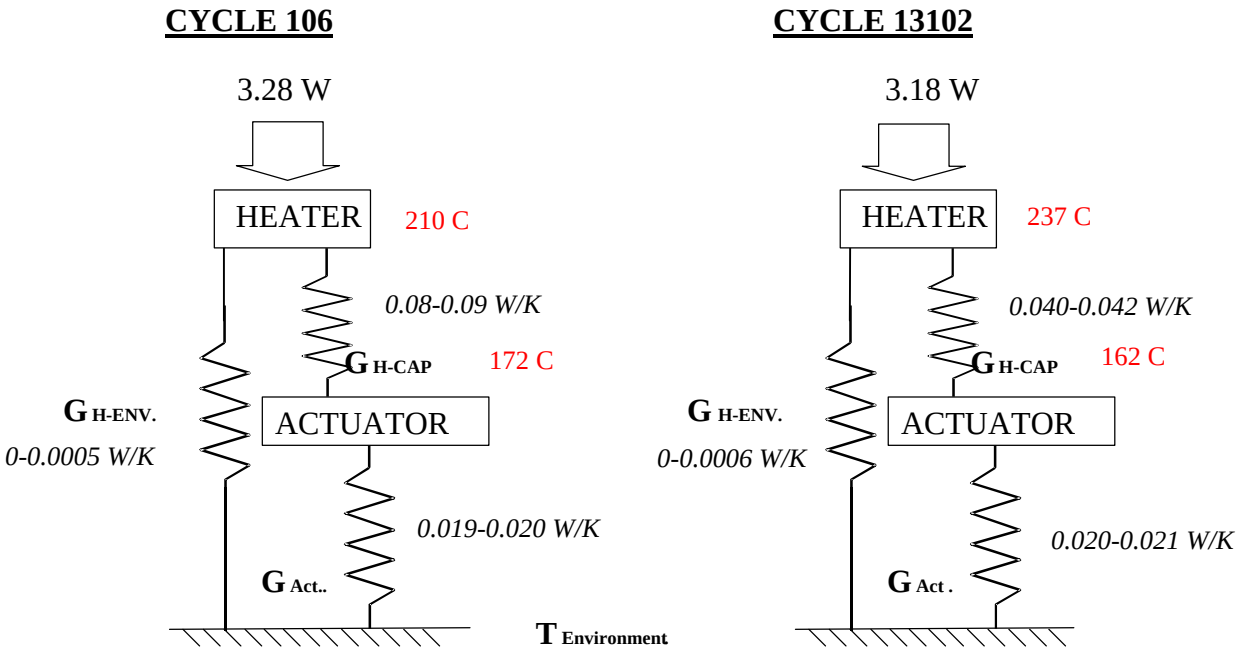

Figure 5-5 Heat conductance schematic of the ZrNi-3 actuator with the heat conductance estimation for the two selected cycles.

It is interesting to observe that the heat conductance from the heater to the cap decreases substantially in 13,000 cycles while the temperature of the cap increased. The heater temperature increasing phenomena was observed directly on ZrNi-1 actuator. In fact, it has been observed and initially verified during the characterization test that the ZrNi-1 temperature sensor was sensing a temperature closer to the heater one rather than the hydride average temperature. By an analogous process, considering a variable resistor of 5 Ω, it is possible to determine the heater temperature of ZrNi-1 at the beginning of

cycle for a power of the ON state of 3.48 W and after 12,000 cycles for a power of 3.3 W. The temperature of the heater is initially about 250 C at 3.5 W and it increases to 300 C for 3.3 W. The temperature measured in the center of the cap and reported in Figure 5-6 follows the temperature increase as expected. The fact that the temperature sensor was following the heater temperature and not the average cap temperature does not permit to establish the degradation of the heat conductance between the cap and the heater to be established.

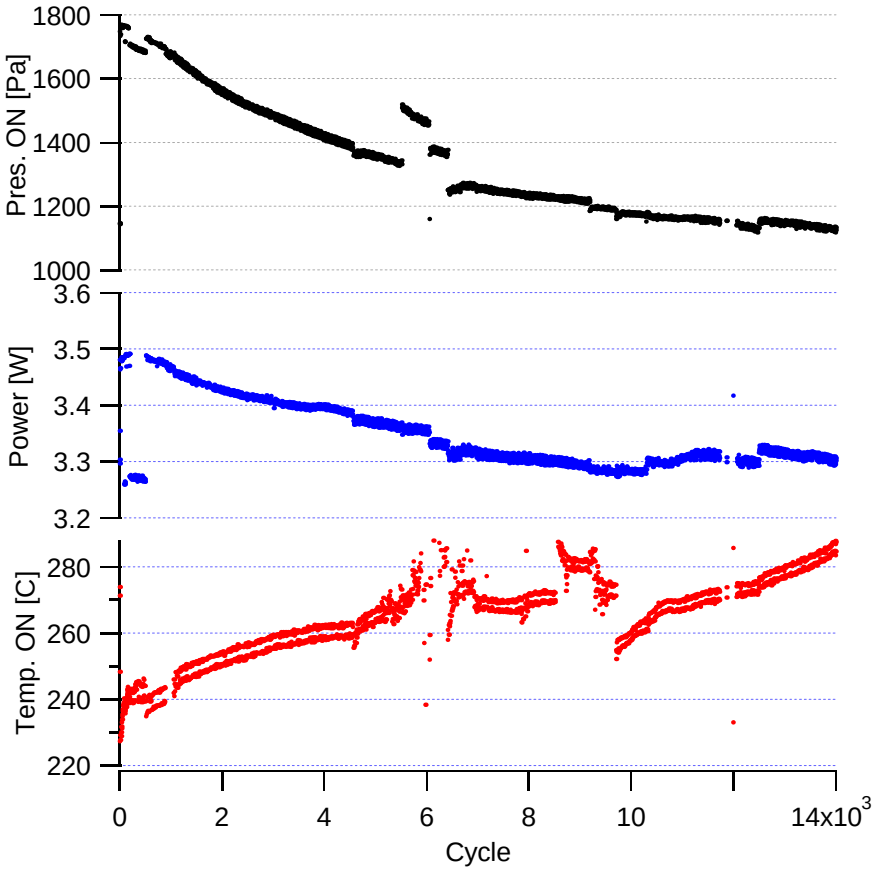

Figure 5-6 Pressure, Power and Temperature at the end of the ON phase for the ZrNi-1 actuator.

It should be observed that the ON state power decrease and the heater temperature increase on ZrNi-1 are double the analogous quantities for ZrNi-2. However, the two actuator assemblies were built and put into test following the same procedures. It is believed that the heater degradation differences could have been determined by small, not controllable parameters during the actuator assembly (i.e., the glue line of the epoxy used in the heater attachment or different epoxy curing conditions). The ZrNi-2 performance

degradation [Figure 5-7] are very similar to what have been observed on ZrNi-3: the ON state temperature, the ON state power and the ON state pressure decrease in time following a similar trend. The calculate heater temperature at the beginning of life test, for a power of 3.21 W is 215 C. After 12,000 the power has decreased to 3.05 W while the heater temperature has increased to 260 C. The heat conductance between the cap and the heater decreased form 0.1 W/K to 0.035 W/K.

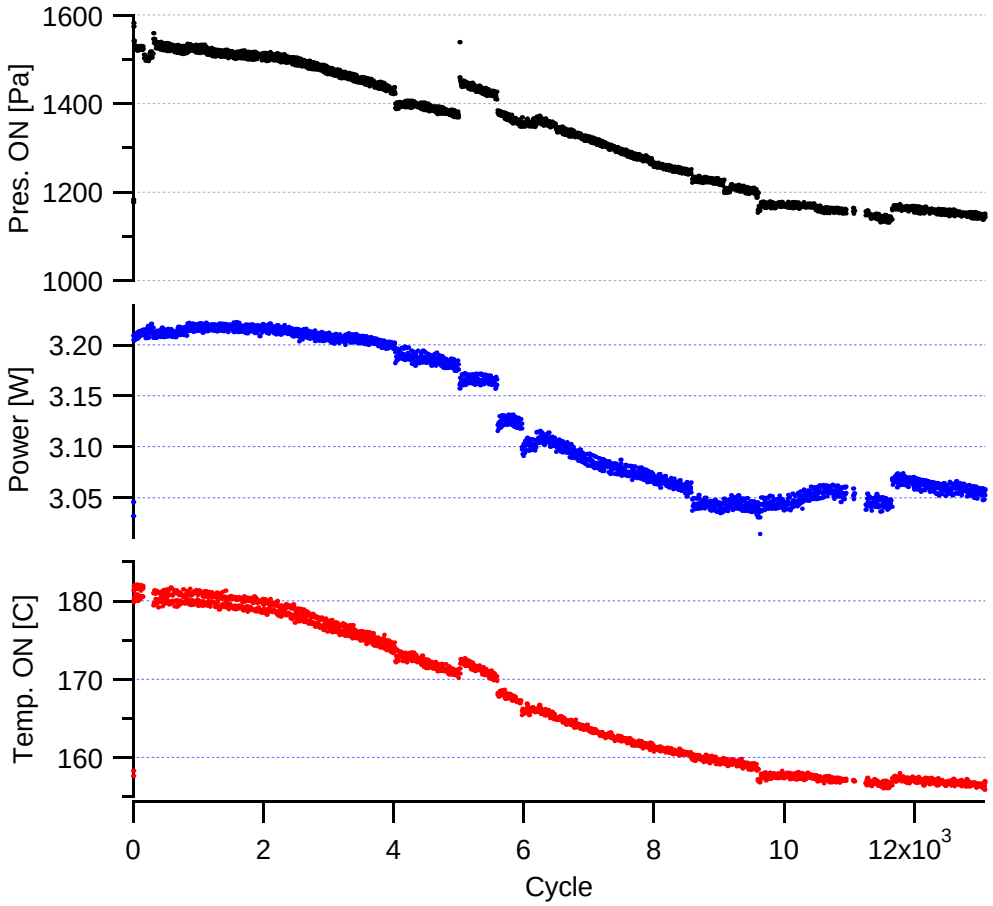

Figure 5-7 Pressure, Power and Temperature at the end of the ON phase for the ZrNi-2 actuator.

Figure 5-8 shows the locus of the pressure-temperature relationship at the end of the ON phase for each cycle of ZrNi-2 with the previously determined characterization data. The points are close to the characterization line but the locus trendline slope is substantially different. In fact, in conflict to what has been observed for ZrNi-3, after around 3600 cycles the points are above the characterization line. Two possible reasons can be suggested: 1) the temperature sensing is not working properly, or 2) material is

degrading and its isotherms are moving as described in section 1.4. The temperature sensor reliability has been verified by observing the operational stability of the sensor during the test; therefore it is believed that sorbent degradation is occurring for this unit. In light of the OFF state pressure results and of the kinetic observation, the degradation cause has been attributed to inadequate cleaning process of the hydride surface by hydrogen during activation.

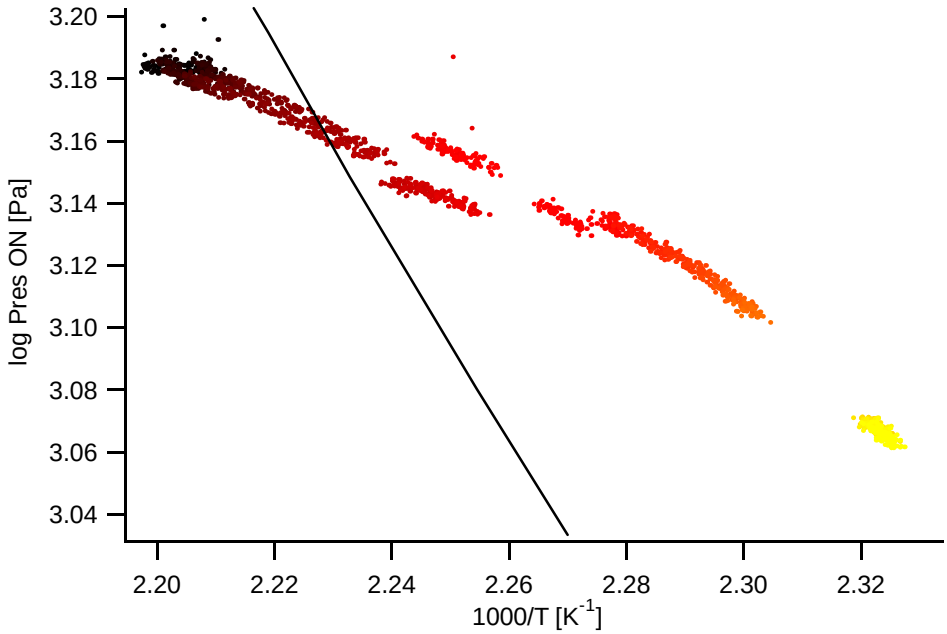

Figure 5-8 Pressure at the end of the ON phase versus 1000/T for the ZrNi-2 actuator. The curve color goes from black to yellow as a function of the cycle number. The black line is the van't Hoff curve determined before the life testing, as described in section 5.1.1

The switch is still running in the specified requirements (P_{ON} above 500 Pa and P_{OFF} below 1 Pa) and a detailed analysis of the degradation process will be performed at the end of the life cycling to determine the phase content of the cycled metal system.

5.1.2.2 OFF state

The OFF pressure was monitored properly on ZrNi-1 and ZrNi-2; they where instrumented with a 266 Pa [2 Torr] range MKS Baratron capacitance manometer with a minimal reading of 0.13 Pa [1 mTorr]. ZrNi-3 low pressure was monitored using a 1.33 kPa [10 Torr] range manometer with a minimal reading of 0.65 Pa. Despite the lower sensitivity of the 1.33 kPa sensor, it was decided to add it to the switch assembly in case

some major hydride performance would occur. The cycling tests have not yet shown any major performance degradation.

In Figure 5-9 the temperature and the pressure for the ZrNi-1 OFF state are reported. There is a big difference between the temperature reading on the cap and the chilled plate temperature. It was previously observed that the temperature of the ZrNi-1 actuator was not sensing the temperature of the cap but rather the heater temperature. The observation at low pressure confirms this conclusion and suggest that the temperature sensor is not thermally well coupled to the cap. The pressure was essentially stable and it raised up to the minimal reading after 4000 thousands cycles. The ZrNi-2 OFF pressure observation suggested that the pressure raising could be a manometer drifting [see Figure 5-10]. The OFF pressure build up after few thousands cycles to 0.6 Pa [4 mTorr].

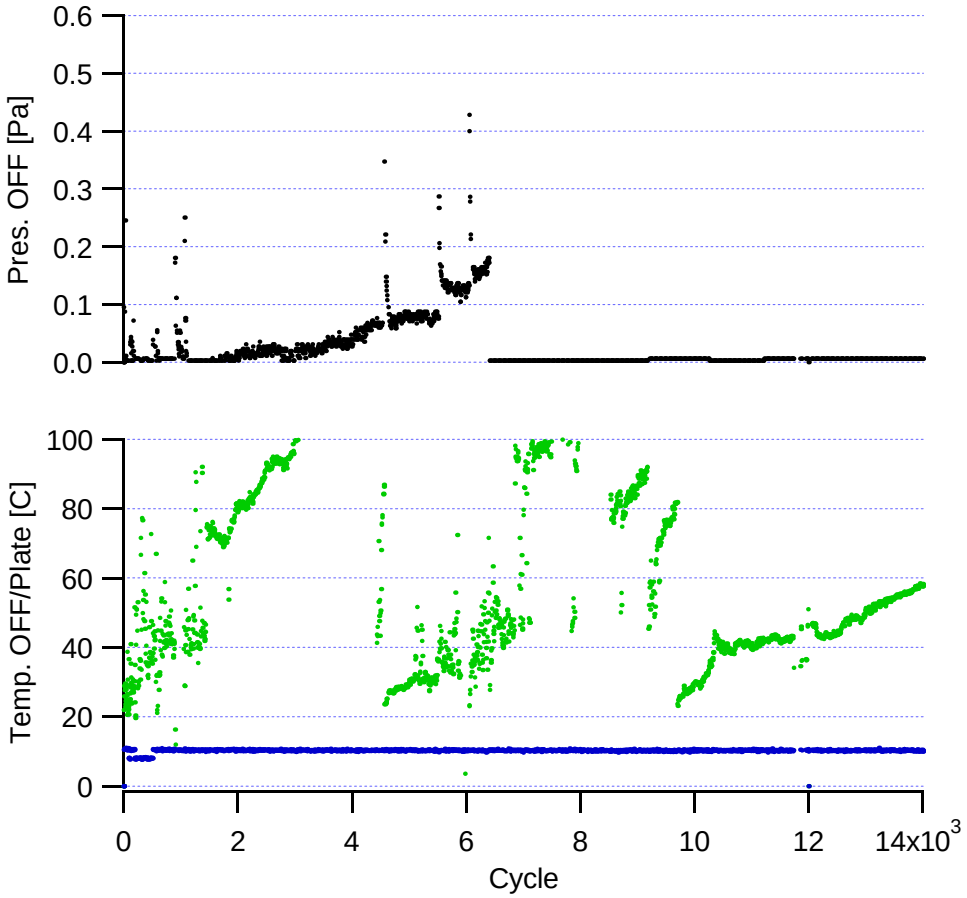

Figure 5-9 Pressure and Temperature of the OFF state for the ZrNi-1 actuator [green]. The blue line shows the temperature of the copper chilled plate.

Initially, it was postulated that the pressure transducer shift in their zero point offset. All the actuator assemblies in test at that time (ZrNi-1, ZrNi-2, ZrNi-3, U-1, U-2) were then removed from the vacuum chamber and connected to the pumping station [see Figure 4-4] to verify and in some case recalibrate the pressure transducers. The calibration procedure for the capacitance manometer consists of re-zeroing the output voltage when the pressure is below the minimal reading of the instrument. Surprisingly, it was observed that the pressure transducers were still calibrated on ZrNi-2 and some minor adjusting was required for ZrNi-1 and ZrNi-3. The increased ZrNi-1 OFF pressure can be attributed to the instruments zero drifting. The "low pressure" transducer [0-266 Pa] on ZrNi-2 was reading the pressure of a residual gas that was slowly accumulated cycle by cycle. The residual gas was analyzed with a quadrupole mass spectrometer and

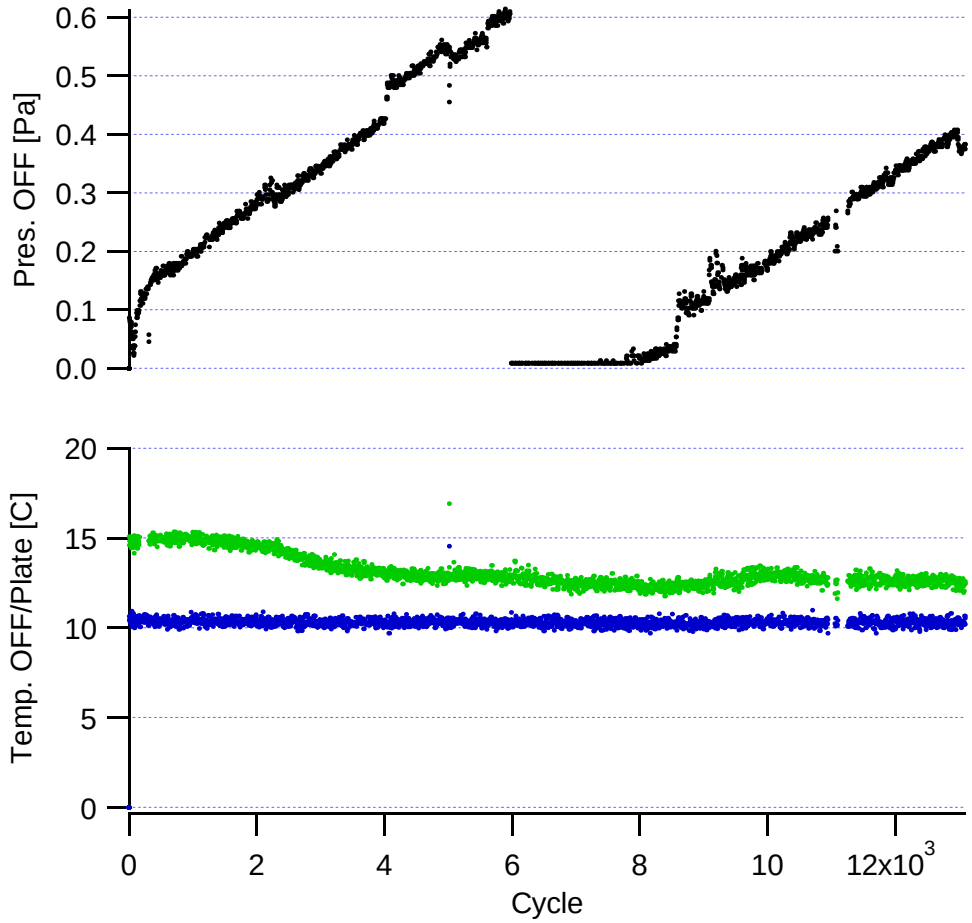

Figure 5-10 Pressure and Temperature of the OFF state for the ZrNi-2 actuator [green]. The blue line shows the chilled copper plate temperature.

the results are reported in the next section.

It is interesting to note that after the ZrNi-1 was re-zeroed the OFF state pressure has not practically changed, with a pressure reading always below the minimal one. In ZrNi-2 the pressure increasing phenomena is instead repeating with a smaller slope.

5.1.2.3 Residual gas data analysis

The residual gas on ZrNi-1, ZrNi-2 and ZrNi-3 was qualitatively analyzed using a quadrupole mass spectrometer (Standford Research System, model QMS 200) [see Figure 4-4]. The test assembly was mounted on the pumping station at the same location where it had been previously filled with hydrogen. The II reference volume, previously used to fill the test assembly with the proper amount of hydrogen, has been used to collect sample the residual gas. The pressure transducer connected to it was replaced with a 0 – 266 Pa [2 Torr] MKS Baratron that was calibrated against the Bayard - Alapert pressure gauge before each sampling. When the actuators were connected to the pumping station, the connecting line was cleaned by heating it under active vacuum and the switch assemblies were leak tested; no leaks were found. Before sampling the residual gas on each actuator the vacuum system background was observed and all the measurements were appropriately corrected. The residual gas analyzing systems were set up to give only qualitative estimates of the constituents; a more refined system would be needed to measure the constituent quantities with greater accuracy.

For ZrNi-1 unit, its low pressure transducer showed a drifting of 0.13 Pa and was recalibrated. It is interesting to observe that the drifting is consistent with the OFF pressure increase observed in the previous section. The residual gas analysis showed the presence of some hydrocarbons, methane, carbon monoxide and propanol.

ZrNi-2 did not show any drifting of the 0-266 Pa pressure transducer. The residual gas not absorbed at the OFF state was analyzed. The major constituent of the residual gas in the ZrNi-2 test assembly was hydrogen. Some amount of propanol, methane, carbon monoxide and in general hydrocarbons chains were found.

5.1.2.4 Switch kinetics comparison

The switch kinetics did not substantially changed during the cycles for all three ZrNi actuators. Figure 5-11 reports three characteristic cycles for the ZrNi-2 actuator. It has been chosen to describe only the ZrNi-2 kinetics because the possible effects of

hydride capacity degradation were suggested by the ON an OFF state analysis. ZrNi-2 actuator kinetics are compared to the ZrNi-3 kinetics on which no signs of degradation have been noted in the ON and OFF status analyses.

In Figure 5-11, it is possible to observe the ON state temperature degradation; the maximum temperature reached at the end of the ON period in the three cycles are decreasing with the cycle number. It should also be noted that the equilibrium temperature of the ON state was never reached. In fact, when the heater was turned OFF the temperature and, as a consequence the pressure, was still raising.

In the three selected cycles the increasing of the residual gas registered at the end of the OFF states can be noted. The effect of the residual gas affects only the lowest pressure achieved by the system and not the cycling behavior of the actuator.

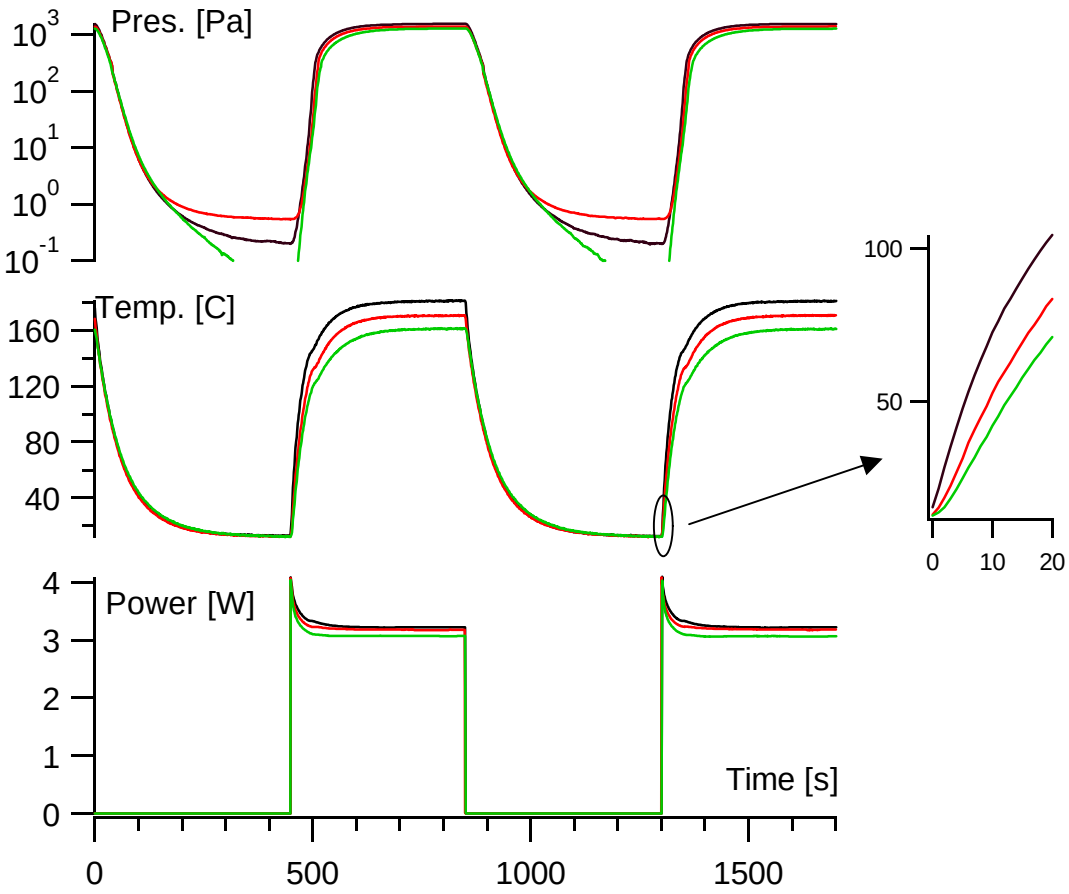

Figure 5-11 Cycle comparison for the ZrNi-2 actuator. Pressure, power and temperature are compared. Black lines for cycle 1006 and 1007, red lines for cycle 5002 and 5003, green lines for cycle 8062 and 8063.The spikes in power supplied are determined by the powering circuit described in 4.5.

It is important to note that in the OFF→ON transition as soon as power is supplied to the heater the temperature rising rate is higher at cycle 106 than the other two cycles. After 10s the actuator temperature reached is 72 C in cycle 1006, 52 C in cycle 5002 and 42 C in cycle 8062 while the heater temperature is instead increasing with the cycles. In fact, by considering the power supplied after 10s it is possible to establish the heater temperature at that moment: 108 C for cycle 106, 130 C for cycle 5002 and 155 C for cycle 8062. The thermal gradient between the heater and the cap increases with time confirming impact of the attachment degradation.

Considering the net power supplied on cycle 106 to the switch assembly and assuming heat losses are linearly temperature dependent, it is possible to approximately estimate the thermal mass of the actuator to be 0.8±0.2 J/K. This estimate is in the range of what predicted in section 4.5.1 (0.85 J/K) and of the value used in the actuator modeling and design (1.18 J/K).

The dynamic behavior of the switches can also be analyzed in a van't Hoff plot to verify kinetic hydride property changes not shown on diagrams such as Figure 5-11. By plotting pressure as a function of temperature the time variable becomes implicit and curves plotted for different cycles should lay on top of each other if no material degradation is occurring and the temperature sensor is working properly. The kinetic van't Hoff representation of the cycles is intended to give an indication on the material performance consistency verifying the relative position of different cycle curves on the plot. A detailed analysis of the van't Hoff kinetic diagram would require a complicate transient conduction analysis of the actuator switching, including the transient hydride phase transition and it is outside the objectives of this study.

In Figure 5-12 the comparison on three cycles for ZrNi-3 is made for the OFF→ON and the ON→OFF switching operations to verify if the initial indication of no material degradation is confirmed. The previously described variations in the ON-state and in the OFF-state are visible: the ON-state points are located below the characterization data; and the curves diverge in the low part of the diagram (OFF) due to the pressure transducer zero drifting (ZrNi-3 was not equipped with adequate pressure transducer to measure accurately the OFF state of the actuator). In the ON→OFF switching, the dynamic behavior approaches a line parallel to the Luo's et al. absorption data for a material not cycled, as shown in the diagram. Those observations confirm that no apparent degradation has occurred in the hydride material.

An interesting behavior is shown in the OFF→ON transition. The curve points at low temperatures are not close to the characterization line. When the temperature increases (1000/T decreases) a sudden pressure change occurs in the region of point A (Temperature ≈390 K, pressure ≈ 120 Pa). For higher temperatures the curves approach the characterization line. The point A is reached at different time after the switch is turned ON in the three cycles: 40s for cycle 106, 51s for cycle 7060 and 53s for cycle 13102. The consistency of the phenomenon in terms of temperature but especially of pressure suggests that its cause be related to material properties rather than to heat diffusion in the actuator assembly. Therefore it can be considered as an additional indication of the hydride material endurance to thermal cycling.

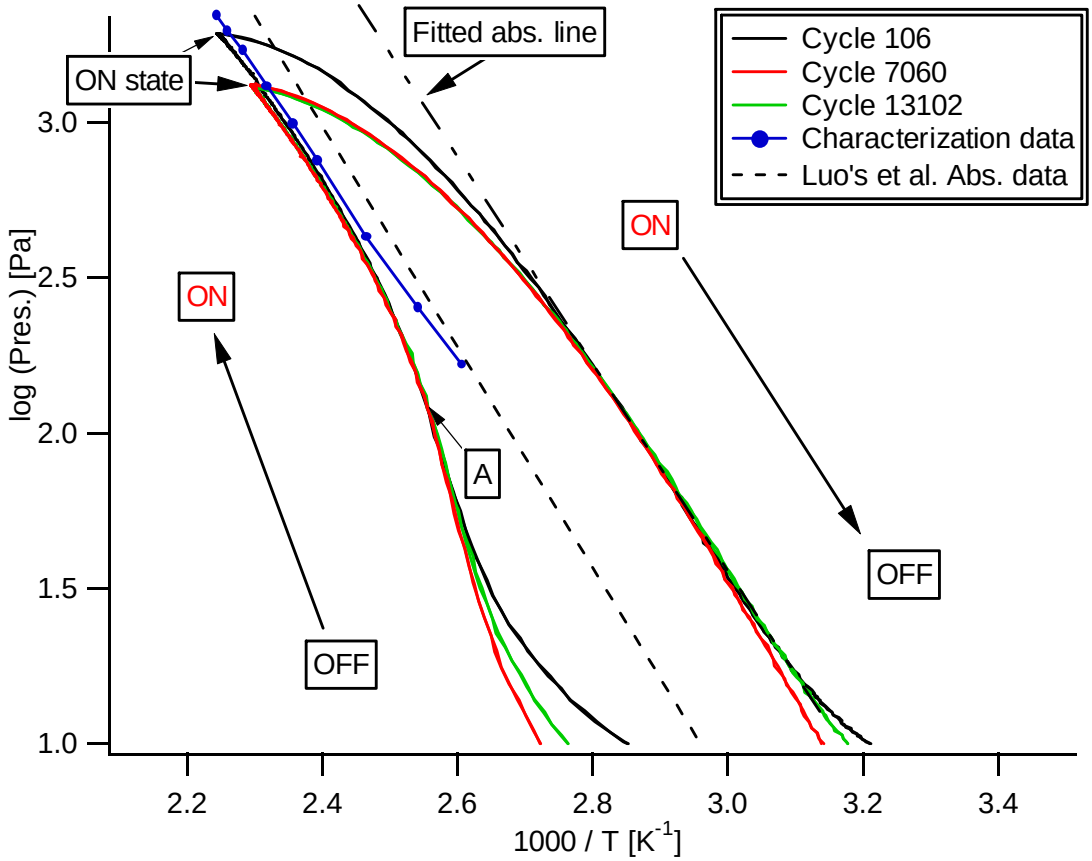

Figure 5-12 Cycles comparison for the ZrNi-3 actuator on the van't Hoff plot of log[Pressure(t)] vs. 1000/Temperature(t), where time is the implicit variable. The characterization data measured before the life test are reported along with the Luo et al. [77] absorption data

The same kinetic transition was monitored in ZrNi-2, as shown in Figure 5-13 where the three cycles are reported. For this actuator the phase transition point (A) is not stable as it had been observed for ZrNi-3, but it changed during cycling. The three points have been highlighted in the diagram and it can be observed that the temperature of the transition decreases with cycling: 418 K for cycle 1006 (after 50s), 408 K for cycle 5002 (after 56s), and 398 K for cycle 8062 (after 61s). It is suggested that the hydride surface is getting cleaned by cycling and that therefore the kinetic activation that occur in A require less energy. The hypothesis is also prompted by the fact that residual gas in the OFF state was formed during the ZrNi-2 cycling, as shown in Figure 5-10. In addition, if the ZrNi-2 results were to be plotted on the same diagram with the ZrNi-3 one, it should be observable that the ZrNi-2 latest cycles are approaching the stable cycle of ZrNi-3, confirming the hypothesis that, by removing initial impurities present in the system, ZrNi-2 is progressing to a stable condition.

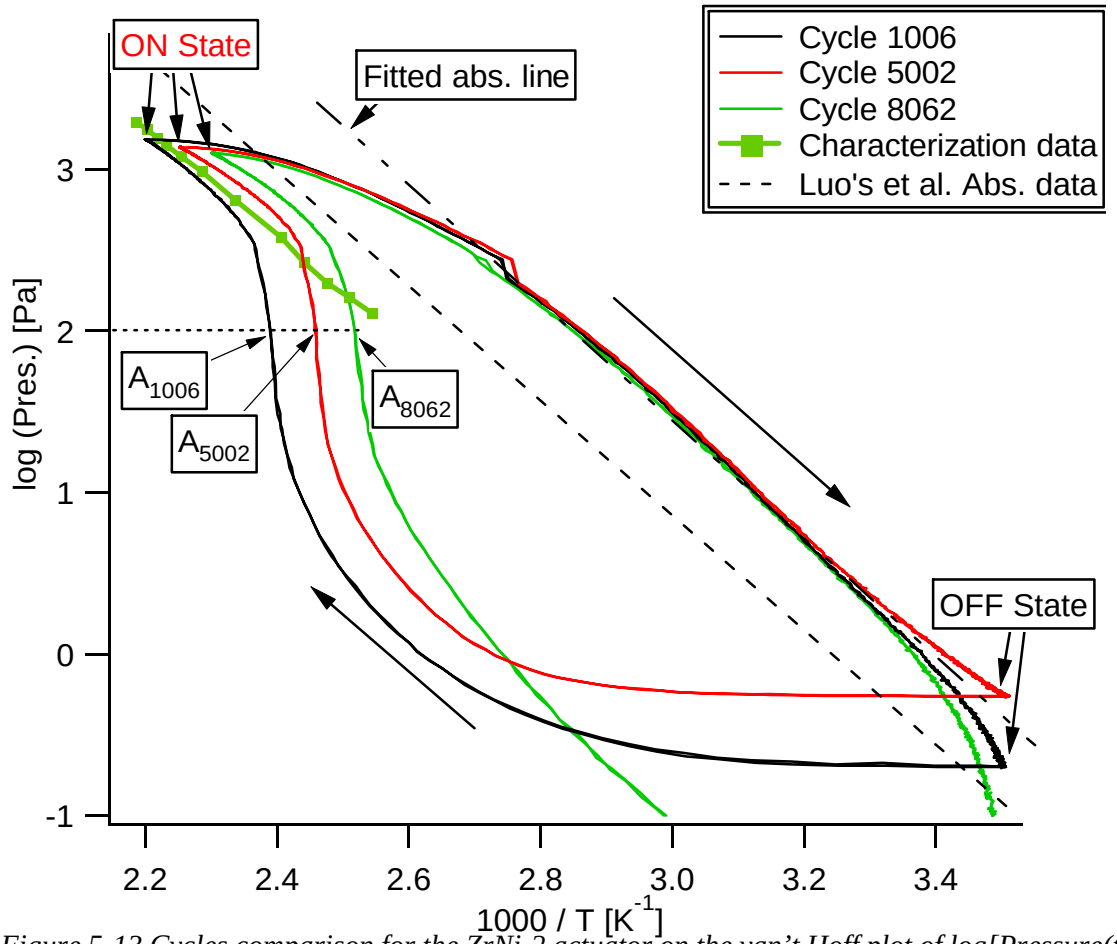

Figure 5-13 Cycles comparison for the ZrNi-2 actuator on the van't Hoff plot of log[Pressure(t)] vs. 1000/Temperature(t), where time is the implicit variable. The characterization data measured before the life test are reported along with the Luo et al. [77] absorption data

It should also be mentioned that the ON→OFF transition is consistent in time: the dynamic behavior approaches a line parallel to the Luo's et al. absorption data as it was observed on ZrNi-3. The variations in the ON, previously observed in Figure 5-7 and Figure 5-8, are visible, as well as the OFF state variation [see Figure 5-11].

5.1.3 Discussion

The characterization data of the three ZrNi actuators have shown that the hydride was operating properly and that the ON state could be reached within the predicted power requirements. In fact, all the points reported in Figure 5-1 were obtained applying to the actuators less than 3.4 W. It was also verified that the hydrogen-hydride system reached the required OFF pressure at the radiator temperature. In fact it can be observed that the characterization line measure after more than 12,000 are very similar to the initial one.

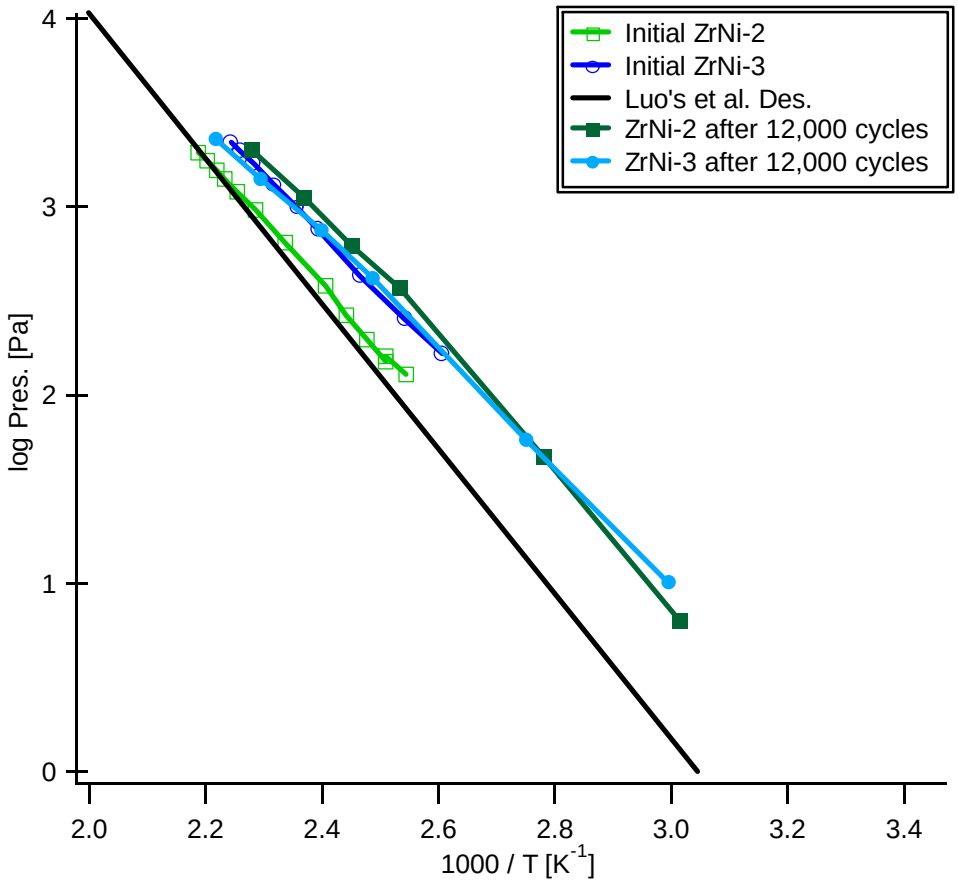

Figure 5-14 Comparison of the characterization data for ZrNi-2 and ZrNi-3 after 12,000 cycles.

The thermal cycling has deteriorated the actuator performance, especially in terms of ON and OFF state pressure. However, it has been observed that the principal cause of the decay has been the degradation of heater attachment to the cap. No major material degradation has been detected; the only evidence observed in regard, the modest OFF state pressure raising in ZrNi-2, has been attributed to the cleaning process of the surface of the material. In fact, it can be observed in Figure 5-14 that the ZrNi-2 characterization line measure after more than 12,000 is very similar to the ZrNi-3 one that has not been affected by any measurable change after the same amount of cycles performed.

Nevertheless, the magnitude of the actuator behavior changes has to be evaluated in light of the overall switch performance. The cycles for ZrNi-1 and ZrNi-2 have been analyzed in terms of *Total Power* and cooling time *Margin*. The fact that ZrNi-3 did not have an adequate pressure transducer to read accurately the low pressure precludes the possibility to estimate the first figure of merit with sufficient accuracy. The locus of the points (*Total Power*, *Margin*) for each cycle of ZrNi-1 and ZrNi-2 is shown in Figure 5-15 . For the ZrNi actuator it was predicted in section 3.3.1 a total power of 5.1 W and a margin of 0.4 for a switch with a thermal mass of 1.2 J/K and a constant ON state power of 3.82 W [the pivotal point in Figure 3-8]. It can be observed in Figure 5-11 that in more than 10,000 cycles the total power has always been below the predicted value and that the cooling time margin has always been between 0.4 and 0.5.

Despite the fact that some hypotheses assumed in the actuator modeling were not confirmed in the experiments, the performances of the test actuators are very similar to the values estimated. Three major discrepancies have been observed in regard to the initial hypothesis: (1) the thermal mass was lower than 1.2 J/K, (2) the power supplied to the actuator was not constant, and (3) the temperature distribution in the actuator assembly was not uniform.

It has been previously noted [section 4.5.1] that ZrNi actuators have a lower thermal mass (0.8 J/K) than the assumed value (1.2 J/K). A lower switch thermal mass would cause a lower total power (4.7 W) of the actuator and a higher margin (0.455), as shown in Figure 3-8.

The power supplied to the actuator is not constant, as described in section 4.5 and has been observed in the ON state description. When the heater is turn ON the power the power has an initial spike that increase the OFF→ON transition switching speed.

However, the spike is short [see Figure 5-11] and its effect on the margin initial prediction is very small (less than 1%). In fact, the integral of the difference between the power supplied and the equilibrium power in the firsts 100 s, assuming for the latter an average of 3.2 W, is approximately 18 J. The error has been calculated based on the extra time needed (5.6 s) to supply that energy at the equilibrium power.

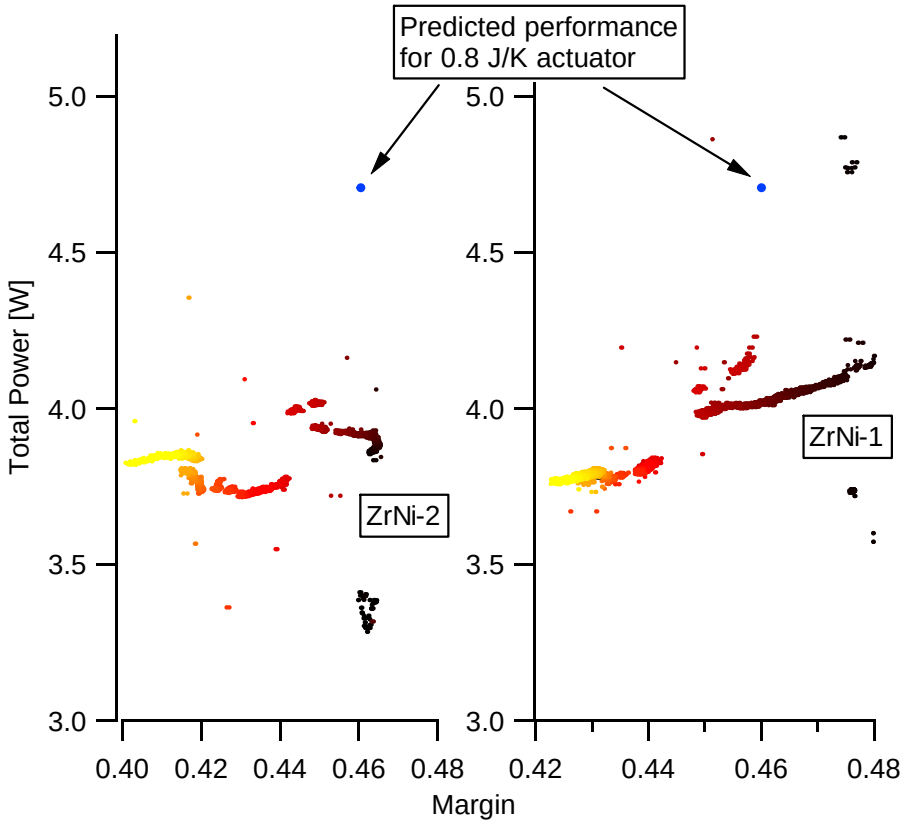

Figure 5-15 Margin and Total Power for the ZrNi-1 and the ZrNi-2 actuator. The curve color goes from black to yellow as a function of the cycle number. The blue point is the performance prediction for a ZrNi actuator with a thermal mass of 0.8 J/K [see 3.3.1]

In the switch modeling, it was assumed a uniform temperature of the switch assembly that, at the designed ON state temperature, would determine a pressure of 1.2 kPa. During the life test, the ON state pressure (for ZrNi-1 and ZrNi-2) varied between 1800 Pa to 1000 Pa. Considering the gap heat conductance as a function of pressure [Figure 2-3] and the ZrNi-1 and ZrNi-2 ON state power [Figure 5-6, Figure 5-7], it is possible to observe that the ON pressure variations are happening above the knee. Their effect on the switch performance is greatly attenuated by the flattening of the gap heat conductance above the transition between molecular and viscous regime. It should be

concluded from Figure 5-15 in fact that the changes in the ON state pressure are slightly impacting the *Margin* while the *Total Power* is almost unchanged. Even the OFF state pressure increasing in the ZrNi-2 actuator have not significantly affected the *DPower*.

It should be observed that the cooling margin plays an important role in the cooler design and it could be used to optimize the overall system performance. The fact that the compressor unit requires less time to cool imposes high power peaks to the radiator, as shown in Figure 5-16 for ZrNi-2. To gain a 43 % margin in the cool down time of the compressor unit, a heat peak of 950 W is dumped to the radiator. Regulating the heat conductance of the gas gap heat switch, by adjusting the hydride temperature, would allow the heat flux to be controlled more effectively.

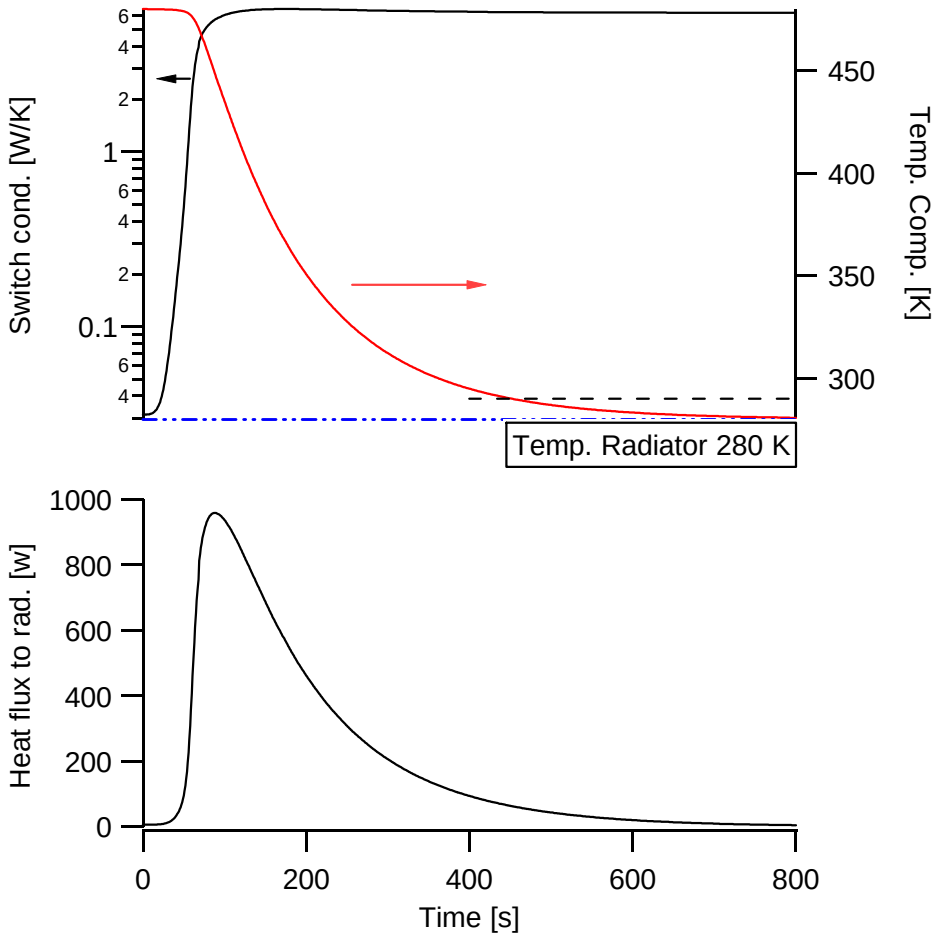

Figure 5-16 Heat flux to the radiator and compressor temperature curve considering ZrNi-2 performance (cycle 8062) in the determination of the gap heat conductance. In the gap heat conductance the measured conductive support heat losses and the radiative losses [Equation 2-7] have been considered. The black dashed line is representing the maximum temperature of absorption [290 K] on which the cooling margin has been calculated (0.43). In fact, it takes only 450 s to cool the compressor unit to 290 K.

5.2 Uranium test results

5.2.1 Initial Characterization data

The characterization data for the three uranium actuators are presented in Figure 5-17 with the relevant literature data reported in Table 3-1. It is interesting to observe that the three lines are very close although two different heater configuration were adopted for U-1 and for U-2 and U-3 [as described in section 4.4].

Considering that higher temperatures are required to reach the ON state pressure whom was needed for the ZrNi system, the hydride system was almost loaded to the maximum concentration to take advantage of possible pressure rising at the end of the pressure plateau region. Based on Figure 3-3 for temperature lower than 400 C and concentration around 3.0 H/M a dashed line is reported indicating no clear data of the end of the plateau line. However the fact that the steady state points are aligned in the van't Hoff plot indicates that all the measurements were describing the same phase transition. In fact, U-1 and U-2 were loaded with almost the maximum amount of hydrogen [H/M ≈

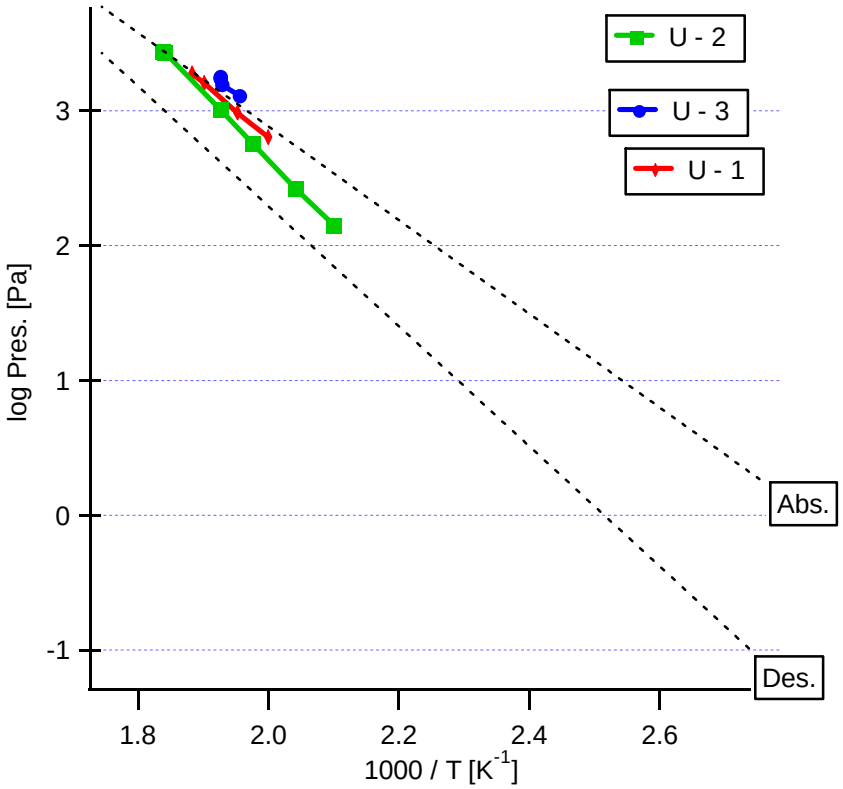

Figure 5-17 Uranium characterization data: van't Hoff plot. The black dotted lines are the literature absorption and desorption data [68]

3] and their characterization lines are very similar to the U-3 characterization data line even if it has been loaded to a concentration of 1.9 H/U.

The pressure lines for the actuator were expected to be similar to the literature desorption line. The slopes of the U-1 and U-3 show an error of 8 and 3 % in respect to the desorption literature data slope. The U-2 characterization line slope shows instead an error of 12 %. Considering the interpolated lines the temperature required to reach 0.13 Pa [1 mTorr] is 348 K for U-1 and U-3 and is 369 K for U-2. Under steady state conditions, the equilibrium pressure reached at the radiator temperature (280 K) should be much lower than the minimal reading of the pressure transducer mounted on U-2 and U-3. U-1, the first built actuator, was equipped with only one pressure transducer with a minimal reading of 6.6 Pa.

During the first 750 cycles of U-2, it was observed that the OFF state pressure was above the predicted values based on the extension at lower temperatures of the characterization data shown in Figure 5-17. The higher OFF pressure has been attributed to a slow kinetic absorption process caused by the high hydrogen concentration. By lowering the concentration to 2.2 H/M as reported in Table 4-1. After the hydrogen removal, the OFF pressure measured after each cycle has always been below the instruments minimal reading (0.13 Pa). The hydrogen removal did not affect the ON state performance of the actuator. The concentration on U-1 was not modified considering that the actuator test did not have a pressure transducer to verify the behavior changes in the OFF state.

5.2.2 Life test data analysis

The three uranium actuators have been cycled for more than 5000 cycles and, as the other test actuators, the life test will be continued to 25,000 cycles. The available life data have been analyzed in terms of ON and OFF state. The variation of the hydride absorption and desorption kinetics have been compared for some characteristic cycles.

For all the uranium actuators it was observed that ON state temperatures decrease in time, indicating a degradation of the heater attachment to the cap. A similar phenomenon was noted on the heater life test [see section 4.5.2.] for a heater configuration similar to the one adopted for U-2, U-3 and St-172. During the cycling of U-2, the heater failed after about 3300 cycles. The heater was replaced with an equivalent

unit (WS-81, see section 4.5.2). After the heater was attached to the cap, a new temperature sensor was mounted and the test was resumed. No external evidences of the PRT failure were found implying internal cause of the open circuit; a microscopic analysis of the heater surface did not reveal any cracking.

5.2.2.1 ON state

In Figure 5-18 the ON state properties for U-3 actuator are reported. The ON state pressure decreased in time by thermal cycling as it was observed previously for the ZrNi actuators. The ON state pressure curve follows the trend of the ON state temperature curve indicating that the performance degradation should be the consequence of the temperature decreasing.

The thermal dependence of the pressure decreasing can be seen in the van't Hoff plot in Figure 5-19. The darker points representing the initial 300 cycles can be interpolated by a linear extension of the characterization line [blue line]. In addition that line is parallel to the literature desorption van' t Hoff data. At a temperature of 222 C

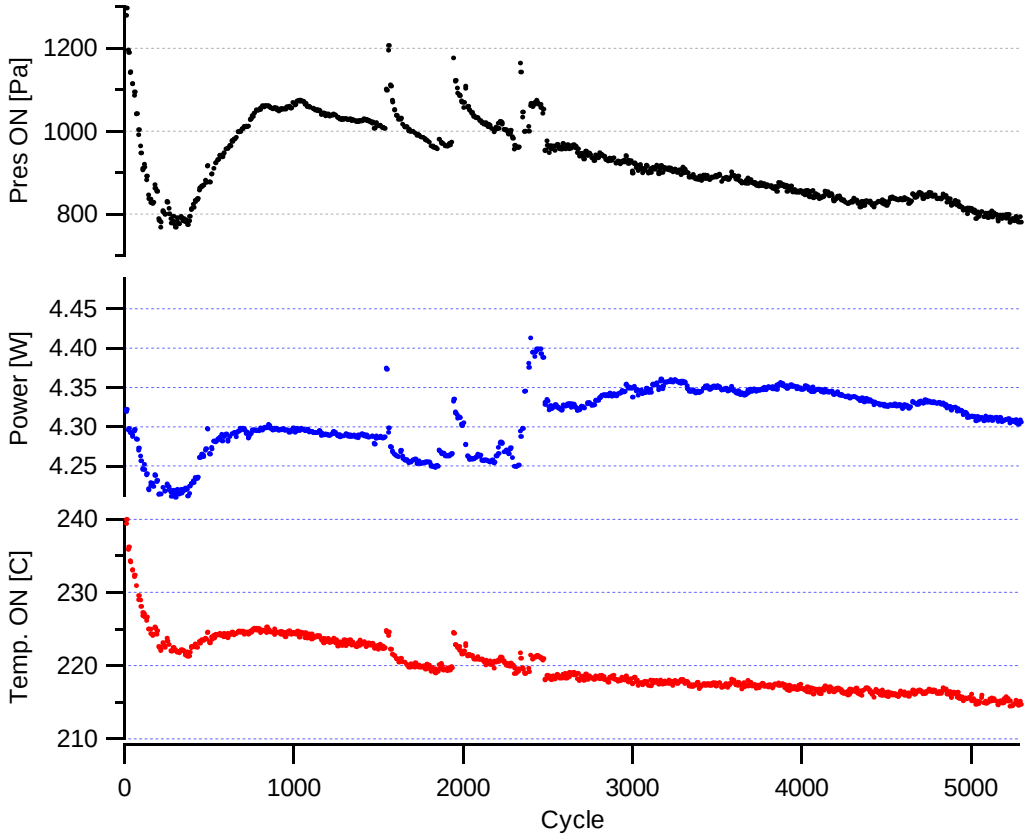

Figure 5-18 Pressure, Power and Temperature at the end of the ON phase for the U-3 actuator.

(1000 / T [K]= 2.02 K^{-1}), the ON state pressure increases. It is suggested that the hydride powder could have been redistributing inside the cap allowing a more efficient heat transfer to the hydride. However with the available data it is not possible to unquestionably determine the cause.

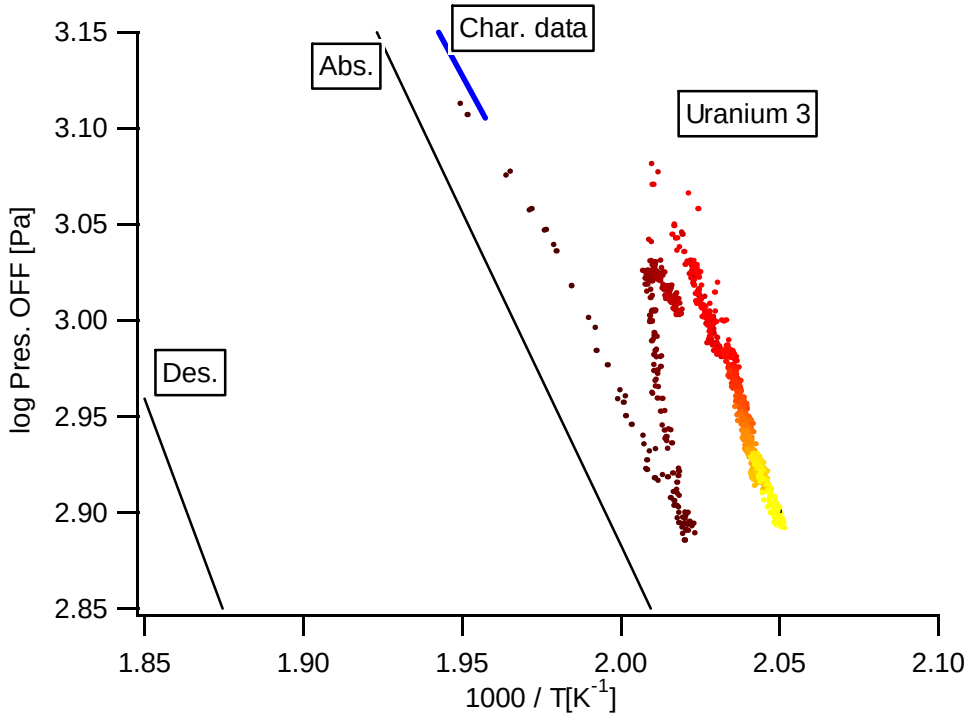

Figure 5-19 Pressure at the end of the ON phase versus 1000/T for the U-3 actuator. The curve color goes from black to yellow as a function of the cycle number. The black lines are the literature data for absorption and desorption and the blue line is the characterization curve determined before the life testing, as described in section 5.2.1

After cycle 1000 the ON state pressure decreases again as a function of the ON state temperature. In fact, a line could interpolate the reddish and yellow points in Figure 5-19.

The same ON state pressure decreasing phenomena was observed on U-1 and U-2 actuators. Figure 5-20 shows the ON state pressure, temperature and power for the U-2. In the first 800 cycles the ON state pressure decreased from 1570 Pa to 316 Pa and the ON state temperature fell from 240.8 C to 203.0 C. The fact that the power supplied to the heater did not comparably change indicates that the heater temperature stayed fairly constant. It is suggested that the radiative heat conductance from the cap to the

environment increased, decreasing the net power supplied to the switch assembly [see the actuator heat conductance schematic reported in Figure 4-7]. In fact, it was observed that the heater surface got darker in time, as previously detected in the heater test and attributed for reactions of the brazing flux.

The actuator test was left cycling in degraded conditions (the ON state pressure was below 500 Pa) until the heater burned out at cycle 2810. The actuator test was removed from the vacuum chamber and the heater and the temperature sensor were replaced.

It is interesting to observe the effect of the new heating configuration in Figure 5-20. Despite the fact that the variable resistor in the U-2 powering circuit was not re-tuned, it was observed a 10% power increase. Considering the diagram show in Figure 4-7, it was deduced that the heater temperature was lower in respect to the previous heater and therefore that the new heater is more efficiently transferring heat to the cap. A higher heat supplied to the hydride is also documented by the large pressure change in

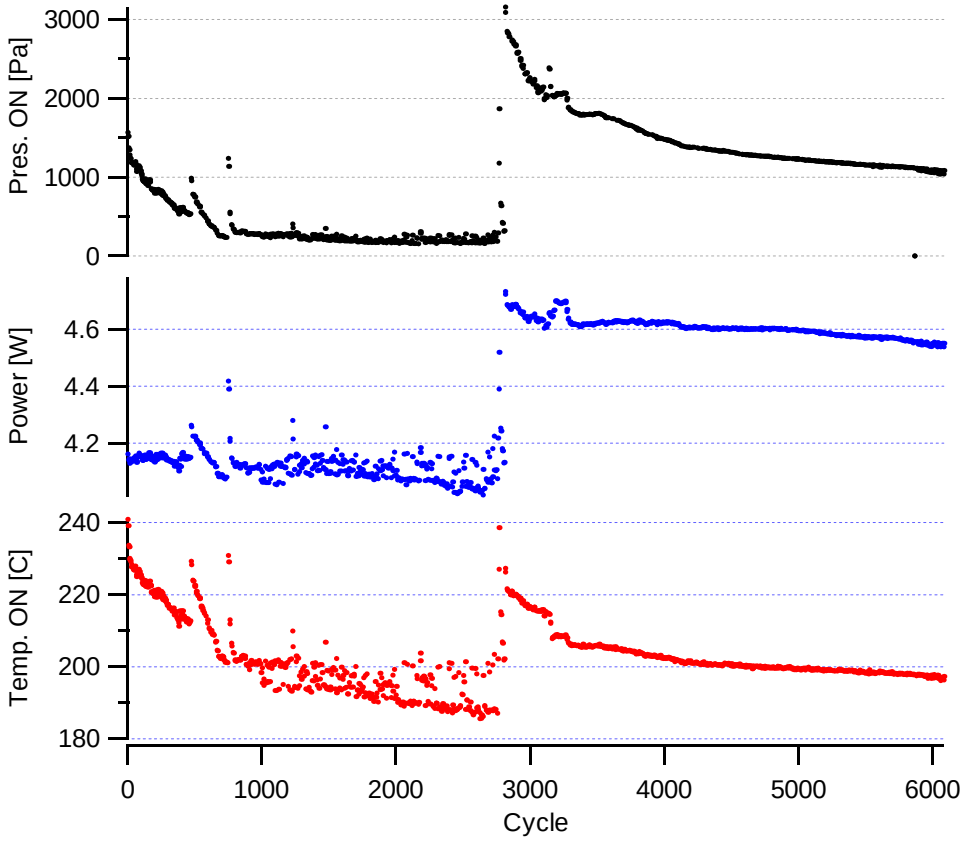

Figure 5-20 Pressure, Power and Temperature at the end of the ON phase for the U-2 actuator.

occurrence of the heater change. Regardless of the initially efficient heat transfer the power, temperature and pressure of the ON state for the U-2 again decreased in time as it was observed for the heater test and for U-3.

The temperature dependence of the pressure decrease for U-2 is shown can be observed in Figure 5-21. The black points show the initial ON state pressure dropping. An interpolated line would be parallel to the previously observed characterization line [blue line]. The light red and the yellow points represent the cycles after the heater replacement. It can be observed that they are considerably above the initial characterization line and that the interpolated line between them would be parallel to it.

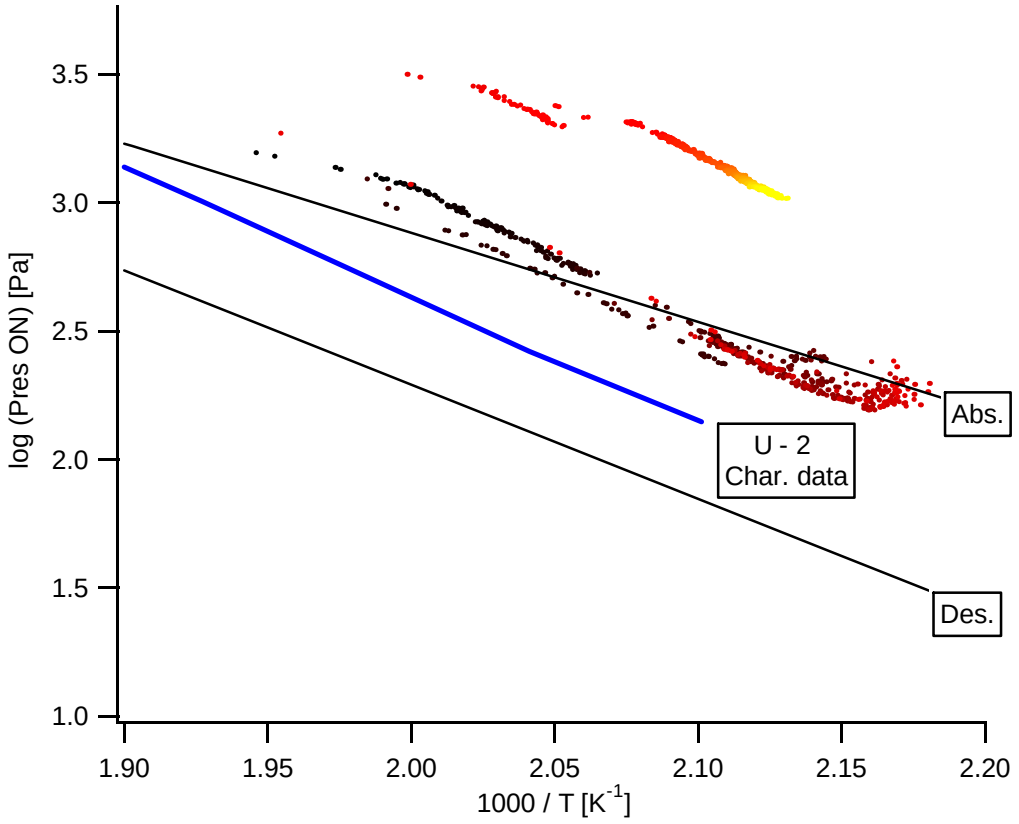

Figure 5-21 Pressure at the end of the ON phase versus 1000/T for the U-2 actuator. The curve color goes from black to yellow as a function of the cycle number. The black lines are the literature data for absorption and desorption and the blue line is the characterization curve determined before the life testing, as described in section 5.2.1

Comparing U-2 and U-3 it is interesting to note the different scale axis of Figure 5-18 and Figure 5-20. The maximum variation of ON state pressure of U-2 during the

first 6,000 cycles was 450 Pa while it was 1 kPa for U-2 with the initial heater configuration and around 2 kPa with the second one.

5.2.2.2 OFF state

The OFF state in the uranium actuators was monitored on U-2 and U-3. At the radiator temperature of 280 K the uranium actuators are expected to be at a pressure below 0.1 Pa [the minimal reading of the pressure transducer mounted on U-2 and U-3]. In fact, considering the interpolation of the characterization lines at the chilled plate temperature of 10 C it is expected that the equilibrium pressure to be below 10^{-4} Pa. It was observed that the U-3 OFF pressure was always below the minimal reading of the instruments. Unexpected higher pressures (up to nearly 1.5 Pa) were observed on U-2 in the first 800 cycles as shown in Figure 5-22. U-3 was initially loaded with hydrogen to a concentration of 2.9 H/U and the unexpected high pressure at the end of the OFF-state

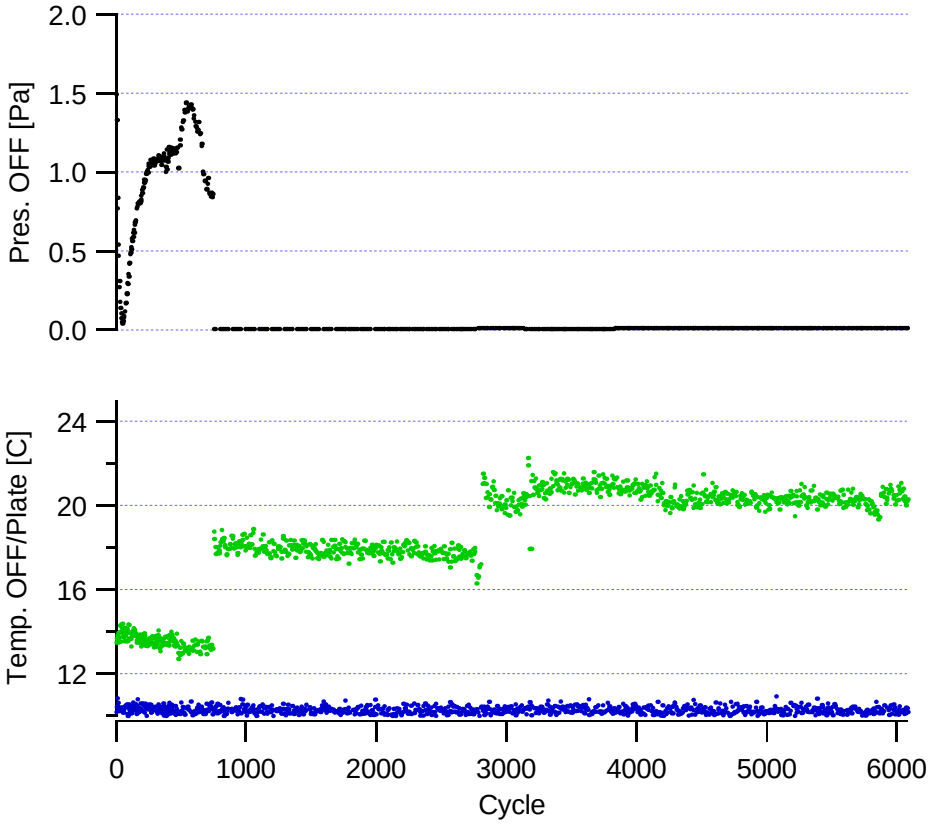

Figure 5-22 Pressure and Temperature of the OFF state for the U-2 actuator [light gray]. The blue line shows the temperature of the copper chilled plate.

was attribute to slow kinetc at the end of the plateau region. The hydrogen concentration was reduced to 2.2 H/U to verify the hypothesis and since then the OFF state pressure has always been below minimal reading.

The two steps in the OFF state temperature corresponds to the repositioning of the switch assembly on the chilled plate; the first one when the hydrogen concentration was reduced and the second one when the heater was replaced.

5.2.2.3 Switch kinetic comparison

Three representative cycles for the U-3 test actuator have been compared in Figure 5-23 in terms of power, temperature and power. It was previously noted that the ON state power did not effectively changed by cycling. It can be observed that also the dynamic power curve did not change in the three cycles reported in Figure 5-23.

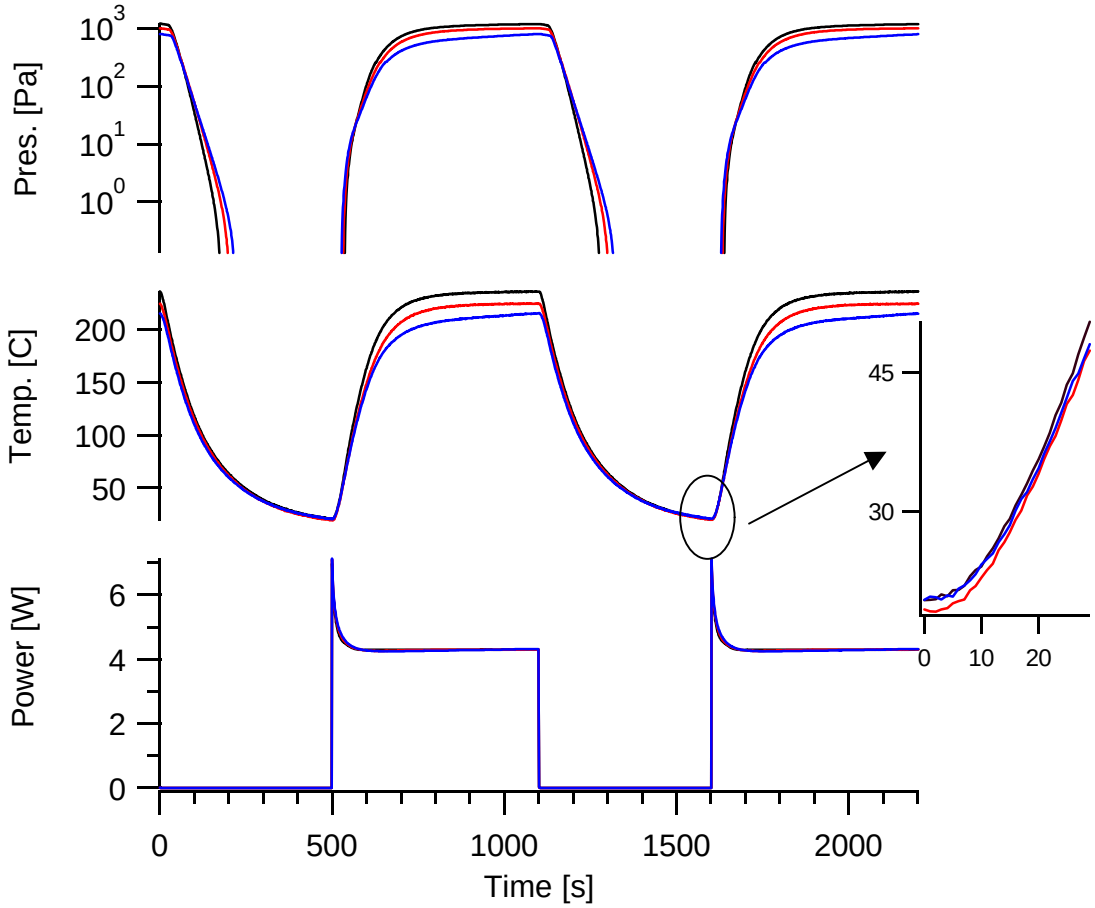

Figure 5-23 Cycle comparison for the U-3 actuator. Pressure, power and temperature are compared. Black lines for cycle 22-23, red lines for cycle 706-707 blue lines for cycle 5010-5011.

It is important to remark that the OFF→ON temperature transition is different compared to the ZrNi actuator temperature curve shown in Figure 5-11. In fact, the temperature rising in the uranium actuator follows with a small delay the step power input. This observation leads to the conclusion that the three thermal masses reported in Figure 4-7, the heater, the temperature sensor and the actuator assembly, cannot be reduced to a single element. The heating system cannot therefore be simplified as a first order system as it had been assumed in the actuator modeling of section 3.3.2.

In the OFF→ON state transition, the time needed to reach 500 Pa for the uranium actuators is almost twice (≈ 180 s) in regard to the same time for the ZrNi ones (≈ 90 s). In the ON→OFF state transition, their speed is comparable; they both take around 200 s to reduce the gap pressure below 1 Pa. The only hydride kinetics change observable in Figure 5-23 is the slowing of the ON→OFF pressure transition. The transition was faster in the 22nd cycle in regard to the other two reported cycles despite the fact that initial ON temperature was higher. However, the available data do not allow one to properly investigate the cause of the variation in the hydride absorption kinetics. In addition, there are indications of a poor heat transfer within the hydride. When the heater is turned off, the measured temperature drops while the pressure do not changed as quickly.

The fact that the temperature curves, and consequently the pressure ones, are not completely flat at the end of the ON state suggest that the equilibrium ON state temperature was never reached.

5.2.3 Discussion

The characterization data of the three uranium actuators have shown that the hydride was operating properly. The ON state could be reached requiring however more power than what was predicted. In fact, the actuator was designed to work at a ON state temperature of 558 K with a power of 3.1 W. The calculation were done assuming an emissivity of the cap of 0.8 and an emitting surface equivalent to the cap area. The heater configuration on U-2 and U-3 had instead higher emitting surface and it required more power (4.2 W).

The actuator thermal performance degraded by cycling. It has been observed that the principal cause of the ON pressure decay has been the degradation of heater attachment to the cap (up to the failure of the heater on U-2). The shifting of the ON state

points in the van't Hoff diagram, visible on Figure 5-19 and Figure 5-21, has been confirmed by a measurement of the characterization data after 6,000 cycles on U-2 and U-3. The origin of the shifting has not been clearly identified. However the fact that the characterization line after cycling and the lines of the ON state points can be aligned parallel to the original characterization line suggest that no major hydride material degradation occurred.

The OFF state pressure was constantly below the instruments minimal reading for U-3 and also for U-2, after the hydrogen concentration was lowered.

The cycles for U-2 and U-3 have been analyzed in terms of *Total Power* and cooling time *Margin* as shown in Figure 5-24. The numerical modeling of the uranium actuator predicted a total power of 4.9 W and a margin of 0.33 [section 3.3.2] for a switch with a thermal mass of 1.2 J/K and a constant ON state power of 3.1 W [the pivotal point in Figure 3-9]. The previous observation that the three thermal masses of the actuators cannot be grouped discourages an attempt of comparing the predicted performance to the experimental data. Considering the different history and behavior of U-2 and U-3 their performance are discussed separately.

The U-2 performance diagram can be separated in three phases: (1) initial 750 cycles before the hydrogen concentration reduction, (2) the cycles after the hydrogen removal and before the heater failure and the (3) the cycles after the heater replacement. The initial cyles are characterized by a high Total Power, up to 36 W, deriving from the slow ON→OFF transition. The OFF state pressure increasing shown in Figure 5-22 deteriorates substantially the actuators total power. In fact, the black points are above 15 W depending on the OFF state pressure. In the margin and total power it was assumed that the heat conductance achieved at the end of the ON or OFF phase was the equilibrium conductance. Until the ON state pressure was above 270 Pa (cycle 890), the switch margin was positive. After that cycle the margin became negative, with the lowest margin value of –0.2 and a total power below 5 W, until the U-2 heater died (darker red points). After the heater replacement, the margin reached its highest peak (0.43) and with a total power of 12.4 W (lighter red points). The margin and the total power decreased with the decaying of the ON state pressure. It is interesting to observe that to achieve the same margin as the ZrNi actuator with the present configuration the total power required is three times greater for U-2.

U-3 performances are less complex: the margin varied between 0.26 and 0.36 with minimal variations in the total power. The margin was sensible to the ON state pressure variations even if they were above the molecular to viscous transition regime.

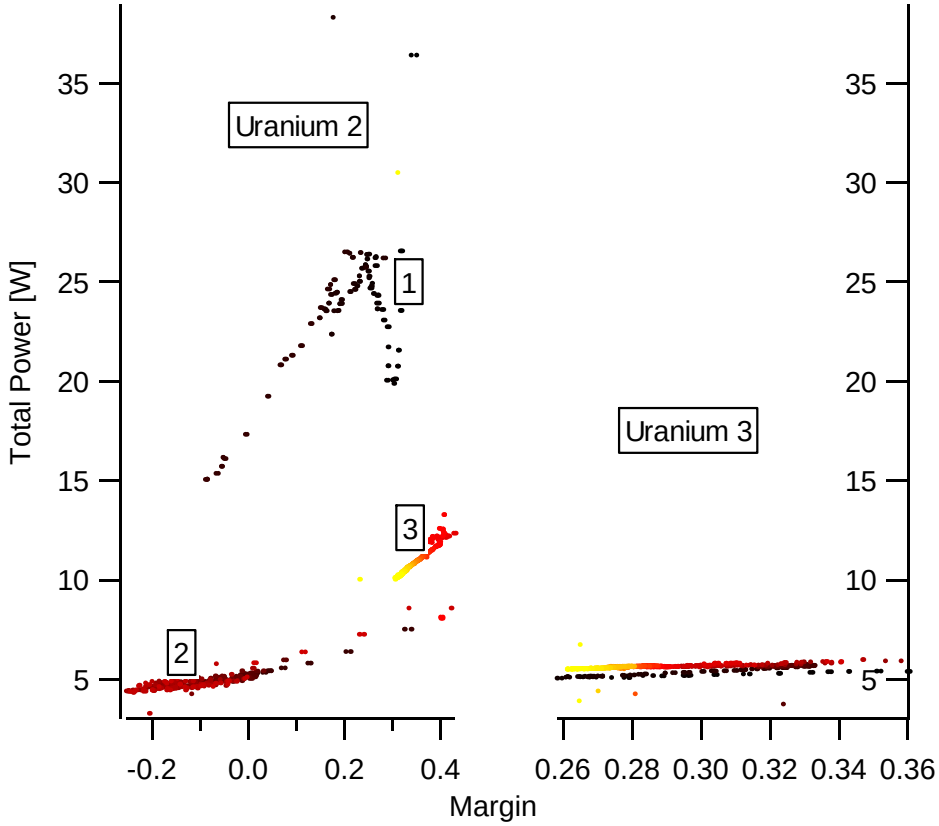

Figure 5-24 Margin and Total Power for the U-2 and the U-3 actuator. The curve color goes from black to yellow as a function of the cycle number. The numbers on the Uranium 2 region indicates (1) cycles before the hydrogen removal, (2) cycles after the removal before heater failure and (3) cycles after the heater replacement

5.3 St-172 test results

Before building the St172-1 actuator, the St172 alloy was tested as a reversible hydrogen pump for more than 500 cycles with no substantial changes in the behavior. The test was conducted utilizing the sintered solid pellet supplied by the manufacturer with a built in heater loaded with a low hydrogen concentration to avoid the embrittlement problem [see Figure 3-6]. In those tests, the temperature required to desorb at a pressure above 270 Pa was almost 1000 K, requiring a large power (34 W). Despite

the high temperature needed to run it, the alloy did not show any degradation and, in addition, fast kinetics were observed. However, it was recognized that the temperature required and the power needed were not practical for a space flight system and it was decided to verify the alloy-hydrogen system properties but at higher concentrations. The material was characterized and thermally cycled (for more than 3,000 cycles up to November 1999) and the hydrogen-hydride system isotherms were measured to characterized the equilibrium pressure vs. temperatures at high hydrogen concentration, since no published data were found for this conditions. After the 3,300 cycle the test was temporarily stopped because the heater power had considerably diminished not allowing reaching a sufficient ON state temperature. Once the heater will be fixed or replaced the test will continue with a 25,000 cycles goal.

5.3.1 Isotherms and characterization data

The behavior of the St172 at a high hydrogen concentration was studied by measuring absorption isotherms on a part of the batch material used for the actuator St172-1. The material was received sintered in solid pellet of 3.2 g that were broken in pieces to be loaded into a stainless steel reactor (3.603 g were loaded). The isotherms were obtained by adding small quantity of hydrogen to the hydride material kept at a uniform temperature, and by measuring the equilibrium pressure of absorption. Objective of these measurements was to obtain a diagram similar the one reported in Figure 3-6 but at higher hydrogen concentrations.

In Figure 5-25 the experimentally data measured isotherms pressures are shown as a function of the hydrogen concentration measured in $mg_H/g_{Hydride}$. No evidences of plateau region are shown. The first isotherm, when the alloy was hydrogenated, was measured at 400C. This isotherm was the only one that started with a zero hydrogen concentration in the hydride system. The main phase in the St172 is zirconium hydride that has a desorption equilibrium pressure of few Pa at 500 C. It was therefore very difficult to remove all the previously stored hydrogen. Between different runs the system was left for 2 to 3 hour at 535 C (the temperature limit of the VCR connecting gasket and gland) pumping on alloy. The positions of the other isotherms in the pressure vs. concentration diagram were measured relatively to the one at 400 C. The concentration offset was determined by taking the system to 400 C and measuring the relative

concentration in respect to measure the isotherms the initial measured isotherm. A description of the system and the procedure used to run it could be found in Appendix C.

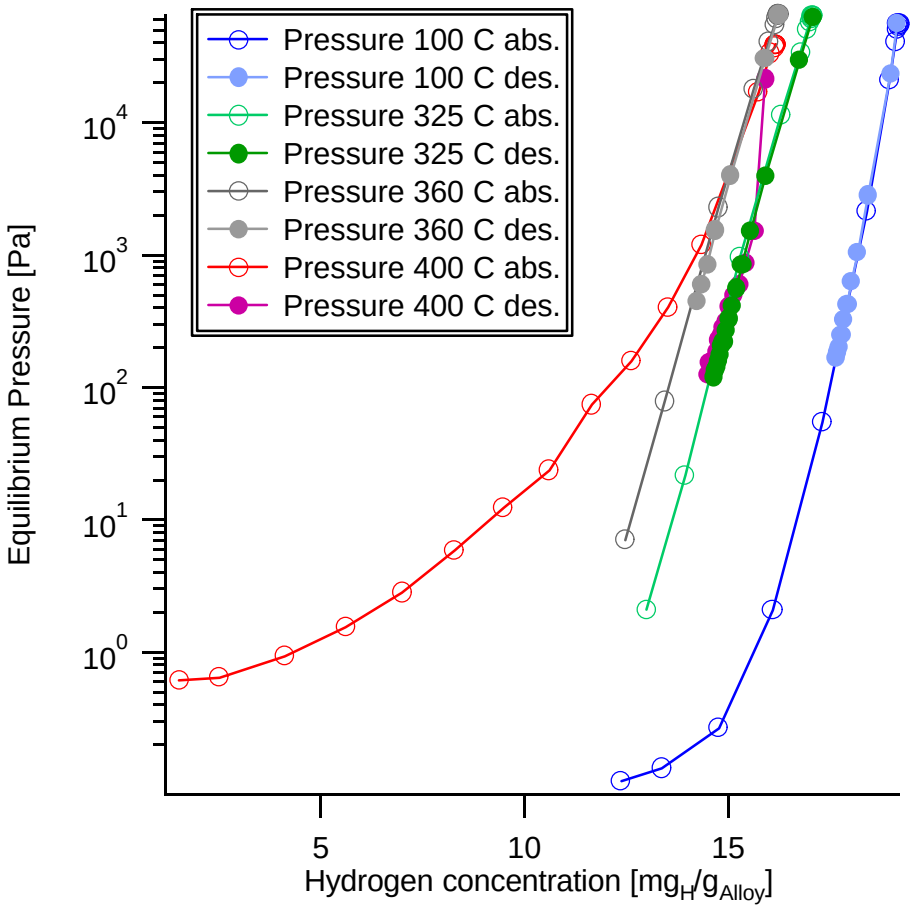

Figure 5-25 Isotherms for the St172 getter alloy with high hydrogen concentration.

To best satisfy the actuator requirements in terms of low power of the ON state and cooling time margin a hydrogen loading close to the maximum concentration of the system would be suggested. Unfortunately, the isotherm measurement were done after the hydrogen loading of St172-1 (at a concentration of 10.14 $mg_H/g_{Hydride}$) because the Sievert's apparatus was not available previously. The concentration has not been changed in consideration of the acceptable actuator performance (see section 4.4). The characterization data for St172-1 are reported in Table 5-1. The characterization data do not agree with the isotherm indicating that the either the temperature reading was not very well related to the hydride temperature or the alloy was subjected to major modifications. In fact, at that actuator hydrogen concentration the equilibrium pressure

derived from the isotherm at 325 C would be below 0.1 Pa. The pressure measured in the actuator assembly at 309 C was instead 1.35 kPa.

Pressure [Pa]	Temperature [C]	Power [W]
338.5	237.2	2.959
659.2	264.5	3.511
908.7	284.3	3.955
1111.0	299.0	4.372
1257.2	309.7	4.742
1349.5	319.7	5.376

Table 5-1 Characterization data for the St172-1.

5.3.2 Life test analysis

The ON state properties of the St172-1 are reported in Figure 5-26. It can be observed that the temperature sensor had initially a problem. The temperature measurement of the ON state in fact fell from 300 C to 130 C after few cycles and since than it was stable at that value. The instrumentation analysis in this case is very complex

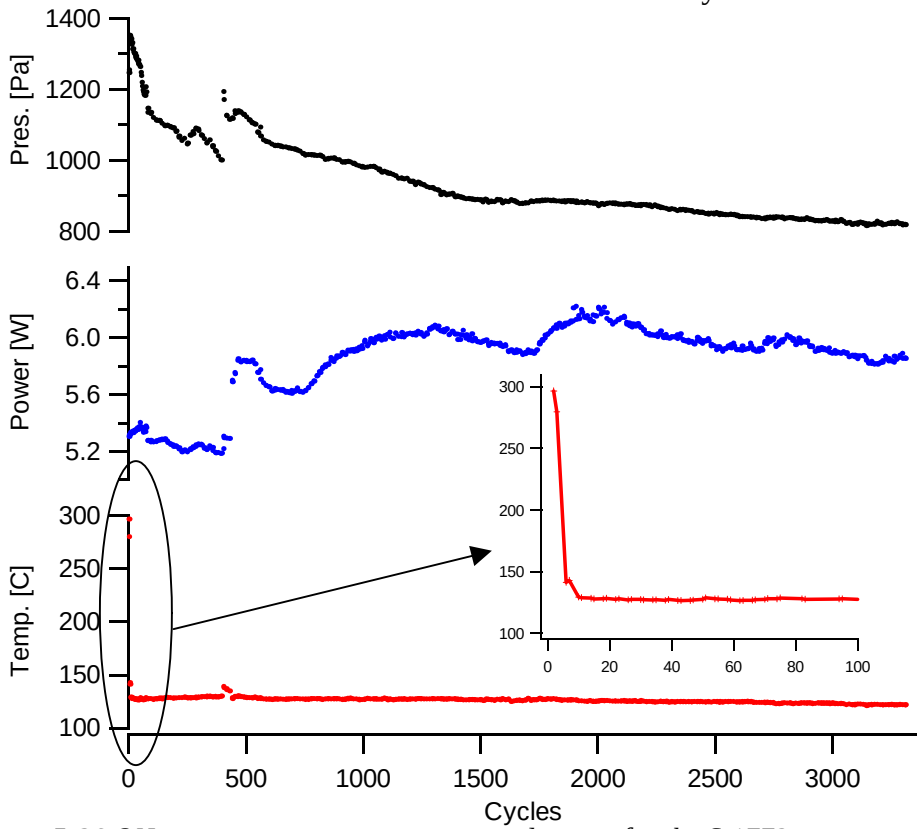

Figure 5-26 ON state pressure, temperature and power for the St1772 actuator.

and would be not sufficiently corroborated by the available data. When the test will be restarted with new instrumentation, namely heater and temperature sensor, more precise indications will be available.

The actuator kinetics did not change in time rather then the different ON state pressure reached at the end of the ON state.

5.3.3 Discussion

The St172 actuator is very demanding in terms of power and heater endurance. In fact it require an average of 5.9 W and the heater lasted little more than 3,000 cycles. In contrast its OFF state power was never above the minimal reading of the pressure transducers and it is high tolerant to potential contaminants.

The cycles for St172-1 have been analyzed in terms of *Total Power* and cooling time *Margin* as shown in Figure 5-27. The total power is slightly above the ON state power [Figure 5-26] indicating that the St172 is originating negligible *DPower*, as it was expected. The cooling time *Margin* is acceptable and, as happened for the ZrNi and U actuators, it degraded by cycling. The major disadvantage of the St-172 actuator is with the heating system.

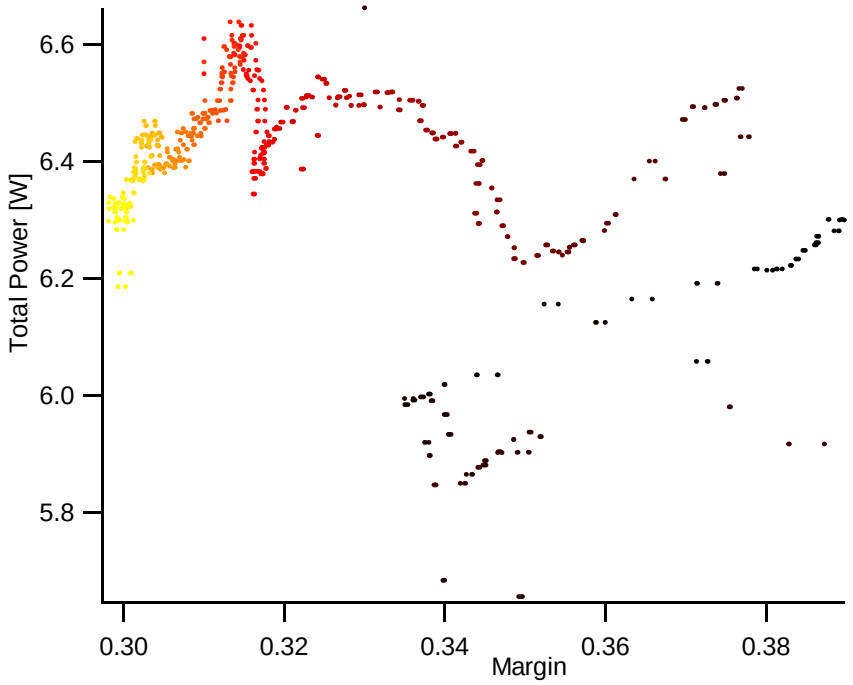

Figure 5-27 Cycle performance of the St172-1: Margin and Total Power for the recorded cycles. The point's color becomes lighter as a function of the cycle number

6. Conclusions

Gas gap heat switches for the Planck sorption cooler have been designed according to measured requirements, have been built, tested and cycled for several months. Operational requirements, such as heat conductance and time to switch, have been derived according to the proposed operational specifications of the sorption cooler and to environmental conditions. The requirements have been validated in the laboratory on prototype compressor units in terms of pressure vs. gap conductance.

The combination of hydrogen and hydrides is a suitable solution for gas gap heat switches and it has been tested in three different designs based on ZrNi, Uranium and St172 hydride. The main objective of this study was to assess the switch design of gas gap actuators for a sorption cryocooler in consideration of the requirements imposed by the cooler and the environmental conditions. In fact, the switch will be used to thermally optimize the compressor elements of a space flight 20 K cooler. The heat transfer on a similar compressor unit was measured at different hydrogen gas pressures in the gap to derive the pressure requirements for the switch actuator.

Three hydrides were selected as a reversible hydrogen storage media for the actuator. Particular regard was taken to the fact that the heat switch is supposed to have a lifetime of at least 1.5 years, equivalent to 16,000 cycles. In fact, the major concern in this technology development was the repeatability of the hydride performances over a long term cycling. Seven actuators were built and tested. After ≈ 13,000 cycles for the ZrNi actuators, ≈ 6,000 cycles the Uranium actuators and ≈ 3,000 cycles the St 172 actuator, the critical characteristics for the three different designs can be summarized as follows:

ZrNi switch. The tested ZrNi switches have shown to be low power consumption units with high cooling margin and no hydride degradation in time. The fact that they require low temperatures to reach the ON state pressure is their major asset, implying a low ON state power, and is not extremely stressing conditions for the heaters and the heater attachment. However, this sorbent is very sensitive to cleaning procedures, with potential of build-up pressure of pressure in the OFF state from impurities (i.e., methane, water, etc.) and increasing the power losses to the radiator.

Uranium and St172 switches. Uranium and St 172 switches do not have any problem in reaching a low pressure in the OFF state but they require high ON state temperature. Consequently they require high power imposing significant thermal stresses on the heater and the heater attachment.

The evaluation of the actuators was based on the two figure of merit: the cooling time *Margin* and the *Total Power*. The *Margin* has been used to appraise the capacity of the switch to cool the compressor unit in the appropriate cycle time, and the *Total Power*, to evaluate the power needed to run the switch and the power losses induced in the compressor unit during its heating phase.

It has been observed that all the switches had a positive *Margin* during the cycles performed up through November 1999 and that the *Total Power* of the switch is below 15 W. An exception was observed for U-2 but, when the issues were fixed, the *Margin* came back to 0.4 and the *Total Power* decreases to 12 W. Some problems were in fact encountered in the assembly and in the instrumentation of the switches, especially in the heater attachment on the cap. In was observed that the heater attachment to the cap deteriorated in time. Most of the actuator performance reductions are attributed to that reason and no major performance decay associated with degradation hydrogen-hydride system was observed. However, it has to be noted that refined information on the hydride degradation cannot be inferred, since the test was not intended to be a material characterization study per se.

Some problems were encountered in the assembling and in the testing of those switches. The major complications were encountered in the heater attachment: the higher the temperature of the ON state made it more difficult to keep the heater attached and to remain in adequate thermal contact with the cap. Therefore a robust switch design must be a major objective in future assessment and test of solid heater configurations.

Considering the difficulties found, it is suggested to use the lowest ON state temperature hydride, ZrNi, in the flight unit switches and to build a heater that could be brazed directly to the cap. The epoxy used in the present study did not have any major problems, but better robustness of the attachment, in consideration of the vibrations during launch, has to be tested. A brazed attachment solution would be preferable providing it does not excessively increase the thermal mass of the switch. It is also suggested to consider a different way of machining the ZrNi slices to use as hydride. The

surface contaminants that could not be removed properly before hydride activation are believed to be responsible of the OFF pressure increasing in time which would enhance the power losses from the compressor unit to the radiator. However, a final decision in the selection of the flight unit actuator hydride implies further system-engineering considerations to balance the risk of gas gap heater failures versus reduction of the heat losses from the compressor unit to the radiator as well as reliable operation during nearly 20,000 heating cooling cycles.

7. References

1 N. Mandolesi, *Low Frequency Instrument for PLANCK proposal to ESA*, February 1998

2 R.B. Partridge, *3 K: The Cosmic Microwave background radiation*, Cambridge University Press 1995

3 B. Collaudin, T. Passvogel, *The FIRST and PLANCK 'Carrier' missions. Descriptions of the Cryogenic Systems*, Cryogenics 39, 157 (1999)

4 P. Bhandari, R.C. Bowman, R.G. Chave, C.A. Lindensmith, G. Morgante, C. Paine, M. Prina, L.A. Wade, *Sorption Cryocooler Development for the PLANCK Surveyor Mission*, submitted to Astrophysics Letters & Communications, (Oct 1998)

5 R.C. Bowman, J.S. Cantrell, T.W. Ellis, T.D. Flanagan, J.D. Clewley, S.Luo, *Hydriding Properties of the Pseudo-Binary Alloys* $LaNi_{5-y-x}Mn_ySn_z$, Hydrogen Energy Process X, edited by D.L Block and T.N. VeziroGlu (Int. Assoc. Hydrogen Energy, Miami FL, 1994)p.1199

6 B.D. Freeman, E.L. Ryba, R.C. Bowman Jr., J.R. Phillips, *Progress toward the Development of Hydrogen Sorption Cryocoolers for Space Applications*, Int. J. Hydrogen Energy, 22, 1125 (1997)

7 L.A. Wade, P. Bhandari, R.C. Bowman, Jr., C. Paine, G. Morgante, C.A. Lindensmith, D. Crumb, M.Prina, R. Sugimura, D. Rapp, *Hydrogen Sorption Cryocoolers for the Planck Mission*, presented at 13th Int. Cryogenic Conf (1999), submitted to Adv. Cryogenic Engineering vol. 45

8 F.P. Incropera, D.P. Dewitt, *Fundamentals of Heat Transfer*, John Wiley & Sons, 1981

9 R.C. Bowman, P.B. Karlmann, S. Bard, *Brilliant Eyes Ten-Kelvin Sorption Cryoooler Experiment*, JPL publication 97-14, issued Sept 1997

10 S. Bard, P. karlmann, J. Rodriguez, J. Wu, L. Wade, P. Cowgill, K.M. Russ, *Flight Demonstration of a 10 K Sorption Cooler*, Crycoolers 9, edited by R.G. Ross, Jr., Plenum Press, 1997

11 R. Wiswall, *Hydrogen storage in metals* in *Hydrogen in metals II*, edited by G.Alefeld and J. Volkl, Springer-Verlag, 1978, 201-242

12 C Boffito, F. Doni, L. Rosai, *The Properties of Some Zirconium-Based Gettering Alloys for Hydrogen Isotope Storage and Purification*, J. Less-Common Metals, 104, 149 (1984)

13 H. Albrecht, U. Kuhnes, A.Asel, *Application of SAES and HWT gas purifiers for the removal of impurities from helium-hhydrogen gas mixtures*, J. Less-Common Metals, 172-174, 1157 (1991)

14 W.T. Shmayda, N.P. Kherani, A.G. Heics, *Tritium removal from noble gas steams*, J. Vac. Sci. Tech. A 6 (3) (1988)

15 W.T.Shmayda, P. Mayer, *Uranium Beds for Temporary Tritium Storage*, J. Less-Common Metals, 104, 239 (1984)p. 2447

16 F. Doni, C. Boffito, B. Ferrario, *Hydrogen Isotope Sorption and Recovery by a non-evaporable getter combined with a chemical compressor material*, J. Vac. Sci. Tech. A 4 (6) (1986), p. 417

17 T.A. Giorgi, B Ferrario, B. Storey, *An updated review of getters and gettering*, J. Vac. Sci. Tech. A 3 (2) (1985)

18 N.P. Kherani, W.T. Shmayda, *Gas Handling Systems Using Titanium-Sponge and Uranium Bulk Getters*, Fusion Technology vol. 8 (1985), p. 2399

19 H. Albrecht, U. Kuhnes, W. Asel, *Application of SAES and HWT gas purifiers for the removal of impurities from helium-hydrogen gas mixtures*, J. Less-Common Met. 172-174, 1157 (1991)

20 K. J. Gross, *Intermetallic materials for hydrogen storage*, Ph.D. thesis n^1217, Institute de Physique-Université de Fribourg, Suisse (1999)

21 C.B. Magee, J. Liu, C.E. Lundin, *Relationships between Intermetallic Compound Structure and Hydride Formation*, J. Less-Common Met. 78, 119 (1981)

22 D.G. Westlake, *Stoichiometries and Interstitial Site Occupation in the Hydrides of ZrNi and other Isostructural Intermetallic Compounds*, J. Less-Common Met. 75, 177 (1980)

23 J.H.Wernick, *Topological Close-Packed Structures* in *Intermetallic Compounds*, R.E. Krieger Publishing Com., 1977

24 P. Dantzer, W. Luo, T.B. Flanagan, J.D. Clewley, *Calorimetrically Measured Enthalpies for the Reaction of H_2 (g) with Zr and Zr Alloys*, Metallurgic Transactions A, 24 A, 1471 (1993)

25 W. Luo, J.D. Clewley, T.B. Flanagan, *Calorimetrically Measured Enthalpies for the Reaction of H_2 (D_2) (g) with Ti and Ti-Ni Alloys*, Metallurgic Transactions B, 24 B, 867 (1993)

26 W. M. Muller, J.P Blackledge and G.G. Libowitz, *Metal Hydrides*, New York Academic, 1968

27 W. Luo, T. Kuji, J.D. Clewley, T.B. Flanagan, *The thrmodynamic properties of the niobium-hydrogen system measured by reaction calorimetry*, J. Chem. Physics 94 (9), 6179 (1991)

28 H. Choi, A.F. Mills, *Heat and Mass Transfer in Metal Hydrides Beds for Heat Pump Applications*, Int. J. Heat Mass Transfer, vol. 33, n 6, 1281 (1990)

29 W. Supper, M. Groll, U. Mayer, *Reaction Kinetics in Metal hydride Reaction Beds with Improved Heat and Mass Transfer*, J. Less-Common Met. 104, 279 (1984)

30 S.Suda, N. Kobayashi, K. Yoshida, Y. Ishido, S. Ono, *Experimental measurement of thermal conductivity*, J. Less-Common Met. 74, 127 (1980)

31 E.Suissa, I. Jacob, Z. Hadari, *Experimental measurements and general consclusions on the effective thermal conductivity*, J. Less-Common Met. 104, 287 (1984)

32 D. Sun, S. Deng, *Theoretical Descriptions and Experimental Measurements on the Effective Thermal Conductivity in Metal Hydride powder Beds*, J. Less-Common Met. 160, 387 (1990)

33 E. Fromm, *Kinetics of Metal-Gas Interactions at Low Temperatures*, Springer-Verlag (1998)

34 K. Ichimura, M. Matsuyama, K Watanabe, *Alloyng effect on the activation processes of Zr-alloy getters*, J. Vac. Sci. Technol., A 5 (2) (1987), p. 220

35 J.S. Cantrell, R.C. Bowman, L.A. Wade, S. Luo, J.D. Clewley, T.B. Flanagan, *Thermodynamic Properties and the degradation of $ZrNiH_x$ at elevated temperatures*, J. of Alloys and Comp. 231, 518 (1995)

36 G.K. White, *Experimental Techniques in Low-Temperature Physics*, Oxford University Press, 1979, volume 3, p. 3.57

37 P.A. Nelson, A.A. Chilenskas, R.F. Malecha, *Variable Pressure Insulating Jackets for High-Temperaure Batteries*, Proc. Of the 27th Intersociety Energy Conversion, 1992

38 S. Burch, F.T. Potter, M.A. Keyser, M.J. Brady, K.F. Michaels, *Reducing Cold-Start Emission by Catalytic Converter Thermal Management*, NREL/TP-473-7025

39 D.K. Benson, T.F. Potter, C.E. Tracy, *Design of a Variable-Conductance Vacuum Insulation*, SAE Tech. Paper # 940315 (1995)

40 D.L. Johnson, J.J Wu, *Feasibility Demonstration of a Thermal Switch for Dual Temperature IR Focal Plane Cooling*, Crycoolers 9 edited by R.G. Ross, (1997), p. 795

41 J.F. Burger, H.J. Holland, H. van Egmong, M. Elwenspoek, H.J. ter Brake, H. Rogalla, *Fast Gas-Gap Heat Switches for a Microcooler*, Crycoolers 10 edited by R.G. Ross, (1999). P. 565

42 L. Duband, L. Hui, A. Lange, *Space-borne ^{3}He refrigerator*, Cryogenics 30, 263 (1990)

43 SAES notes for INTELLIGETTER devices

44 M. Prina, P. Bhandari, R.C. Bowman, C. Paine, L.A. Wade, *Development of Gas Gap Heat Switch Actuator for the Planck Sorption Cryocooler*, presented at 13th Int. Cryogenic Conf (1999), submitted to Adv. Cryogenic Engineering vol. 45

45 E. H. Kennard, *Kinetic Theory of Gases with an Introduction to Statistical Mechanics*, McGraw-Hill Book Company, New York, 1938.

46 W.van Willingen, *Angular Distribution of Hydrogen Molecules Desorbed From Metal Surfaces*, Physics Letters, 28A, 80 (1968)

47 G. Comsa, R. David, K.D. Rendulic, *Velocity Distribution of H2, HD, and D2 Molecules Desorbing from Polycrystalline Nickel Surfaces*, Physical Review Letters, 38, 775 (1977)

48 L. B. Loeb, *Kinetic theory of gases*, McGraw-Hill Book Company, New York, 1934.

49 S. Dushman, *Scientific Foundations of Vacuum Technique*, John Wiley & Sons, second printing, 1962,

50 I. Langmuir, K.B. Blodgett, *Accommodation coefficient of Hydrogen: a sensitive detector of surface films*, Physical Review, vol. XL, N. 1, 78, 1932

51 H.Y. Wachman, *The Thermal Accommodation Coefficient: A Critical Survey*, American Rocket Society, 32, 2, 1962

52 E.R. Grilly, W.J Taylor, H.L. Jonhston, *Accommodation Coefficients for Heat Conduction between Gases and Bright Platinum, for Nine Gases between 80 K (or their Boiling Points) and 380 K*, Jour. Chem. Phys., 14,435,(1946)

53 R.B. Scott, *Cryogenic Engineering*, D. van Nostrand Co, (1959)

54 H.Y, Wachman, *The Thermal accommodation coefficient and Adsorption on Tungsten*, ph.D. dissertation, University of Missouri (1957)

55 J.H. Jeans, *An Introduction to the Kinetic Theory of Gases*, The MacMillan Co., 1940

56 R.D. Penzhorn, M Devillers, *Evaluation of ZrCo and other getters for tritium handling and storage*, Journal of Nuclear Materials 170, 217-231 (1990)

57 R.C. Bowman and R. Scott Dowling, *Evaluation of Metal Hydrides and Design of Low - Pressure Sorption Bed for the Production of Solid Hydrogen via Joule Thomson Expansion – Final Report* , Aerojet Report 9786, issued 1991

58 C. Lartique, A. Percheron-Guégan, J.C. Archard, F. Tasset, *Thermodynamic and Structural Properties of $LaNi_{5-x}Mn_x$ compounds and their related hydrides*, J. Less-Common Met., 75, 23 (1980)

59 W. Luo, S. Luo, J.D. Clewley, T.B. Flanagan, R.C. Bowman, J.S. Cantrell, *Thermodynamic and degradation studies of $LaNi_5$ (closely stoichiometric)-H and $LaNi_{5-x}Mn_x$-H with x=0.5-2*, J. Alloys and Compounds, 202, 147 (1993)

60 M. Gupta, L. Schlapbach, *Electronic Properties* in *Hydrogen in Intermetallic Compounds I*, edited by L. Schlapbach, Springer-Verlag, 1988 pag.139

61 S. Konishi, T. Nagasaki, T. Hayasashi, K. Okuno, *Equilibrium Hydrogen Pressure on the Solid Solutions of ZrCo-HfCo Intermetallic Compound*, J. of Nuclear Materials 223, 300 (1995)

62 M.Devillers, M. Sirch, S. Bredendiek-Kamper, R.D. Penzhorn, *Characterization of the Zr-Co Hydrogen System in View of Its Use for Tritium Storage*, Chem. Mater., 2, 255 (1990)

63 S.J.C. Irvine, I.R. Harris, *The effect of Induced Disorder on the Hydrogenation Behavior of the Phase ZrCo*, included in *Hydrides for Energy Storage* by A.F. Andresen, A.J. Maeland, Pergamon Press (1977)

64 R.D. Penzhorn, M. Devillers, M. Sirch, *Storage of Tritium in ZrCo Alloy: Effect of pre-exposure to impurities relevant to the fusion cycle*, J. of Nuclear Materials, 179-181, 863 (1991)

65 M. Devillers, M. Sirch, R.D. Penzhorn, *Hydrogen Isotopes in Pure and Nitrated ZrCo*, Zeitschrift fur Physikalische Neue Folge, 164, 1355 (1989)

66 W.M. Mueller, J.P. Blackledge, G.G. Libowitz, *Metal hydrides*, Academic Press 1968

67 D.L. Lindner, *Isothermal Decomposition of Uranium Hydride*, J. Less-Common Met., 157, 139 (1990)

68 E. Wiche, K. Otto, *The Uranium-Hydrogen System and the Kinetics of Hydride Formation*, Z. Phys. Chem. Frankfurt 31, 222 (1962)

69 R.M. Alire, B.A. Mueller, C.L. Peterson, J.R. Mosley, *Reaction Kinetics of Uranium and Deuterium*, Jour. Of Chem. Phys. Vol. 52, 1 (1970)

70 J.B. Condon, E.A. Larson, *Kinetics of the uranium-Hydrogen System*, Jour. Of Chem. Phys. Vol. 59, 2 (1972)

71 G.L Powell, W.L. Harper, J.R. Kirkpatrick, *The Kinetics of the Hydriding of Uranium Metal*, J. Less-Common Met., 172-174, 116 (1991)

72 G.L. Powell, R.N. Ceo, W.L. harper, J.R. Kirkpatrick, *The Kinetics of the Hydriding of uranium metal II*, presented at the Int. Symp on Metal-Hydrogen Systems, Sweden (1992)

73 T. Kabatumori, Y. Wakisaka, K. Tsuchiya, H. Kawamura, *Improvement of Hydriding Properties of Zr1Ni Alloy by Adding Third Transition Metals for Tritium Recovery*, Jour. Of Nuclear Materials, 258-263, 481 (1998)

74 K. Nakamura, T. Hoshi, *Supply and Recovery of Hydrogen Isotopes in High Vacuum Systems using ZrNi Hydride Getter Pumps*, J. Vac. Sci. Technol., A 3 (1985), p. 34

75 J.M Joubert, M. Latroche, A. Percheron-Guégan, *Hydrogen Absorption Properties of Several Intermetallic Compounds of the Zr-Ni System*, J. of Alloys and Comp. 231, 494 (1995)

76 R. Kronski, T. Schober, *A Transmission Electron Microscopy and Differential Thermal Analysis Study of NiZr-H System*, J. of Alloys and Comp. 205, 175 (1994)

77 W. Luo, A. Craft, T. Kuji, H.S. Chung, T.B. Flanagan, *Thermodynamic Characterization of the ZrNi-H System by Reaction Calorimetry and p-c-T Measurements*, J. Less-Common Met., 162, 251 (1990)

78 K. Watunabe, M. Hara, M. Matsuyama, I. Kanesaka, T. Kabutoori, *Stability of ZrCo and ZrNi to Heat Cycles in Hydrogen Atmosphere*, Fusion Technology, 28, 1437 (1995)

79 D.H. Meikrantz, J.D. Baker, G.L Bourne, R.J. welko, R.A. Anderl, D.G. Tuggle, H.R. Maltrud, *Tritum Process Applications Using SAES Getters for Purification and Collection from Inert Gas Streams*, Trans. Of Fusion Tech., 27, 14 (1995)

80 G. Bonizzoni, F. Ghezzi, M. Nassi, L. Succi, *New Getter Clean-up System for Tritiated Glove Box Atmosphere*, J. Vac. Sci. Technol., A 8 (2) (1990), p.961

81 K. Ichimura, M. Matsuyama, K. Watanabe, T. Takeuchi, *Recovery and Storage of Tritium by Zr-V-Fe Getter*, Fusion Tech. 8, 2407 (1985)

82 K. Ichimura, M. Matsuyama, K. Watanabe, T. Takeuchi, *Absorption/Desorption of Hydrogen Isotopes and Isootpic Waters by Zr-Alloy Getters*, J. Vac. Sci. Technol., A 6 (4) (1988), p. 2441

83 C. Boffito, F. Doni, L. Rosai, *The properties of some Zirconium-based Gettering Alloys for Hydrogen Isotope Storage and Purification*, J. Less-Common Met., 104, 149 (1984)

84 SAES Getter private communication.

85 Mott Filters manufacturer specifications, [www.MottCorp.com]

86 Watanabe K., K. Tanaka, M Matsuyama, K. Hasegawa, *Zr Ni Alloys as candidate getter materials for tritium processing*, Fusion Eng. And Design, 18, 27 (1991)

7. APPENDICES

HYDROGEN SORPTION CRYOCOOLERS FOR THE PLANCK MISSION

L. A. Wade[1], P. Bhandari[1], R. C. Bowman, Jr.[1], C. Paine[1], G. Morgante[2], C. A. Lindensmith[1], D. Crumb[3], M. Prina[4], R. Sugimura[1], D. Rapp[1]

[1]California Institute of Technology, Jet Propulsion Laboratory
Pasadena, CA 91109, USA
[2]CNR-Te.S.R.E.
Bologna, Italy
[3]Swales Aerospace
Pasadena, CA 91107, USA
[4]Politecnico di Milano
Milano, Italy

ABSTRACT

Two continuous operation 18 K/20 K sorption coolers are being developed by the Jet Propulsion Laboratory (JPL) as a NASA contribution to the European Space Agency (ESA) Planck mission that is currently planned for a 2007 launch. The individual sorption coolers will each be capable of providing a total of 230 mW of cooling at 18 K and 1.45 W at 20 K given passive radiative precooling at 50 K. The hydrogen sorption coolers will directly cool the Low Frequency Instrument HEMT amplifiers to approximately 20 K and will also serve to intercept parasitics and precool a RAL 4.5 K closed-cycle helium J-T cooler to 18 K for the separate High Frequency Instrument. The operating conditions and mission requirements for the Planck sorption cooler are presented. The concept design of the 20 K coolers is described along with the predicted performance. $La_{1.01}Ni_{4.78}Sn_{0.22}$ hydride sorbent beds are currently in fabrication and initial test data on their performance are presented.

INTRODUCTION TO PLANCK

Planck, the third Medium-sized ESA mission M3, will be launched in 2007 in combination with the Far InfraRed and Sub-millimetre Telescope (FIRST). Planck will carry two instruments: the High Frequency Instrument (HFI) and the Low Frequency Instrument (LFI). Together they will observe and image the full sky in nine spectral bands between 30 and 857 GHz. The LFI utilizes an InP HEMT amplifier radiometer cooled to 20 K through a combination of passive cooling to <50 K and the hydrogen

sorption coolers. The HFI observes using bolometers cooled to 100 mK through a combination of passive coolers, the 18 K/20 K sorption cooler, a 4.5 K RAL Mechanical J-T cooler and an Benoit style open cycle dilution cooler[1].

Planck is the third generation space mission (following COBE and MAP) to be designed for observation of the Cosmic Microwave Background (CMB) anisotropies. Planck will observe the full sky and produce maps with an accuracy limited only by cosmic variance and astrophysical foregrounds at all angular scales larger than 10' for the LFI and 6' for the HFI. In addition, both instruments will be capable of measuring the polarization in the CMB. The unprecedented angular resolution and sensitivity ($\Delta T/T \sim 2 \times 10^{-6}$) will allow the primary cosmological parameters (Hubble constant, deceleration parameter, curvature of space, baryon density, amplitude and spectral index of the primordial scalar density perturbations, and the gravity wave content of the Universe) to be determined to an accuracy of a few percent. In doing so a number of truly fundamental questions will be answered about our Universe: How fast is the Universe expanding? What is the ultimate fate of the Universe? What are its material constituents (baryons, dark matter,…)? Where did the initial perturbations come from? When did the first structures form in the Universe? What is the nature of particle physics at energies $\sim 10^{16}$ GeV?

PLANCK PAYLOAD DESIGN OVERVIEW

As with most fundamental physics experiments, the data to be taken by Planck are more coupled to the specifics of the experimental apparatus and environment than to the science of interest. Uncertainties or oscillations in pointing, supply voltages, thermal fluctuations, straylight (much of this is thermal emission from different surfaces) all impact the data collected by the instrument. As an example, the spacecraft emits approximately 10^3 W. The HFI is sensitive to energy levels on the order of 10^{-18}W. As a consequence, even extraordinarily minute spacecraft thermal emission fluctuations that reach the HFI detector could be confused with sky emission.

Changes over some timescales, especially at about the 1 minute spin period, are particularly critical, as they are difficult to distinguish from the observed sky. Even worse, this does not mean that these changes necessarily have a frequency of 0.01667 Hz; but only that they have a non-zero Fourier component at this frequency. The result is that the mission configuration and design, along with the instrument designs, operational and data analysis strategies, must all be driven to minimize systematic effects on the final science data products by reducing the level of these effects and ensuring that they are well understood so that the residual effects can be confidently removed in software without adversely affecting the science results. Ensuring the successful accomplishment of the science goals is the major factor affecting the mission design, and therefore the 18/20 K coolers design.

Planck will fly in a Lissajous orbit around the Earth-Sun L_2 point, and spins at about 1 rpm about an axis that points towards the sun. The 1.5 m aperture telescope looks 80^o to the spin axis and scans circles in the sky. Figure 1 shows a crossection view of a likely configuration for the Planck spacecraft. As the Architect Study is still underway, some changes from this figure will occur.

All warm components of the instruments are mounted on the service module. This includes not only the instrument electronics but the warm compressors of the sorption coolers and the RAL 4.5 K mechanical J-T cooler, the gas storage tanks for the dilution refrigerator and all their associated electronics. The optical bench and telescope are thermally isolated from the warm spacecraft bus by low conductance struts and v-groove shields. V-groove shields are a set of two or more angled low-emissivity specular surfaces typically 2 to 5 degrees out of parallel. The radiative heat transfer between two

facing surfaces of the V-groove shield with emissivity ε is proportional to ε^2, while that between infinite parallel planes is ε/2. The extra energy in the V-groove case is radiated to space. The V-groove shield therefore can provide extremely good radiative isolation between objects at different temperatures even with surfaces of only moderately low emissivity. In addition, it can be highly efficient at intercepting conductive thermal loads and radiating them to space. The reduction in heat transfer in this arrangement is significantly superior to that typically achieved by conventional Multi-Layer Insulation (MLI) between two parallel plates. The v-groove design concept was originally invented by Ray Garcia at JPL. Since then this new technology has been validated in thermal vacuum and vibration tests[2,3]. Similar 'bounce-view-of-space' tricks are commonly employed in high performance radiators (e.g. the NIMS radiative cooler for the Galileo orbiter[4]) and therefore substantial flight heritage date exists for evaluating the long term behavior of such surfaces.

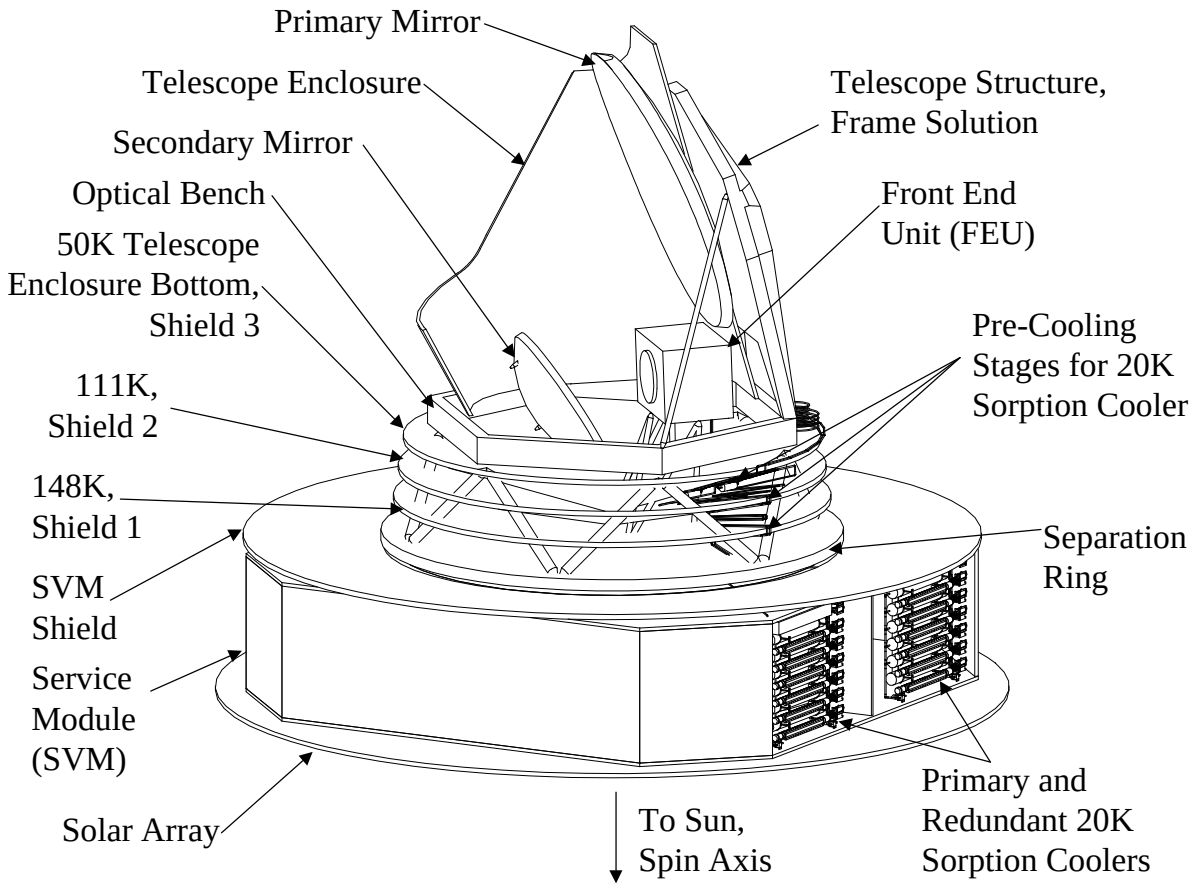

Figure 1. The Planck configuration optimizes passive radiative cooling and minimizes straylight and other systematic effects on the final science data.

The current estimates for shield temperatures are 148 K for the first thermal shield, 111 K for the second and 50 K for the telescope enclosure[5]. The Front End Unit (FEU) is located within the telescope enclosure. This contains the frontend radiometer of the LFI as well as the HFI bolometer array.

PLANCK 18 K/20 K COOLERS OVERVIEW

Two sorption coolers will be flying on the Planck mission. One will provide the primary cooling of up to 230 mW at 18 K for HFI parasitic interception and RAL 4.5 K J-T cooler precooling, and up to 1.45 W of cooling at 20 K for the LFI. The second will be turned off and used as a backup unit should anything happen to the primary cooler. Each cooler is sized to achieve a two year operating life. The cooler input power is 520 W at end-of-life plus an additional 30 W estimated for the cooler electronics. Figure 2 shows a schematic of the sorption cooler that will be used on the Planck spacecraft.

The inherently split design of continuous operation sorption coolers both enables, and maximally benefits from, the passively cooled design needed to minimize systematic impacts on the data gathered but which requires the spacecraft to be located over a meter from the 20 K Front End Unit. The very long operating cycle of the sorption cooler enables easy thermal fluctuation characterization and removal from the science data.

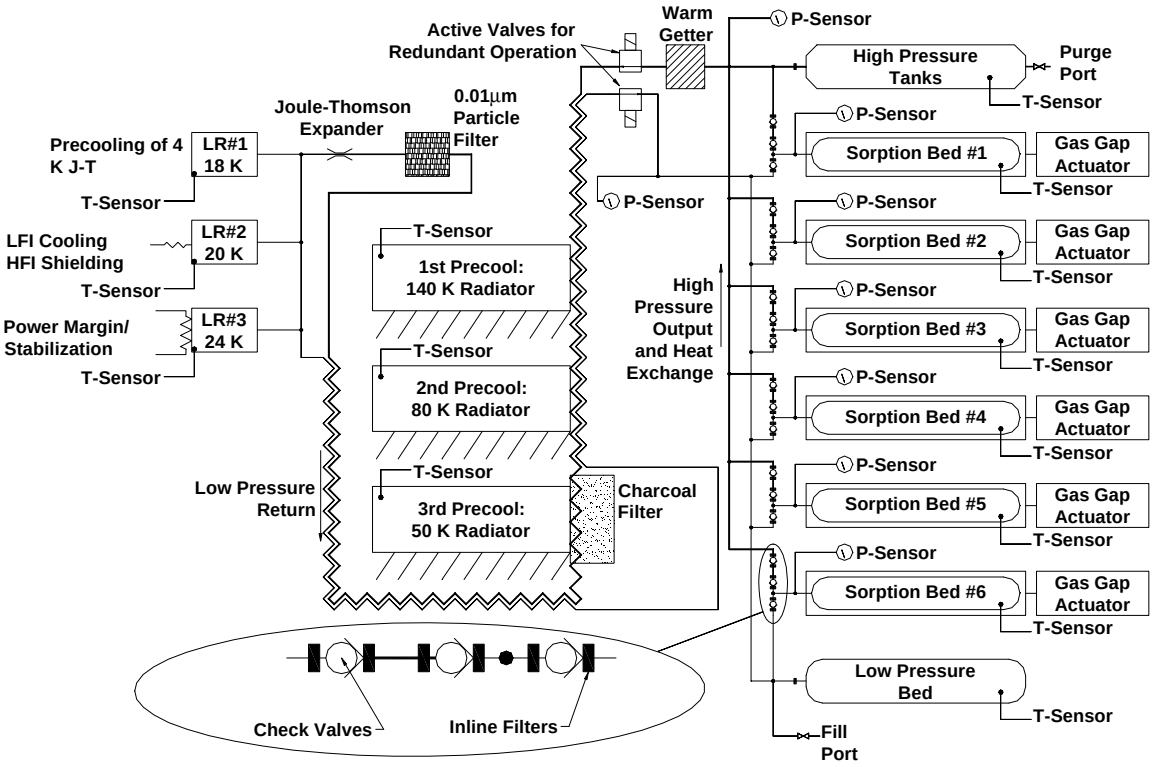

Figure 2. Planck sorption cooler schematic.

The compressor assembly shown in figure 3 is composed of six identical sorption compressor elements, each filled with metal hydride and provided with independent heating and cooling which will be described later. Each compressor element is connected to both the high pressure and low pressure sides of the plumbing system through check valves, which allow gas flow in a single direction only. The check valves are indicated on the schematic as single arrows, which indicate the direction of gas flow through them. In addition to the compressors, there are five one-liter high-pressure

stabilization tanks connected to the high pressure side of the system to damp out oscillations of the high pressure gas, and a low pressure stabilization sorbent bed to damp out pressure fluctuations of the low pressure gas.

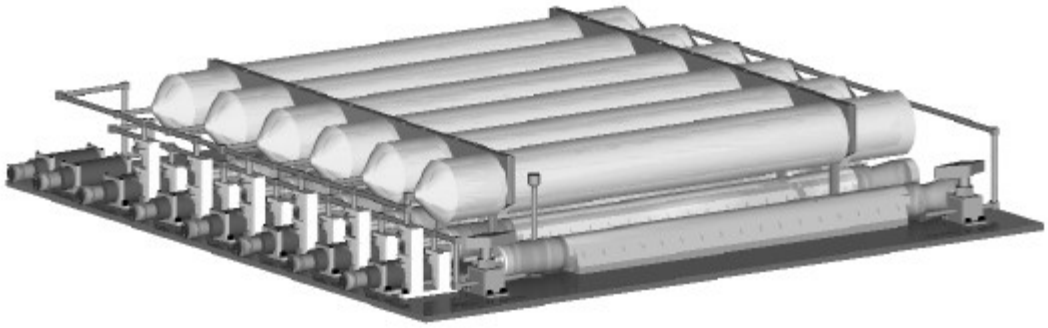

Figure 3. Planck sorption cooler compressor assembly

Refrigerant travels from the compressors through a series of heat exchangers and radiators, which provide precooling to approximately 50 K, through the J-T expander at the FEU. The cold end assembly shown in figure 4 includes three liquid reservoirs in the system: a first reservoir providing 18 K cooling of the 4.5 K RAL mechanical J-T and the HFI thermal shielding, a 20 K reservoir providing cooling to the LFI, and an overflow reservoir for unused cooling capacity. Each of the reservoirs is filled with a wicking material in order to retain the liquid in the reservoirs without gravity. The third reservoir is maintained above the hydrogen equilibrium temperature, to wick and then sublimate any liquid which reaches it, providing an even gas flow back to the sorbent bed.

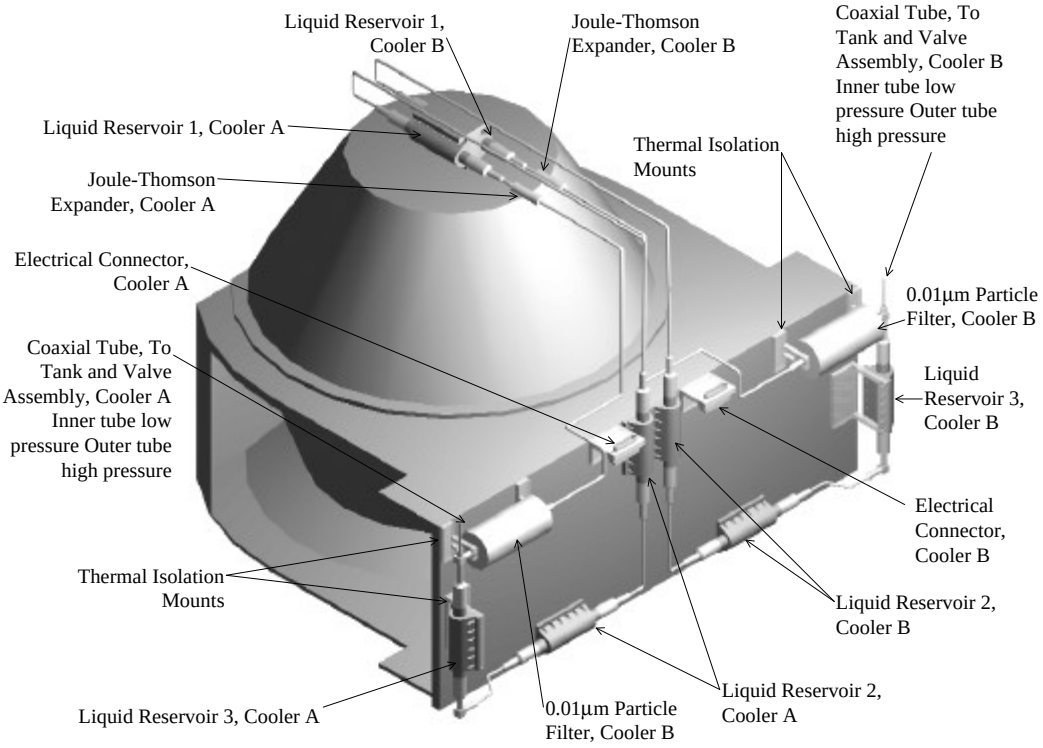

Figure 4. Planck sorption cooler cold end assembly

All regulation of the system is done by simple heating and cooling, with no active control of valves being necessary. Normal operation of the compressors can be done with only a minimum of active feedback: The heaters for the compressors are controlled by a simple timed on-off heater system. In addition to the on-off heater power, each heater will have up to 30 W of additional heating supplied by a proportional controller to compensate for any degradation of hydride or gas-gap properties that might occur.

Compressor Assembly

The compressor assembly is comprised of the six compressor elements, high-pressure stabilization tanks, the low pressure stabilization bed, check valves, and manifolding. The switch time is 667 s leading to an overall cycle time of 4000s. The compressor assembly mounts directly onto the heat rejection radiator. This radiator is sized to reject the cooler input power at 270 K +10 K/-20 K. The low heat rejection temperature was selected to ensure precooling of the 4.5 K RAL cooler at less than 19 K. The compressor assembly mass is 40 kg. It's volume is 0.25 m x 0.8 m x 0.8 m.

A single compressor element is comprised of two concentric cylinders closed with end caps. The inner of these tubes contains the $La_{1.01}Ni_{4.78}Sn_{0.22}$ hydride material and the outer forms a vacuum jacket around the inner cylinder. An exploded view of an compressor element is shown in figure 5. This vacuum jacket is used as a gas-gap heat switch. A recently assembled compressor element which is being used for gas-gap thermal switch characterization is shown in figure 6. The hydrogen gas for the gas-gap heat switch is supplied through a tube penetrating the side of the outer cylinder.

The heater passes through the hydride material and is designed to uniformly distribute heat to ensure a high degree of temperature uniformity when at the maximum temperature of 465 K. Heat transfer to the hydride is provided by aluminum foam that fills the inner cylinder and makes tight contact to the heater. The foam is 89% empty, and is cut to allow penetration by the various other components, which are located in the inner cylinder. A vent tube passes through the center of the hydride material. This vent tube is fabricated from sintered 316 stainless steel, and has a sub-micron porosity, which excludes the powdered hydride from the hydrogen gas flow.

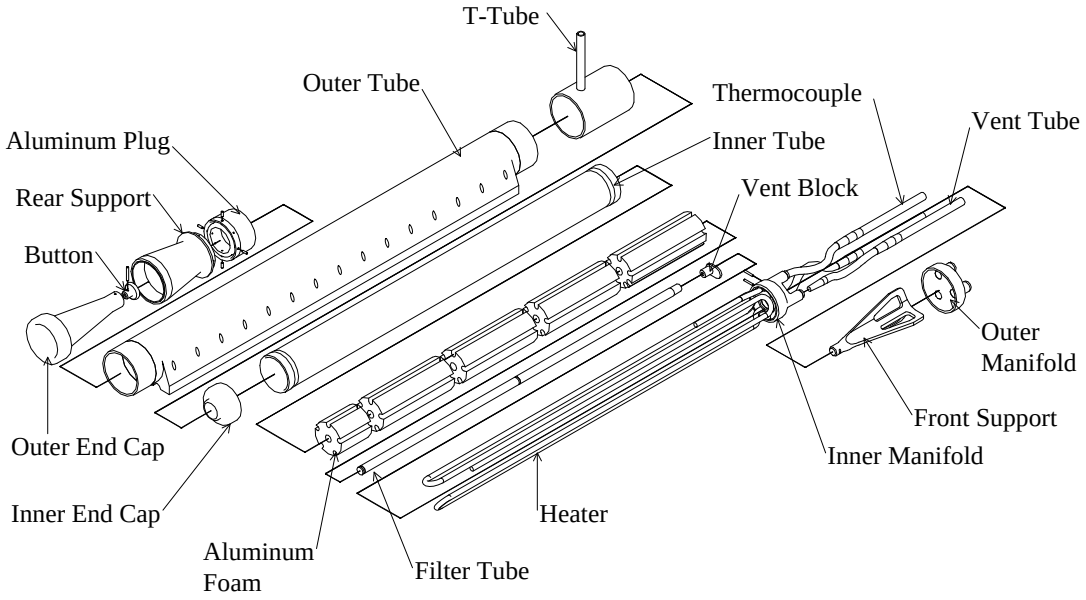

Figure 5. Exploded view of compressor element piece parts.

Figure 6. Compressor element used for gas-gap characterization tests.

A heater, thermocouple, and vent-tube lead run from the end cap of the inner cylinder to that of the outer cylinder. Each has a small bend for stress reduction, which defeats the potential for any of these elements to carry load. Therefore the only elements taking significant load are those designed to be structural, load carrying elements. There are two of these structural end supports: one at either end of the tube assembly. At one end provision is made for thermal compliance, without strain, between the inner and outer
tubes. The outer tube assembly is primarily fabricated of 6061-T6 aluminum. This outer tube also provides the primary structural attachment point for the single compressor bed.

Nearly all parts of the compressors and the gas-handling system which come in contact with hydrogen are made of 316L vacuum arc remelt (VAR) stainless steel which has been electropolished on the surfaces exposed to the hydrogen. This choice of material also serves to prevent the degradation of the compressors structural parts by reaction with the hydrogen. There are two components which are made of other materials. The aluminum foam, which provides heat conduction to the hydride in the compressor, and the seals of the check valves, which are made of Viton. Stringent cleaning and assembly methods are used during construction.

The space between the inner compressor vessel and the outer tube assembly is used as a gas-gap thermal switch. It is preferred that this switch be operated in a closed cycle using a hydride to pump the gap to approximately 0.01 Torr when 'off' and to approximately 10 Torr when 'on.' A test program is currently in place to characterize candidate materials and to determine the operational pressure requirements for closed cycle operation[6]. Closed cycle operation will require approximately 8 W per switch which is 'on.'

In figure 7 conductance test data at approximately 300 K is presented for the compressor assembly shown in figure 6. The sum of conductive and radiative parasitics at the highest temperature difference (475 K inner vessel and 289 K outer vessel), which occurs in operation with the gas-gap volume evacuated, is 31 mW/K. This is slightly better than the predicted performance of this assembly. The conductance across the gas-gap matches theoretical predictions based on a model with one adjustable parameter, the accommodation coefficient, which has a value of 0.4. At high pressure (above approximately 30 Torr) the gas-gap switch conductance saturates at approximately 7.8 W/K, in good agreement with expectations.

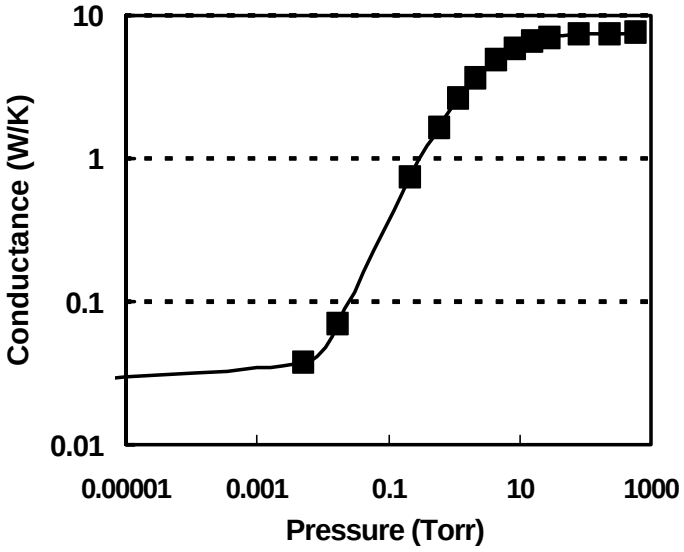

Figure 7. Gas-gap conductance from rarified gas regime through continuum flow at approximately 300 K.

J-T Cryostat Assembly

The J-T cryostat assembly includes a warm contaminate filter, active valves to allow redundant operation of the coolers, four heat exchangers, an approximately 50 K charcoal filter, an approximately 30 K 0.01 micron particulate filter, a porous plug J-T expander, and three liquid reservoirs. The four tube-in-tube heat exchangers are all 6.35 mm outer diameter tubing with a 3.18 mm outer diameter inner tube. The high pressure gas is held in the annulus. The heat exchangers are heat sunk at each thermal shield.

Contaminate trapping is done at room temperature with either a hydride getter or a resin bed (to be determined), with activated charcoal and a particulate filter at 50 K and a 0.01 micron filter at ~30 K. All of the components at the cold end were shown in figure 4. The J-T expansion is done through a porous plug device nearly identical to those described previously[7]. The first two liquid reservoirs are designed to separate the liquid refrigerant from the two-phase fluid leaving the J-T expander. This fluid is wicked to the wall of the reservoirs. The fluid in each reservoir is at essentially the same pressure and temperature. However the heat flux into each is very different. The first liquid reservoir interface temperature is approximately 18 K when providing < 230 mW of refrigeration to the HFI and the 4.5 K RAL cooler. The second reservoir has an approximately 20 K interface temperature due to the higher heat flux from the LFI. The third reservoir is designed to vaporize any excess liquid refrigerant to ensure a stable mass flow and pressure at the cryostat. This helps significantly to remove temperature fluctuations in the range of 1 Hz.

Figure 8 presents the predicted performance of the Planck sorption coolers as a function of temperature as compared with the predicted combined instruments cooling requirement. The difference between these predictions is the predicted margin. At a precooling and telescope enclosure temperature of 50 K, a 77 % margin is predicted. With an environment of 60 K the margin is 0%.

The flight cooler electronics and software will be supplied by the Institut d'Astrophysique Spatiale in Orsay France and an industrial partner. The electronics consist of a CPU, relay boards and several temperature and pressure sensor boards. The details of these electronics will be presented in a future paper.

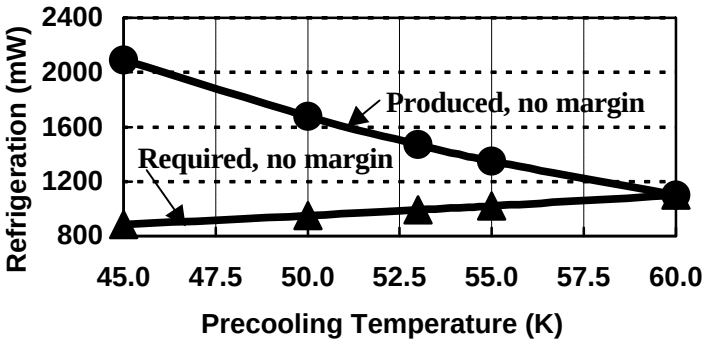

Figure 8. Predicted performance of the Planck sorption coolers and predicted combined Planck instruments cooling requirement as a function of precooling/telescope enclosure temperature.

DEVELOPMENT PLAN SUMMARY

1999 and 2000 will be primarily spent completing the technology development for this program. In 1999 an accelerated lifetest of the hydride material will be performed, several compressor elements will be built and begin parametric performance tests, gas-gap and characterization and actuation materials testing will be completed, and a demonstration of a three liquid reservoir cryostat will be made. In 2000, this development will continue leading up to initiation of testing of a flight-like 'elegant breadboard cooler' in December. The qualification model cooler is scheduled for delivery in January 2003. After qualification, this cooler will be refurbished and fly as the redundant cooler. The flight model cooler will be delivered in January 2004.

SUMMARY

A pair of sorption coolers are being developed for the ESA Planck mission. These coolers will be combined with passive cooling, a 4.5 K RAL cooler and a Benoit style dilution cooler to provide refrigeration. The resulting cryogen-free mission design will likely prove a pathfinder for many other future astrophysics missions.

ACKNOWLEDGMENT

The research described in this paper was carried out by the Jet Propulsion Laboratory, California Institute of Technology, under a contract with the National Aeronautics and Space Administration.

REFERENCES

[1] B. Collaudin and T. Passvogel, *Cryogenics* 39:157 (1999).
[2] S. Bard, *J. Spacecraft and Rockets*, 21:150 (1984)
[3] S. W. Petrick, and S. Bard, presented at AIAA 26th Aerospace Sciences Meeting, Reno, NV, 11/14/88.
[4] T. T. Cafferty, in: "Spacecraft Radiative Transfer and Temperature Control," T. E. Horton, Editor, 1982.

[5] Alcatel Planck Payload Architect Team, Plank Payload Module Architect Technical Assistance Phase 1 Presentation, 29/04/99 ESTEC, private communication.
[6]M. Prina, P. Bhandari, R. C. Bowman Jr., C. G. Paine, and L. A. Wade, "Advances in Cryogenic Engineering," Vol. 45 (In Press).
[7] A. R. Levy and L. A. Wade, in: "Cryocoolers 10," R. G. Ross, Jr., Ed., Plenum Press, New York, (1999) p. 545.

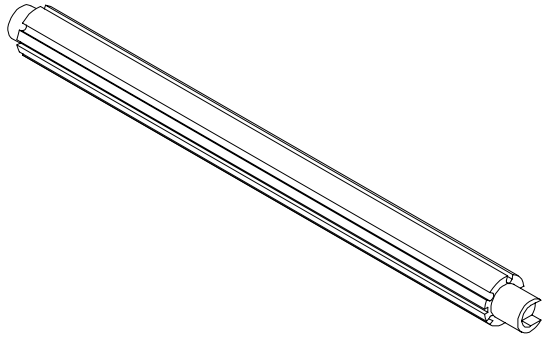

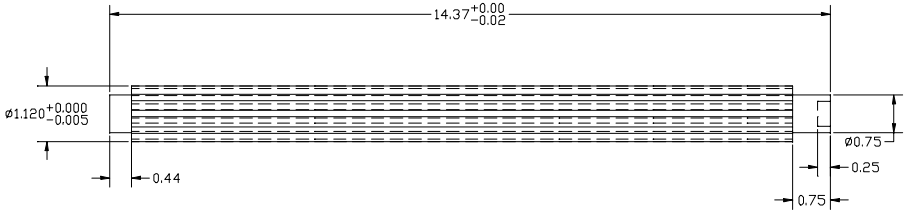

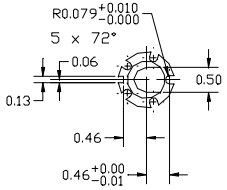

NEXT ASSEMBLY / USED ON: APPLICATION	UNLESS OTHERWISE SPECIFIED DIMENSIONS ARE IN INCHES. TOLERANCES: DECIMALS .XX ± .01, .XXX ± .005, .XXXX ± .0010; ANGLES ±1/2°. MACHINE FINISH. DO NOT SCALE DRAWING. INTERPRET DWG PER ANSI Y14.5M. MATERIALS	CONTRACT NO. APPD ____ DATE ____. DWN, CHK, STRUCT, MATL, QUAL, ENGR, DSGN, SUPV	JET PROPULSION LABORATORY. CALIFORNIA INSTITUTE OF TECHNOLOGY. PASADENA, CA 91109. RELEASE THROUGH SECTION 354. Copper Rod. Gas Gap Test. Hydride Compressor. SIZE D. CASE NO. REV A. SCALE 1/1. March 2, 1999. SHEET OF

Sievert apparatus description

A Sievert apparatus is used to survey gas reactions as a function of pressure, temperature and concentration, as for the characterization of a hydrogen- metal system reaction. This system is set up to automatically dose hydrogen into and out of the reactor vessel and compute the concentration of hydrogen absorbed into the hydride. It records both reduced data (concentration and pressure ordered pairs) and sufficient data to reproduce the Pressure versus Concentration graph. The entire measurements, including: the control of valves and sensor, data-recorded, data-reduction and output is executed by a program in Labview(National Instruments) software.

The apparatus was build and tested at JPL by Chris Lindensmith to take high pressure isotherms (up to pressure of 15 MPa). I adapted it with minor changes to measure low equilibrium pressure hydrogen-metal system by adding two pressure transducers (MKS Baratron 100 Torr and 2 Torr) and modifying the software. The installed pressure transducers are identical to those mounted on the switch assemblies.

The system operation process for an absorption isotherm measurement can be summarized as a repetition of the following steps:

- Fill the appropriate reference volume
- Record the amount of gas stored in the volume
- Open up the volume to the reactor
- Wait until the pressure is constant (the temperature and pressure measurement are at equilibrium)
- Close the valves between the reference and the reactor
- Subtract the gas left in the reference from the amount stored before desorption, and add that to the mass in the reactor volume. The relative concentration increases in the system are known.

The system follow a similar path for desorption, but dose the gas out through the reference instead of in. Before starting the automatic measurements, it is needed to calibrate the volume of the reactor and dead volumes (see schematic) and set the absorption pressure. For the low pressure measurements it is suggested to keep the pressure below 80 kPa to not saturate immediately the sorbent material.

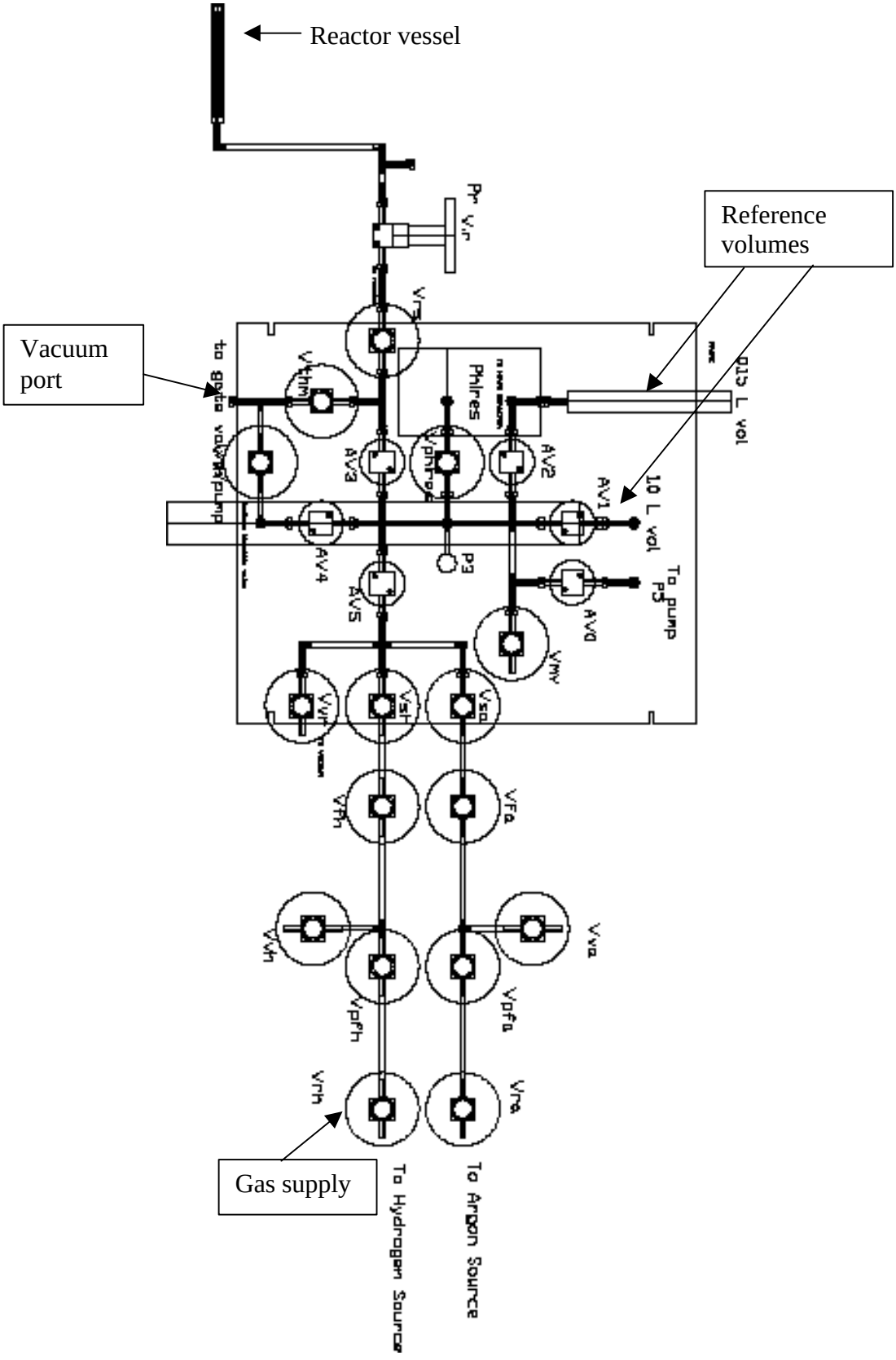
Reactor vessel
Reference volumes
Vacuum port
Gas supply
10 L vol
To pump P3
To Hydrogen Source
To Argon Source